ISTANBUL TECHNICAL UNIVERSITY ★ GRADUATE SCHOOL OF SCIENCE ENGINEERING AND TECHNOLOGY

APPLICATIONS OF ISOGEOMETRIC THEORY ON STRUCTURAL ANALYSIS OF BEAMS

M.Sc. THESIS

Murat DEMİRTAŞ

Department of Aeronautics and Astronautics Engineering

Interdiciplinary Aeronautics and Astronautics Engineering Program

DECEMBER 2011

ISTANBUL TECHNICAL UNIVERSITY ★ GRADUATE SCHOOL OF SCIENCE ENGINEERING AND TECHNOLOGY

APPLICATIONS OF ISOGEOMETRIC THEORY ON STRUCTURAL ANALYSIS OF BEAMS

M.Sc. THESIS

Murat DEMİRTAŞ
(511091144)

Department of Aeronautics and Astronautics Engineering

Interdiciplinary Aeronautics and Astronautics Engineering Program

Thesis Advisor: Assoc. Prof. Dr. Halit S. TÜRKMEN

DECEMBER 2011

İSTANBUL TEKNİK ÜNİVERSİTESİ ★ FEN BİLİMLERİ ENSTİTÜSÜ

İZOGEOMETRİK ANALİZ TEORİSİ'NİN KİRİŞLERİN YAPISAL ANALİZİ ÜZERİNE UYGULAMALARI

YÜKSEK LİSANS TEZİ

Murat DEMİRTAŞ
(511091144)

Uçak ve Uzay Mühendisliği Anabilim Dalı

Disiplinler Arası Uçak ve Uzay Mühendisliği Yüksek Lisans Programı

Tez Danışmanı: Doç. Dr. Halit S. TÜRKMEN

ARALIK 2011

Murat Demirtaş, a **M.Sc.** student of ITU **Graduate School of Science Engineering and Technology** student ID **511091144**, successfully defended the **thesis** entitled "**APPLICATIONS OF ISOGEOMETRIC THEORY ON STRUCTURAL ANALYSIS OF BEAMS**", which he prepared after fulfilling the requirements specified in the associated legislations, before the jury whose signatures are below.

Thesis Advisor :	**Assoc. Prof. Dr. Halit S. TÜRKMEN** Istanbul Technical University	.....
Jury Members :	**Assoc. Prof. Dr. Halit S. TÜRKMEN** Istanbul Technical University	.....
	Assoc. Prof. Dr. Mehmet ŞAHİN Istanbul Technical University	.....
	Assoc. Prof. Dr. Hasan KURTARAN Gebze Institute of Technology	.....

Date of Submission : 19 December 2011
Date of Defense : 24 January 2012

To my family,

FOREWORD

I would like to express my deep appreciation and thanks to my supervisor in İ.T.Ü. Doç. Dr. Halit S. Türkmen for his support and guidance to encourage me to participate the ERASMUS exchange program that makes this work possible. I would like to thank my supervisor in TU Delft Prof. Dr. Zafer GURDAL as well for accepting to work on this subject and his support.

My deepest thanks go to one of the most talented man I have ever met in my life, Attila P. Nagy. I was so lucky as I had the chance to connect his impressive knowledge river and I tried to gain as much flow as I can to my composed stream.

I would like to thank for his great patience and every single help he generously offered all along this challenging thesis study.

December 2011

Murat DEMİRTAŞ
Aerospace Engineer

TABLE OF CONTENTS

Page

ABBREVIATIONS

CAD	**:** Computer Aided Design
FE	**:** Finite Element
FEM	**:** Finite Element Method
FEA	**:** Finite Element Analysis
NURBS	**:** Non-Uniform Rational B-Splines

LIST OF SYMBOLS

A : Area

b : Width of cross section

$\boldsymbol{B_i}$: Control points

$\boldsymbol{C^n}$: Continuity level

$\boldsymbol{C(\xi)}$: B-spline function / NURBS function

dS : Differential arc length

$\underline{\boldsymbol{f}}$: Vector of concentrated load

h : Height of cross section

k : Number of knot repetition

n : Number of control points.

$\boldsymbol{N_{i,p}}$: Basis function

$\underline{\boldsymbol{n}}$: Normal vector of a the NURBS curve

p : Polynomial order of basis functions

$\boldsymbol{p_0}$: Pressure load

$\boldsymbol{q_0}$: Vector of distributed load

R : Radius of curvature

$\underline{\underline{\boldsymbol{R}}}$: Interpolation matrix

$\boldsymbol{R_i^p}$: Rational basis function

$\underline{\boldsymbol{r}}(\boldsymbol{\xi})$: Position vector of a location on a NURBS curve

$\boldsymbol{U}$: Strain energy stored in an elastic rod

$\underline{\boldsymbol{u}}$: Displacement of the control points

$\tilde{\boldsymbol{u}}$: Continuous displacement field

$\boldsymbol{V}$: Potential energy of applied external forces

w : Weight value

Greek Symbols

$\boldsymbol{\xi}$: Parametric coordinate on x direction

Ξ : Knot vector

Π : Total potential energy

$\boldsymbol{\varepsilon}$: Change in length

$\boldsymbol{\rho}$: Change in curvature

$\boldsymbol{\kappa}$: Curvature

$\boldsymbol{\sigma_m}$: Membrane stress

$\boldsymbol{\sigma_b}$: Bending stress

LIST OF TABLES

Page

LIST OF FIGURES

Page

APPLICATIONS OF ISOGEOMETRIC THEORY ON STRUCTURAL ANALYSIS OF BEAMS

SUMMARY

A novel method in numerical analysis called isogeometric analysis is applied on structural analysis of straight and free shaped slender beams as well as isotropic and composite thick beams in this thesis framework. Eventual goal of isogeometric approach is based on the idea of combining CAD tools and FEM solvers under a single software structure. This is simply ensured by appying same blending functions both to define the distribution of analysis variables and for modeling the problem geometry to be analysed.

In isogeometric analysis approach, the CAD tool that constructs the computational domain are the NURBS which are already used in computer graphics which offers distinguished flexibility and precision for generating and representing curves and surfaces. Since NURBS allows defining exact geometry of even conic sections and surfaces, when the mesh structure is constructed by NURBS, computational domain exactly matches with the geometry of the problem. This is ensured with relatively lower number of elements. As a result same accuracy can be maintained by using relatively fewer elements with a lower number of degrees of freedom than standard finite element method.

Since the geometry of the problem and the computational domain created with two different mathematical models in ordinary numerical analysis process, when the problem geometry is needed to be modified, computation mesh must be reconstructed from the beginning. However, isogeometric concept allows easy manipulation on the geometry. Exactly the same mathematical model creates the mesh structure and the original geometry of the problem. As a result, when the geometry modified, mesh is also modified as an exact representation of the new geometry in one operation.

Relying on linearly isotropic constitutive law and geometrically non-linear structural response, stiffness matrix is generated by successive derivation of the strain energy functional of the beam with respect to the vector of control point displacements. Then linearized form of equilibrium equation is solved at the undeformed configuration which yields the control point displacement values. Hence, evaluation of the displacements in control points allows to plot a new NURBS geometry that represents the deformed geometry under defined loads and boundary conditions.

Once displacement field is known, the total stress at a distance to the neutral axis that contains bending and membrane stress components is evaluated.

After the presentation of the isogeometric approach and elaborating the advantages over standard finite element method, some numerical structural analysis applications are carried out on both straight and arched beams and the results are compared with a standard finite element package and analytic solutions.

In the following applications codes to realize the isogeometric structural analysis of isotropic thick beams under several load cases are developed. Finally codes to carry our the isogeometric structural analysis of thick composite beams under cylindrical bending are developed. Isotropic thick beam analyses are compared with the results obtained from ABAQUS while composite cylindrical analysis results are compared with analytic elasticity solutions. In order to create the benchmark results with the analytic elasticity results, a code is developed to realize the analytic solution for the corresponding cases.

Eventual results exposed that using higher order basis functions allows isogeometric analysis to get more accurate results than conventional FEM even in the analyses of free formed slender beams and composite thick beams with a fewer number elements and degrees of freedom.

Since the results are clearly satisfactory, this work indicates that isogeometric analysis theory is a suitable tool for the structural analysis of the beams and can be a very strong alternative of conventional FEM in numerical analysis area.

İZOGEOMETRİK ANALİZ TEORİSİ'NİN KİRİSLERİN YAPISAL ANALİZİ ÜZERİNE UYGULAMALARI

ÖZET

Gerek doğada bulunan geometrik çeşitliliğin sonucu olarak meydana gelen gerekse insan emeği ile üretilen cisimlerin analizleri çoğu zaman belirli bir kısmi diferansiyel denklem systemi ile temsil edilen bir fiziki tanımlama gerektirir. Bu fiziki tanımlamanın yanı sıra söz konusu cisimlerin geometrik tanımı da analizin başarısı için oldukça önemlidir.

Bilgisayarların kullanılmaya başlandığı ilk yıllardan başlayıp günümüze kadar geçen zaman diliminde ileri düzey matematik problemlerinin bilgisayarlar yardımı ile çözülmesinde kullanılan yöntemlerin daha hassas ve daha verimli hale gelmesi için durmaksızın çaba sarf edilmiştir. Bu zaman diliminin başlangıcında gelişmiş analiz uygulamaları için sadece tek aşamalı hesaplama mümkün olabilmiştir. Ancak geçtiğimiz birkaç on yıl içinde teknolojinin ivme kazanarak ilerlemesi ve bilgisayarların kapasitesinin her geçen gün artması ile kullanım alanlarının sadece hesaplama ile sınırlı kalmayıp görsel ve fiziksel modelleme gibi farklı uygulama alanında da kullanılabilmesine olanak sağlamıştır. Farklı uygulamalar için farklı bilgisayar sistemleri geliştirilmiş zaman geçtikçe bu bilgisayar sistemlerinin bütünleşik olarak çalışması ve birçok uygulamaya aynı anda cevap verebilmesi sağlanmıştır. Bilgisayar sistemleri bütünleşik olarak çalışmak zorunda oldukları bir yapıya büründükçe farklı görevler üslenen bilgisayar sistemleri arasında gözlenen tanımlama ve yaklaşım uyuşmazlıkları daha belirgin olmaya başlamış ve bu uyuşmazlıklar analiz dünyasında aşılması gereken birincil sorunlardan biri haline gelmiştir. Söz konusu uyuşmazlıklar bilgisayar sistemleri arasında elektronik bilgi alışverişinin gündemde olmadığı yıllar boyunca sorumlu oldukları görev doğrultusunda ve dönemin sınırlı işlem gücü ile kendi içlerinde optimize edilmeye çalışılmış ve analiz sonuçlarının hassaslığı bu şekilde arttırılmaya çalışılmıştır. Ancak günümüz koşullarında bilgisayar sistemlerini arasındaki uyumun önemi oldukça artmış ve bütünleşik bir yapı ile çalışan sistemler adeta bir zorunluluk haline gelmiştir.

Bilgisayar destekli modelleme ve sonlu elemanlar analizi birbiriyle yüksek uyum ile çalışması istenen bilgisayar sistemleri görevlerinin başında gelmektedir. Çünkü bu görevleri üslenen sistemlerin geometrik tanımlama ve sayısal yaklaşım alanında birbiri ile iletişimi sırasında oluşan uyumsuzluklar sonuçların hassasiyetini ciddi ölçüde etkilemektedir. Özellikle havacılık ve gemi mühendisliği alanında ortaya çıkan karmaşık akışkanlar mekaniği ve yapısal analiz problemlerinin çözümüne duyulan ihtiyaç sonucu sonlu elemanlar analizinin bilim dünyası içindeki popülerliği ve mühendislik dallarında kullanım alanı genişlemiştir. Bunun sonucu olarak uygulamalı matematikçilerin ve bilgisayar mühendislerinin ilgisi de geometrik tanımlama için daha yüksek doğruluğa sahip bir matematiksel taban yaratmaya doğru yönelmiştir.

Analiz sonuçlarının hassaslığında önemli bir role sahip olan yüksek doğruluklu geometrik tanımlamanın gerekliliği ve geliştirilmesi için çeşitli hesaplamalı mekanik uygulamaları üzerine birçok çalışma yapılmış ve sonlu elemanlar analizinde kullanılmak üzere en hassas geometrik tanımlamayı gerçekleştirebilecek alternatif yöntemler geliştirilmiştir. Bu yöntemlerin en yenilerinden biri olan izogeometrik analiz, bilgisayar destekli modelleme ve sonlu elemanlar analizi için gelecek yıllar boyunca kalıcı bir kullanım alanına sahip olabilecek, yüksek verimli bütünleşik bir çalışma alanı oluşturma potansiyeline sahiptir.

Bu çalışma kapsamında öncelikle izogeometrik analizin dayandığı matematiksel temel olan B-Spline eğrileri ve bu eğrilerin özelleşmiş bir hali olan uniform olmayan rasyonel B-Spline eğrilerinin (NURBS) özellikleri detaylarıyla açıklanmış daha sonrasında ise bu matematiksel temel kullanılarak düz ve serbest eğrisel kirişlerin yapısal analizi üzerinde uygulamalar gerçekleştirilmiştir.

İzogeometrik analiz yaklaşımının nihai amacı ve avantajı, bilgisayar destekli tasarım aracı ile sonlu elemanlar metodu işlemcisini aynı yazılım içerisinde birbirleriyle direkt ilişki içerisinde çalışmasını sağlayacak bir analiz ortamının yaratılmasıdır. Bu da yer değiştirme, sıcaklık, hız gibi analiz değişkenlerinin dağılımının hesaplamında kullanılan dağılım fonksiyonlarının aynı zamanda problem geometrisinin oluşturulmasında da kullanılması ile gerçekleştirilir. Başka bir deyişle çözüm ağı yapısının da problemin çözümünde kullanılan dağılım fonksiyonlarının uygun bir şekilde harmanlanması ile oluşturulması, tüm sayısal içeriğin aynı fonksiyonlardan türetilmilmesine olanak sağlar.

İzogeometrik analiz yaklaşımında çözüm ağını oluşturmak için kullanılan CAD aracı, eğri ve serbest şekilli yüzeylerin oluşturulması konusunda seçkin esneklik ve hassasiyet sunan NURBS eğrileridir. NURBS eğrileri ile gerçekleştirilen geometrik tanımlama siteminin temeli Bezier eğrilerinin geliştirilmesine dayanmaktadır ve ortaya çıkmaları serbest şekilli yüzeylerin kusursuz matematiksel tanımının yapılması ihtayıcı sonucu olmuştur. Özellikle hava araçlarının, otomobillerin ve gemi gövdelerinin dış yüzeylerinin teknik gereksinimlerden ötürü, belirli bir matematiksel tanıma göre tekrar oluşturulması gerekebilir. Bu yapılar göz önünde bulundurulduğunda NURBS sistemi bu tip tasarımların ilk yapıldığı yıllarda tasarımcı tarafından oluşturulmuş ve modifikasyonu mümkün olmayan tek bir fiziksel modele nazaran büyük avantaj ortaya koymuştur.

NURBS geometrik tanımlama sistemi konik kesitleri ve yüzeyleri dahi kusursuz biçimde tanımlayabildiği için nümerik analizde kullanılan çözüm ağının NURBS ile oluşturulması hesaplama alanının problem geometrisini ile tamamen eşleşmesini sağlamaktadır. Burada çözüm ağı oluşturulurken gerçek geometriyi temsil etmek ve yakınsama ihtiyacı söz konusu değildir. Zira çözüm ağı geometrisi problem geometrisi ile tamamıyla örtüşmektedir. Üstelik bu durum standart sonlu elemanlar metodu yöntemi ile oluşturulmuş bir çözüm ağına göre daha az sayında eleman kullanılarak veya aynı sayıda eleman kullanılmasına karşın daha az serbestlik derecesi ile sağlanabilmiş ve tatmin edici sonuçlar ortaya çıkarmıştır.

Alışılagelmiş sonlu elemanlar metodu kullanan paketlerde gerçek geometrinin ve çözüm ağının iki farklı matematik model kullanılarak oluşturulması, problem geometrisinin modifiye edilmesi durumunda tüm çözüm ağının tamamıyla tekrar oluşturulması gereğini doğurur. Buna karşın izogeometrik analiz, problem geometrisi üzerinde esnek modifikasyon olanağı sağlar. Çünkü çözüm ağı yapısı ve orijinal problem geometrisi aynı matematik model ile ifade edilir. Bunun sonucu

olarak da problem geometrisinde bir değişiklik yapılması durumunda çözüm ağı da yeni geometrinin mutlak temsili olacak şekilde değişmektedir. İki ayrı matematik model söz konusu olmadığından bu değişim tek bir işlemle gerçekleşir.

Bu çalışma içerisinde düz ve serbest eğrisel kirişlerin analizinde lineer izotropik temel kanunu ve lineer olmayan geometrik yapısal cevap kabulü yapılmıştır. Bu kabul gereğince elastik gerinme enerjisi fonksiyonunun serbestlik derecesi vektörüne göre birinci türevi iç kuvvet vektörünü vermektedir. Bu iç kuvvet vektörünün tekrar serbestlik derecesi vektörüne göre türevinin alınması ise sistemin katılık matrisinin elde edilmesini sağlar. Söz konusu türevler analitik olarak alınmıştır. Bu işlem boyunca gerek ifadeler içindeki terimlerin türevleri gerekse de elastik gerinme enerjisi fonksiyonunun birinci ve ikinci türevleri, sonlu farklar yöntemi kullanan bir yazılım geliştirilerek hesaplanmış, bulunan sonuçlar kağıt üzerinde sonuçlarla karşılaştırılarak sağlaması yapılmıştır.

Elde edilen katılık matrisi, denge denkleminin kiriş geometrisinin deforme olmadan önceki durumu için lineerleştirilmiş hali içerisinde kullanılarak kontrol noktalarının yer değiştirme değerleri yani serbestlik derecesi vektörü bulunur. Kontrol noktalarının yer değiştirme miktarı ile kontrol noktalarının yeni konumları belirlenir. Böylece yeni kontrol noktaları ile oluşturulan NURBS geometrisi uygulanan yük ve sınır şartları altında kirişin deforme olmuş halini oluşturmaktadır.

Yer değiştirme alanı kiriş boyunca tanımlandığında kiriş üzerindeki herhangi bir noktadaki kesitte asal eksenden belirlenen bir uzaklıkta eğilme ve çekme kuvveti bileşenlerinden oluşan toplam gerilme miktarı bulunur.

Çalışma kapsamında öncelikle izogeometrik analiz yaklaşımı anlatılmış ve standart sonlu elemanlar yönteminden temel farklılıklarına ve avantajlarına değinilmiş düz ve serbest formlu eğrisel kirişler üzerinde izogeometrik nümerik analizleri gerçekleştirecek kodlar geliştirilmiş ve bu kodlardan elde edilen sonuçlar analitik çözümlerden ve paket programlardan elde edilen sonuçlarla karşılaştırılmıştır.

Takip eden uygulamalarda ise çeşitli yükleme koşulları ve sınır şartları altında izotropik kalın kirişlerin çeşitli yüklemeler altında ve çeşitli katman sıralamasına sahip kalın kompozit kirişlerin silindirik eğilme etkisi altındaki izogeometrik nümerik analizlerini gerçekleştirecek kodlar geliştirilmiştir. İzotropik kalın kiriş analizleri yine paket programlardan elde edilen sonuçlarla karşılaştırılmış, kompozit kalın kirişlerin silindirik eğilme sonuçları ise N.J. Pagano'nun bir çalışması içerisinde yayınlanmış analitik elastisite çözümleri ile karşılaştırılmıştır. Bunun için analitik tam çözümü gerçekleştiren bir fonksiyon geliştirilmiş ve nümerik izogeometrik analiz kodu ile iletişim halinde çalışması sağlanmıştır. Böylece herhangi bir durum için nümerik ve analitik tam çözüm sonuçlarının karşılaştırmalı grafik çıktısını oluşturan bir kod elde edilmiştir.

Nihai sonuçlar izogeometrik analiz içinde kullanılan fonksiyonların polinom derecesi yükseltildikçe, serbest eğrisel kirişler ve kompozit kalın kirişler de dahil olmak üzere, serbestlik derecesi düşük tutularak hassas sonuçlara ulaşılabilineceğini göstermiştir.

İzogeometrik analiz sonucu elde edilen sonuçlar öncelikle validasyon amacıyla halihazırda piyasada bulunabilen bir paket programdan elde edilen sonuçlarla karşılaştırılmış daha sonra ise yüksek dereceden polinom derecesi kullanılarak daha hassas sonuçlar elde edilmeye çalışılmıştır.

Kalın kompozit kirişlerin silindirik eğilme altındaki analizinde düşük serbestlik derecesi ile halihazırda ticari bir paket programın sahip olmadığı hassaslık elde edilmiştir. Sonuçlarda çok yüksek doğruluk sağladığından bu çalışma, izogeometrik analiz teorisinin söz konusu koşullar altında kirişlerin yapısal analizinde alışılagelmiş sonlu elemanlar metoduna alternatif olarak kullanılabileceğini göstermiş ve ileri çalışmalar için gerekli olan yazılım birikiminin oluşturulmasını sağlamıştır.

1. INTRODUCTION

The importance of an accurate geometrical model have been pointed out by numerous authors in the last decade for diverse computational mechanics problems and different alternatives have been studied to implement accurate or exact geometric representations for finite element simulations. This study proposes a novel analysis method, the isogeometric structural analysis. It allows creating not an approximation of the geometry but the exact geometry description of the solution domain, by means of the CAD representation with NURBS. Furthermore, it also allows simplification of mesh refinement by eliminating the necessity of subsequent communication with the CAD geometry once the initial mesh is constructed.

This chapter describes the necessity of an accurate geometric description in the numerical solution of structural mechanics applications and points out the role of isogeometric analysis with its historical background. Then the objectives of the work are described and a brief overview of the study is presented.

1.1 Literature Review

Finite element method originated from the need for solving complex elasticity and structural analysis problems in civil and aeronautical engineering.

As the popularity of the finite element method began to grow in the engineering communities, more applied mathematicians became interested in improving the method to achieve a firm mathematical base. As a result, a number of studies were aimed at estimating discretization error, rates of convergence, and stability for different types of finite element approximations.

Besides enriching solution approximations, the need of improving the quality of the geometrical representation has been rising. Isoparametric elements were the first approach introduced to efficiently deal with curved boundaries, see Zienkiewicz[1].The key idea was to employ the same polynomial functions to approximate the solution and the geometry, hence the term called “isoparametric”. It

does not take a long time for the researchers to apply this approach on solid mechanics applications due to its simple implementation and relatively better accuracy.

Luo et al. [2] are derived parallel conclusions for linear elasticity problems. The importance of a realistic geometric model for some applications in solid mechanics is pointed out by Munoz [3] as well, where the B-splines are employed for modelling the geometries of frictionless contact problems.

In the 1980s, CAD technology started to get involved in the FE analysis. In fact, researchers on the field of shape optimization were the first ones who took the advantage of the cooperation of CAD and FE. In a shape optimization process, the integration of CAD into the analysis stage is vital to avoid the geometric approximation habit while constructing the mesh structure of the problem.

The relevance of an accurate geometry description also motivated, in the last half of 1990s, an innovative group of FE-like techniques founded on CAD, which is the subject of this thesis and still the subjects of many other researches: isogeometric methods. The key idea is to use the same CAD entities for both the modelling of the geometry and the solution of the problem. As a result, contrary to classical FE approaches, not only the domain boundaries but also the entire solution domain treated as a CAD entity. Moreover, contrary to classical polynomial approximations, the solution is approximated with the same basis fuctions used to design the problem geometry. The first example again encountered on shape optimization in the research of Kagan et al. [4]. B-splines are proposed for the geometrical description, as well as for the mechanical analysis.

More recently, NURBS have been used to develop isogeometric methods, Hughes et al. present a more general framework known as isogeometric analysis.[5] This innovative study is not only intended the accurate geometrical representation, but also employed the features of NURBS for the solution approximation as similar as current work. The use of several connected patches in isogeometric analysis has been pointed out by Cottrell et. al.[6] while the use of T-Splines to take the advantage of local refinement is proposed by Dorfel et. al.[7] Cottrell et al. also employed the isogeometric analysis for vibration problems [8]. Another colleague of Cottrell and Hughes, Bazilevs, published a work on stability and error estimates for refined

meshes in isogeometric analysis. [9] Nagy et al. applied isogeometric analysis into to shape optimization and sizing of beam structures. [10]

Zhang et al. employed the isogeometric method for accurate blood flow modeling [11]. Benson et al. proposed a shear deformable shell formulation based on the isogeometric analysis methodology [12]. Gómez et al. studied the Cahn–Hilliard phase-field model problem via isogeometric analysis [13]. Echter and Bischoff analyzed the efficiency and locking issues for NURBS-based analysis [14]. The robustness of isogeometric discretizations were also investigated by Lipton et al. [15]. Kim et al. Performed the isogeometric analysis for trimmed CAD surfaces [16]. Besides based upon the isogeometric concept Lu constructed a circular element [17]. Sevilla et al. proposed a NURBS enhanced finite element method [18]. Shaw and Roy constructed a NURBS-based parametric meshless method [19].

1.2 Objectives and Overview

The objective of this thesis is to present a novel numerical analysis approach, isogeometric analysis, studying its superiorities over conventional FEM, and applying isogeometric analysis on various cases of structural analysis of beams. Although the method is already verified by some examples in the litrerature initial simple applications, such as 1D slender beam analysis, are more likely to validate the method. These applications are presented in this thesis for a better understanding of the isogeometric concept and to maintain a solid foundation for more complex applications in the following chapters. Besides this since isogeometric analysis concept is a novel method, a contribution to current inventions is crucially necessary as it is the eventual objective of this study. Since the isogeometric analysis codes can achieve more accurate the results than a conventional FEM package for 2D isotropic thick beam and 2D composite thick beam applications, this objective has been accomplished successfully.

In the second chapter, B-splines, the key basis of NURBS, are explained in details with proper refinement methods and NURBS, which are the building blocks of isogeometric analysis, presented in the third chapter. In Chapter 4 the main equations and mathematical background employed in the isogeometric structural analysis codes developed for both 1D and 2D cases are introduced.

In the fifth chapter applications on a straight beam for two different boundary conditions realized followed by an analysis of a free formed arched beam. Straight beam applications are compared with analytical solutions while arched beam application benchmarked with a commercial FEM package, ABAQUS.

In Chapter 6 the most challenging and remarkable section of this study which is isogeometric structural analysis of isotropic and composite thick beams is introduced. Isotropic thick beam cases compared with the results obtained from ABAQUS while composite cases benchmarked with analytic elasticity solutions. Besides the code for isogeometric analysis of composite thick beams, a subroutine code is also developed for these elasticity solutions and for each case isogeometric analysis code calls this subroutine and creates the benchmark plots for the stress values through the beam thickness as presented at the end of the chapter. In addition, all the results for various element numbers and basis degrees are presented in the appendix.

2. B-SPLINES

Since B-Splines are the progenitors of the NURBS, definition of the B-Splines is an essential starting point on the way to comprehend the NURBS which is the key structure to implement isogeometric analysis.

A B-spline is a spline function that has minimal support with respect to a given degree, smoothness, and domain partition. A fundamental theorem states that every spline function of a given degree, smoothness, and domain partition can be represented as a linear combination of B-splines of that same degree and smoothness, and over that same partition. [20] Unlike in standard finite element analysis, the B-spline parametric space is local to patches. Patches are used to define the parametric space partitions within which element types and material models are assumed to be uniform likely the elements do in conventional finite element method.

To avoid misunderstandings in the cases when computational geometry and finite element method are applied together as it is done in isogeometric approach; it is useful to state that in finite element literature $p = 0,1,2,3...$ etc. refers to constant, linear, quadratic, cubic etc. polynomials respectively. However, this is usually referred to as "degree" in the computational geometry literature.

2.1 Knot Vectors

In order to define the patches, a one dimensional vector comprise of non-decreasing ($\xi_i \leq \xi_{i+1}$) coordinates in the parametric space is used. This is called "knot vector". Knot vectors are written as follows; $\Xi = \{\xi_1, \xi_2, ...\xi_{n+p+1}\}$ where $\xi_i \in \mathbb{R}$ is the ith *knot, i* is the knot index $i = 1,2,3...,n+p+1$, p is the polynomial order, and n is the number of the basis functions which comprise the B-Spline.

There are two types of knot vector are used, periodic and open. Then they can be either uniform or non-uniform. $[0 \quad 1 \quad 2 \quad 3 \quad 4]$ and $[-0,2 \quad -0,1 \quad 0 \quad 0,1 \quad 0,2]$ are uniform knot vectors since the knot values are evenly spaced otherwise they are

called non-uniform. Generally uniform knot vectors are normalized in the range between 0 and 1.Knot vectors can be normalized as follows; when $p=2$ $[0 \quad 0 \quad 1 \quad 2 \quad 3 \quad 4 \quad 4]$ is normalized we get the following knot vector $p=2$ $[0 \quad 0 \quad 1/4 \quad 1/2 \quad 3/4 \quad 1 \quad 1]$.

More than one knot can appear at the same parametric coordinate. If a knot vector is open then its first and last knots are repeated $p+1$ times. For example: $[0 \quad 0 \quad 0 \quad 0.25 \quad 0.5 \quad 0.75 \quad 1 \quad 1 \quad 1]$ is an open knot vector for quadratic $(p=2)$ basis functions. In one dimension; for the basis functions formed from open knot vectors, this repetition is compulsory to provide interpolative property at the internal and end coordinates of the parametric interval $[\xi_1, \xi_{n+p+1}]$. In multiple dimensions; it is also the way of providing interpolative property of the corners of patches while they are not interpolatory at interior knots. This is a distinctive feature between knots and "nodes" in finite element analysis.

2.2 Basis Functions

B-spline basis functions are defined recursively starting with piecewise constants when p=0

$$N_{i,0}(\xi) = \begin{cases} 1 & \text{if } \xi_i \le \xi < \xi_{i+1}, \\ 0 & \textit{otherwise.} \end{cases} \qquad \textbf{(2.1)}$$

For $p=1,2,3...,$ they are defined by the following formula;

$$N_{i,p}(\xi) = \frac{\xi - \xi_i}{\xi_{i+p} - \xi_i} N_{i,p-1}(\xi) + \frac{\xi_{i+p+1} - \xi}{\xi_{i+p+1} - \xi_{i+1}} N_{i+1,p-1}(\xi) \qquad \textbf{(2.2)}$$

This is referred to as the Cox-de Boor recursion formula [21]. Because the Cox-de Boor formula used to calculate B-spline basis functions is a recursion relation, a basis function of a given order p depends on lover-order basis functions down to order 1. For a given basis function, $N_{i,p}$, this dependence forms a triangular pattern given by;

$$N_{i,p}$$

$$N_{i,p-1} \quad N_{i+1,p-1}$$

$$N_{i,p-2} \quad N_{i+1,p-2} \quad N_{i+2,p-2}$$

$$\vdots \qquad \vdots \qquad \vdots \qquad \ddots$$

$$N_{i,1} \qquad N_{i+1,1} \qquad N_{i+2,1} \qquad \cdots \qquad N_{i+p-1,1}$$

Applying (eq.2.1) and (eq.2.2) to a uniform knot vector $\Xi = [0 \quad 0.1 \quad 0.2 \quad 0.3 \quad 0.4 \quad 0.5 ...]$ provides the quadratic B-Spline basis functions which is useful to make a comparison with standard finite element method shape functions in Figure 2.1.

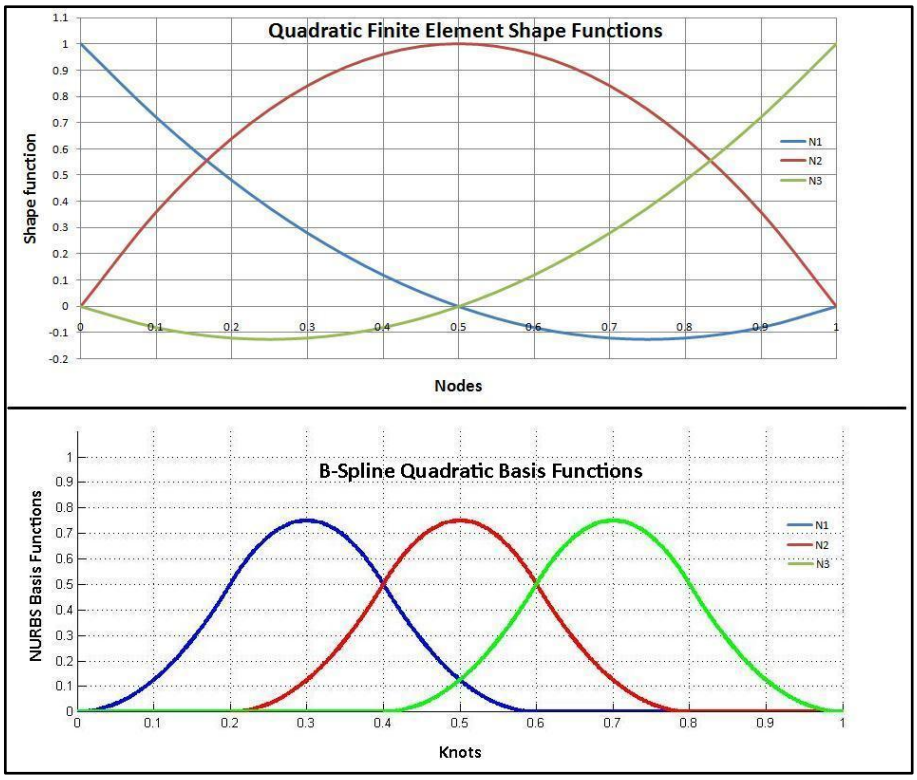

Figure 2.1 : Comparison of quadratic finite element shape functions and B-spline basis functions.

When the basis functions of standard FEM and B-Spline compared with each other, for $p = 0$ and $p = 1$, the basis functions of two different methods give the same plots respectively. However for $p \geq 2$ B-spline basis functions differ from their FEM counterparts. Quadratic B-spline basis functions are exactly alike but shifted while shape of a quadratic finite element function differs whether it corresponds to an internal or an end node. This is the first distinguishing and noteworthy feature of

quadratic and higher order B-spline basis functions (and NURBS basis functions, as will be discussed later) superior to standard finite element method as this homogeneous feature provides significant advantages in equation solving over finite element functions. In addition, support of each B-Spline basis function that shown as $N_{i,p}$ is compact and contained in the interval $\left[\xi_i, \xi_{i+p+1}\right]$. Finally, unlike the standard finite element shape functions each basis function of a B-Spline is pointwise non-negative over the entire domain, that is, $N_{i,p}(\xi) \geq 0, \forall \xi$. Accordingly, all of the coefficients of a mass matrix computed from these bases greater than, or equal to zero.

Non-uniform knot vectors allow maintaining much richer behavior than uniform knot vectors. A quadratic example is shown in Figure 2.2 for the open non-uniform knot vector $\Xi = \left[0 \quad 0 \quad 0 \quad 0.2 \quad 0.4 \quad 0.4 \quad 0.6 \quad 0.8 \quad 1 \quad 1 \quad 1\right]$. Note that the basis functions are interpolatory at the ends of the interval and also at $\xi = 0.4$ where the knot repetition occurs. At this repeated knot only C0 continuity is attained. Elsewhere the functions have C1 continuity. Thus when the multiplicity of a knot value is exactly p, the basis is interpolatory at that knot. When the multiplicity is p + 1, the basis becomes discontinuous and the patch boundary is formed.

Notice that the knot repetition on any parametric location on the curve decreases the support of some of the functions, which lies around the repeated knot. However this does not override the feature stated previously as the support of the each function still contains p+1 knot spans. That is, all the functions still begin at knot ξ_i and end at ξ_{i+p+1} however functions influenced by knot repetition has zero measure in some of those knot spans. Furthermore, none of this has any effect on the bandwidth.

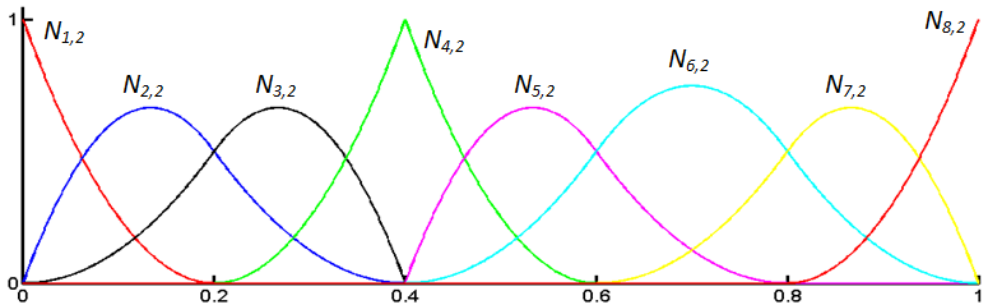

Figure 2.2 : Quadratic basis functions of $\Xi = \left[0 \quad 0 \quad 0 \quad 0.2 \quad 0.4 \quad 0.4 \quad 0.6 \quad 0.8 \quad 1 \quad 1 \quad 1\right]$.

2.3 B-Spline Curves

Linear combination of B-spline basis functions constructs the B-spline curves in $\mathbb{R}^d$ where the coefficients of the basis functions are called "control points". Control points have a similar role in the analysis as the nodal coordinates do in finite element method. When the control points are added together with straight lines starting from the first to the last, the resultant polygon is referred to as "control polygon".

B-spline curves are defined by;

$$C(\xi) = \sum_{i=1}^{n} N_{i,p}(\xi) B_i \tag{2.3}$$

where $B_i \in \mathbb{R}^d$ are the corresponding control points for the given parametric length. For the knot vector $\Xi = [0 \quad 0 \quad 0 \quad 0.2 \quad 0.4 \quad 0.4 \quad 0.6 \quad 0.8 \quad 1 \quad 1 \quad 1]$ the example shown in Figure 2.3 is built from quadratic basis functions in Figure 2.2.

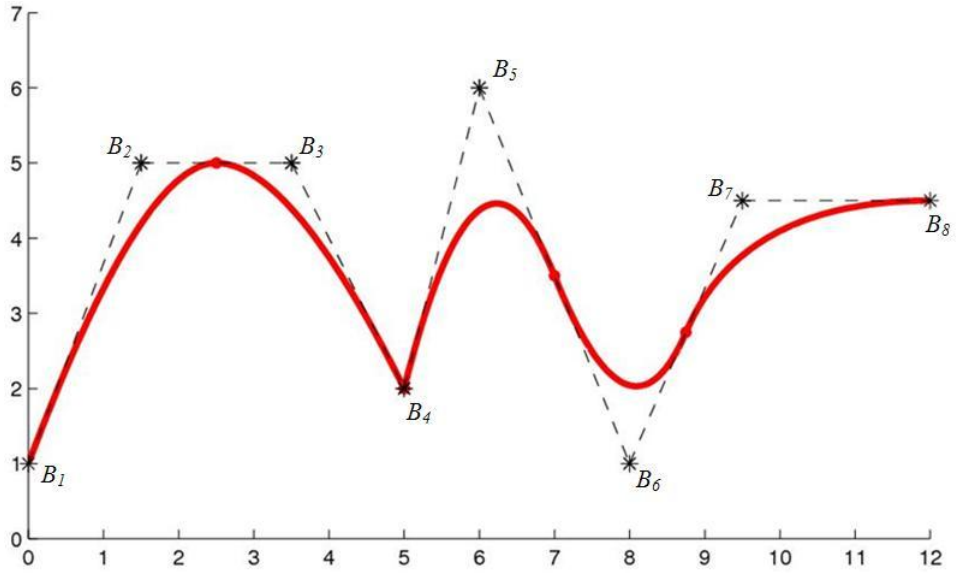

Figure 2.3 : Quadratic B-Spline curve in $\mathbb{R}^2$ constructed by the basis functions and the knot vector in Figure 2.2.

2.4 Refinements

Mesh refinement processes for the B-spline geometries are simply developed from a blend of knot insertion and order elevation strategies. These bring analogues with standard finite element method such as h-refinement and p-refinement. However

advantageous k-refinement technique is a characteristic feature that is applicable on B-splines.

2.4.1 Knot insertion: h-refinement

The analogue of h-refinement is knot insertion. For an existing knot vector $\Xi = \left[\xi_1, \xi_2, ..., \xi_{n+p+1}\right]$ let $\bar{\xi} \in \left[\xi_k, \xi_{k+1}\right[$ be the inserted knot. Then the new knot vector will be $\Xi = \left[\xi_1, \xi_2, ..., \xi_k, \bar{\xi}, \xi_{k+1}, ..., \xi_{n+p+1}\right]$.When a new knot inserted to the knot vector, number of the control points and the basis functions also increase by 1. The new n+1 control points $\left\{\bar{B}_1, \bar{B}_2, ..., \bar{B}_{n+1}\right\}$ are formed from the original control points, $\left\{B_1, B_2, ..., B_n\right\}$ by;

$$\bar{B}_i = \alpha_i B_i + (1-\alpha_i) B_{i-1} \qquad \textbf{(2.4)}$$

where;

$$\alpha_1 = \begin{cases} 1 & , 1 \le i \le k-p \\ \dfrac{\bar{\xi} - \xi_i}{\xi_{i+p} - \xi_i} & , k-p+1 \le i \le k \\ 0 & , k+1 \le i \le n+p+2 \end{cases} \qquad \textbf{(2.5)}$$

Knot values in the existing knot vector may be repeated as well but in this case the continuity of the basis will be reduced. Continuity of the curve is preserved by choosing the control points as in **(2.4)** and **(2.5)**. Each unique internal knot value may appear no more than p times or the curve becomes discontinuous as it is discussed before.

An example of knot insertion is shown in Figure 2.4. A new knot is inserted at $\bar{\xi} = 0,5$ to the existing knot vector $\Xi = \left[0 \quad 0 \quad 0 \quad 1 \quad 1 \quad 1\right]$ which is used to create the original curve consist of quadratic B-Splines. Although the new curve is geometrically and parametrically identical to the original curve the basis functions and control points are changed. Thus, repeating h-refinement process allows enriching the solution space by adding more basis functions of the same order while keeping the original geometry.

Main idea of the knot insertion is creating new knot spans by splitting the present knot spans while adding new knot values. For that reason, it has significant similarities with h-refinement procedure in standard finite element analysis. On the other hand the number of new functions that are created and the basis continuity at the newly created element boundaries are different (continuity remains p-1). However when each newly added knot is repeated *p* times, basis functions will have C^0 across the new boundaries then it will be completely identical with h-refinement.

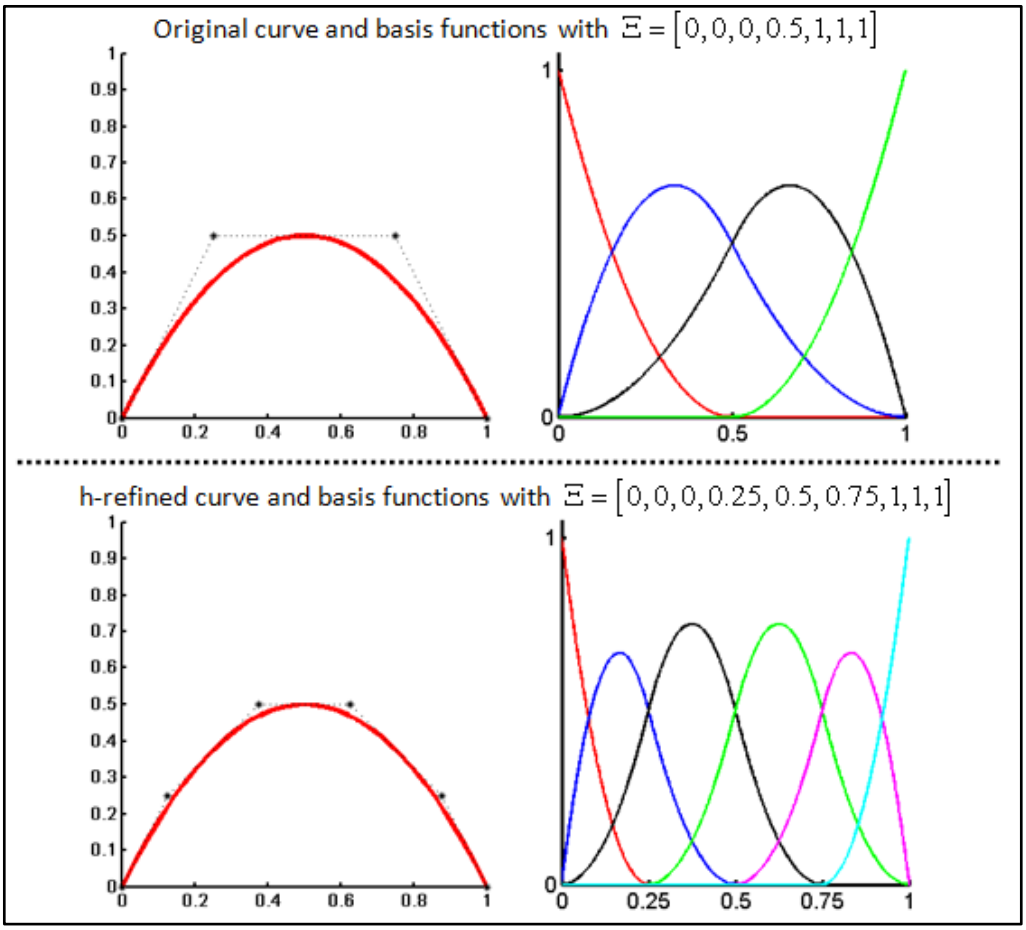

Figure 2.4 : h-refinement (knot insertion). Control points are denoted by "*".

2.4.2 Order elevation: p-refinement

In this refinement method the polynomial order of the basis functions are increased. This action does not change the geometry or parameterization. In addition, to preserve the desired discontinuities in the pth derivative of the elevated curve each knot value in the knot vector must be repeated.

The solution space spanned by the order elevated basis functions includes the space spanned by the original functions. Thus, as well as in h-refinement, it is possible to

elevate the polynomial order of basis functions without changing the geometry of the B-spline curve. It is also possible to keep the parameterization structure unchanged. Parameterization can be maintained as it was before the order elevation by splitting the curve into many Bézier curves by knot insertion (see [22] for more info about Bézier curves), then order elevating each of these segments and finally removing the unnecessary knots to merge the segments to create one unified, order-elevated B-spline curve.

An example of order elevation is presented in Figure 2.5. When p-refinement is applied, the number of the control points and basis functions also increase by one as seen in the figure. Although the control points appeared in different positions after p-refinement, the elevated curve is still geometrically and parametrically identical to the original curve. As a result, while original curve has three quadratic basis functions, elevated curve has four cubic basis functions.

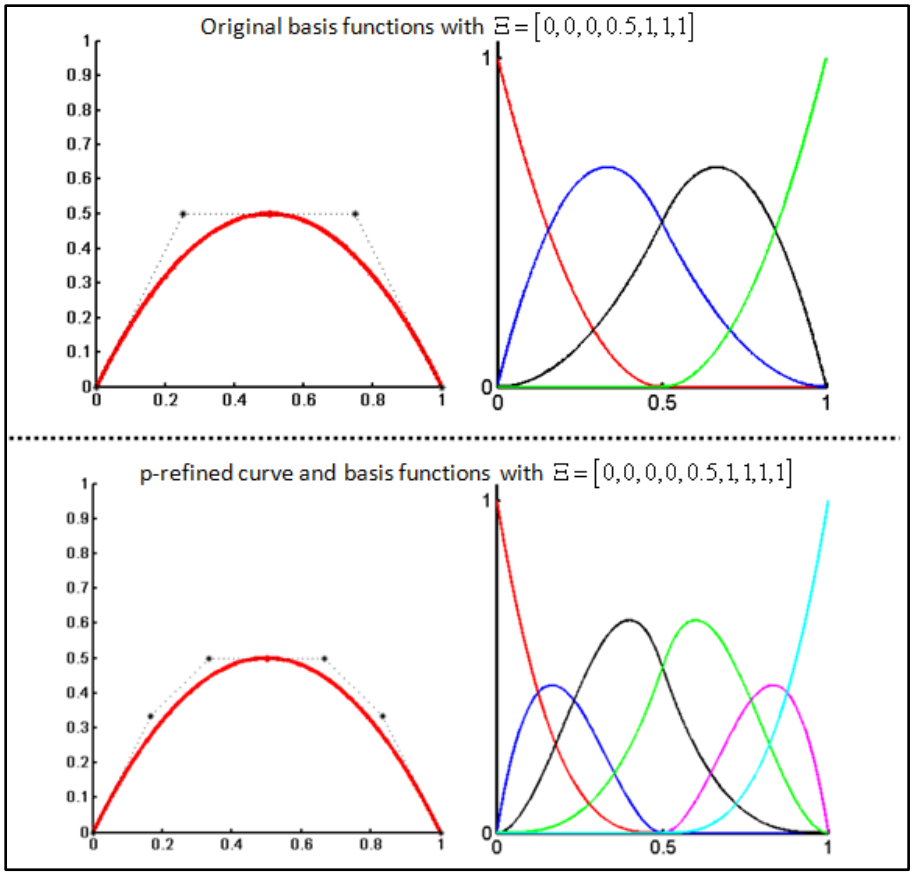

Figure 2.5 : p-refinement (order elevation). Control points are denoted by "*".

2.4.3 Combined refinement for high orders and high continuity: k-refinement

If a unique knot value, $\bar{\xi}$, is inserted between two distinct knots in a curve of order p, the number of continuous derivatives of the basis functions at $\bar{\xi}$ is p-1. Even if we elevate the order after knot insertion the basis still has p-1 continuous derivatives at $\bar{\xi}$. However if we change the sequence i.e. if the order of the original curve elevated to q first and only then insert a unique knot value, the basis will have q-1 continuous derivatives at $\bar{\xi}$ .Thus an alternative order elevation method which has significant advantages over standard order elevation reveals. This procedure called k-refinement. There is no analogous refinement method similar with k-refinement.

There are many superiorities of k-refinement over p-refinement. Unlike the p-refinement, k-refinement creates a homogeneous structure within patches and it doesn't raise the number of knots while maintaining the desired continuity. So applying the order elevation before the knot insertion i.e. "k-refinement" creates different basis function than applying the order elevation after knot insertion.

In order to make it more clear, these two different sequences of refinement process are compared with an example in Figure 2.6. Initial domain consist of an element and p+1 basis functions. h-refinement is applied followed by p-refinement on the left side of the figure. In this process, to maintain the continuity at the p-1 level each distinct knot value are replicated and the total number of basis functions is increased by n-p to 2n-p. As a result, nine piecewise quadratic basis functions that has zero continuity at internal knots are created.

By comparison, begin with the same element domain and proceed by k-refinement. In this case for each order elevation, total number of basis functions increases by only 1. Then domain can be h-refined until having n-p elements. If the domain is exposed to order elevation for a times, the number of total basis functions will be n+a while each of them has r+p-1 continuity. Thus at the right side, by applying k-refinement, six piecewise quadratic functions that are continuous at internal knots are created. That is, k-refinement allows covering the same element domain with fewer number of basis functions while having higher level of continuity.

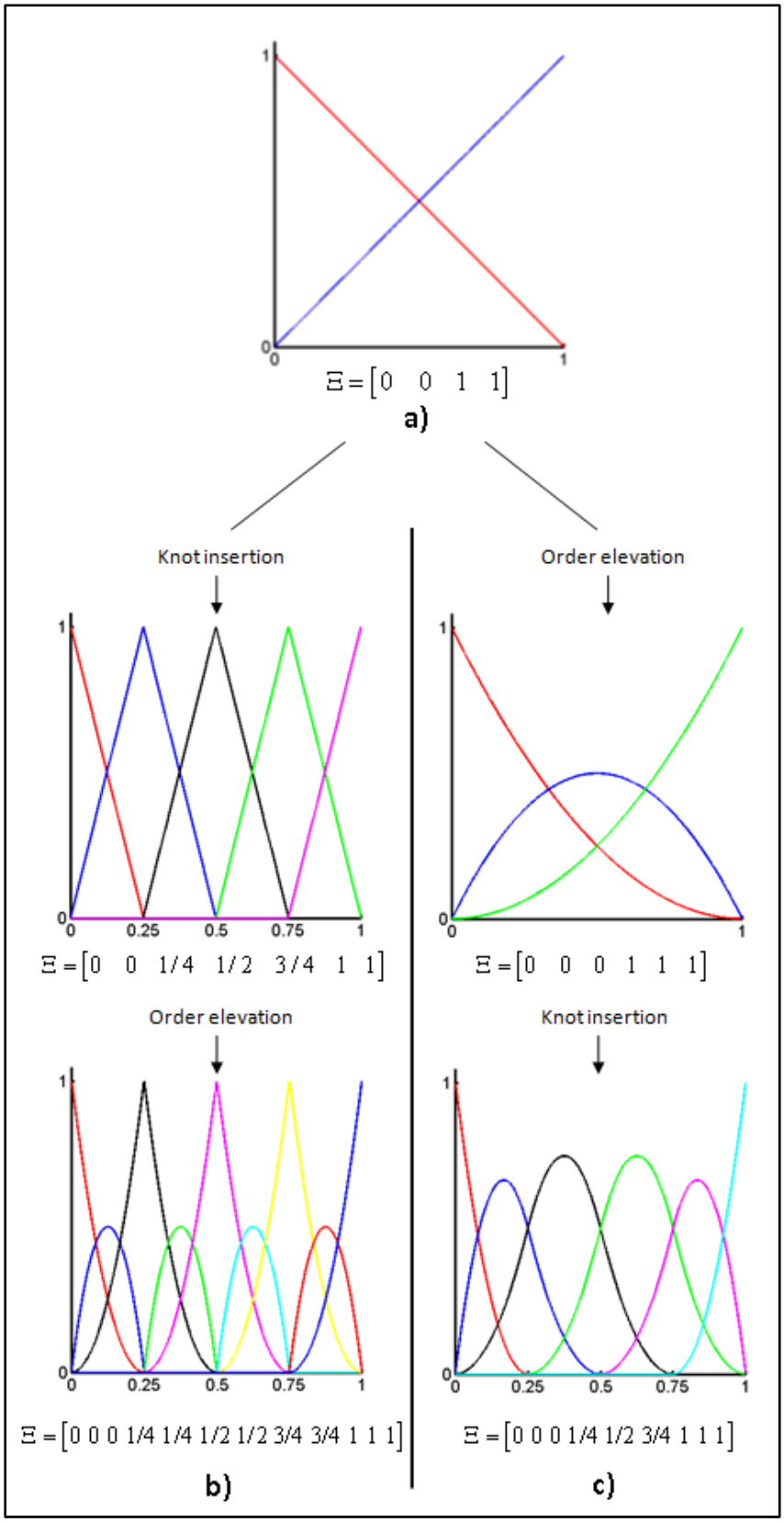

Figure 2.6 : Comparison of k-refinement (right) and the reverse sequence of refinement process.

3. NON-UNIFORM RATIONAL B-SPLINES: NURBS

3.1 Formulation of NURBS

A rational B-spline is similar to a non-rational B-spline with the following exception. A "weight" is added to each of the control points. This weight value usually ranges from 0 to 1 and reflects how much the particular control point affects the curve. So it can be stated that a B-spline is actually a rational B-spline with all weight values equal to 1.

Although non-rational B-splines already have some advantageous features such as having more homogenous basis structure as it is discussed in Chapter 2.2, using rational B-splines adds a new significant ability which is exact representation of geometries that cannot be exactly represented by polynomials. NURBS provide the ability of obtaining desired geometric entities in $\mathbb{R}^d$ by projective transformations of B-spline entities in $\mathbb{R}^{d+1}$. In order to define an exact definition of conic sections such as circles and ellipses, transformations of piecewise quadratic curves are used. This is illustrated in Figure 3.1 [6] in which a circle in $\mathbb{R}^2$ is constructed by the projection of piecewise quadratic curves. Here $\{B_i^w\}$ is the set of control points for a B-spline curve in $\mathbb{R}^{d+1}$ with knot vector Ξ. These are the projective control points that are used to construct the desired NURBS curve in $\mathbb{R}^d$. The control points in $\mathbb{R}^d$ are formed from these points in $\mathbb{R}^{d+1}$ by the following relations:

$$\left(B_i\right)_j = \left(B_i^w\right)_j \Big/ w_i \qquad j = 1,\ldots,d \tag{3.6}$$

$$w_i = \left(B_i^w\right)_{d+1} \tag{3.7}$$

where $(B_i)_j$ is the jth component of the vector B_i and w_i is corresponded the ith weight.Rational basis functions are defined by;

$$R_i^p(\xi) = \frac{N_{i,p}(\xi) w_i}{\sum_{i=1}^{n} N_{i,p}(\xi) w_i} \tag{3.3}$$

Substituting this rational basis functions in B-spline definition gives NURBS geometry as follows;

$$C(\xi) = \sum_{i=1}^{n} R_i^p(\xi) B_i \tag{3.4}$$

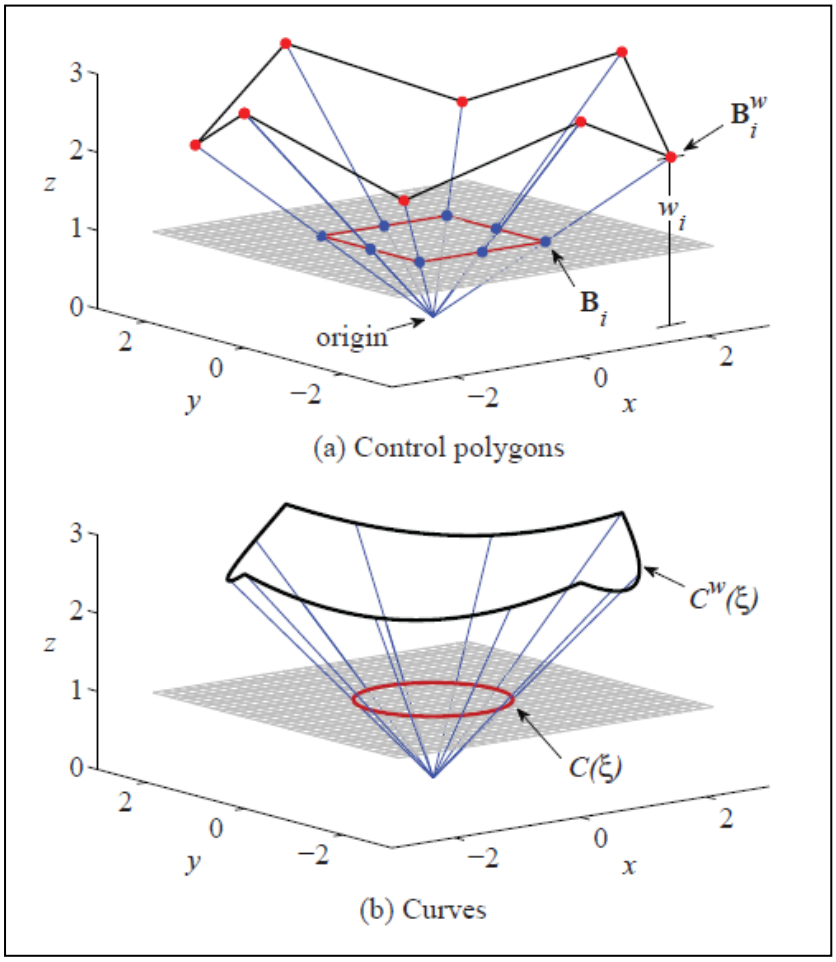

Figure 3.1 : Circle in $\mathbb{R}^2$ constructed by projective transformation of piecewise quadratic B-spline in $\mathbb{R}^3$. [6]

Similarly rational surfaces and solids can be defined analogously in terms of the rational basis functions as follows;

$$R_{i,j}^{p,q}(\xi,\eta) = \frac{N_{i,p}(\xi) M_{j,q}(\eta) w_{i,j}}{\sum_{\hat{i}=1}^{n} \sum_{\hat{j}=1}^{m} N_{\hat{i},p}(\xi) M_{\hat{j},q}(\eta) w_{\hat{i},\hat{j}}} \tag{3.5}$$

$$R_{i,j}^{p,q}(\xi,\eta)=\frac{N_{i,p}(\xi)M_{j,q}(\eta)w_{i,j}}{\sum_{\hat{i}=1}^{n}\sum_{\hat{j}=1}^{m}N_{\hat{i},p}(\xi)M_{\hat{j},q}(\eta)w_{\hat{i},\hat{j}}} \tag{3.6}$$

As an example Figure 3.2 [23] shows a control net and the corresponding NURBS surface description of a torus. (see [23] for details)

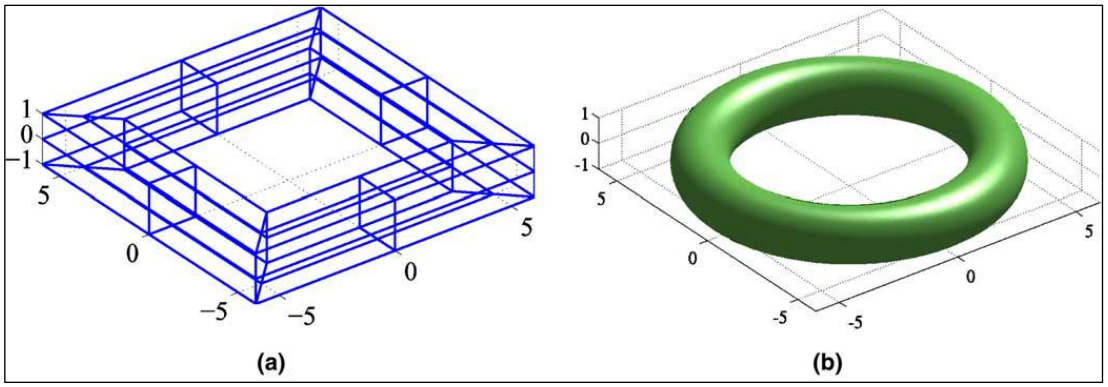

Figure 3.2 : a) Control net for toroidal surface. **b)** Torodial surface [23].

3.2 Properties of NURBS Basis Functions

Important properties of rational B-Spline basis functions which are the results of being a special case of non-rational B-spline basis functions (all weights equals to 0) are;

- ✓ They form a partition of unity, that is,

$$\forall\xi \quad \sum_{i=1}^{n}N_{i,p}(\xi)=1 \tag{3.7}$$

- ✓ Over the entire domain, basis functions always have positive values, that is, $N_{i,p}(\xi)\geq 0$. This makes all the entities of mass matrix positive.

- ✓ The basis functions with p^{th} order have $p-1$ continuous derivatives across the knots which enables some advantages of the use of splines as a basis of analysis.

- ✓ The support of each B-Spline function $N_{i,p}$ compact and contained in the interval $\left[\xi_i,\xi_{i+p+1}\right]$, i.e. the support of B-Spline functions with an order of p is always $p+1$ knot spans. Thus, when compared to classical FEM functions,

higher order B-Spline functions have support over much larger portions of the domain.

They also have following useful features which differ from non-rational B-Splines;

- ✓ They produce the correct results under projective transformations (while non-rational B-splines only produce the correct results under affine transformations).

They can be used to represent lines, conics, and when generalised to patches, can represents planes, quadrics, and tori.

4. ISOGEOMETRIC STRUCTURAL ANALYSIS OF BEAMS

It is obvious that NURBS are quite functional as a CAD tool when flexibility and exact representation is needed. Today most CAD systems (e.g. Rhino, Npower etc.) use spline basis function and often Non-Uniform Rational B-Splines (NURBS) of different polynomial order. In the previous chapter NURBS itself, their features on geometry representation and refinement processes explained in detail. However, properties of NURBS are also very convenient for a wide range of computational engineering applications as they provide unique accuracy and reduce the time consumed for the communication between design and analysis. Briefly, the robustness of the combination of geometric and analytic capabilities is the key feature of the isogeometric analysis.

A NURBS based isogeometric analysis procedure contains following factors and features;

- ✓ Knot vectors are the structures to define a mesh for the solution of NURBS based analysis. In a one dimensional analysis, knot vector represents the mesh itself. For two or three dimensional analyses mesh is created by the products of knot vectors. e.g. in three dimensions a mesh is defined by $\Xi \times H \times Z$.
- ✓ Since knot vales used to define the mesh, knot spans define the elements in a domain.
- ✓ Each basis function used to define a NURBS patch has a support which consists of a small number of elements.
- ✓ As a new approach, NURBS based analysis allows k-refinement process beside classical h-refinement and p-refinement.
- ✓ A set of control points coordinates and control point variables are used as the coefficients of the basis functions to realize the required representations.
- ✓ Control points and blended basis functions are used to define the geometry.

- ✓ Same basis functions are used to define both the geometry and the analysis variables such as displacement, temperature etc. This feature enables isogeometric solution that will be explained in details in Chapter 3.

Local arrays of the isoparametric NURBS patches can be assembled into global arrays likewise as it is done in finite elements. In order to achieve the compatibility of NURBS patches, same NURBS edge and surface representations are used on both sides of patch interfaces.

4.1 Potential Energy Functionals

Although NURBS can be used to solve any kind of computational engineering problem in the area of standard finite element method, the present work is one focused on isogeometric structural analysis of beams. Objective of this chapter is explaining the theory and algorithm of the code to calculate potential energy functional to get the internal and external force vectors and stiffness matrix by using isogeometric concept. Then these vectors and stiffness matrix will be used in a linear solver to calculate the displacements and the stresses along the beam.

It is important to notice, that in a NURBS patch there is a continuous distribution of properties. The geometric representation of NURBS is also capable of defining geometrically non-linear structural responses. In order to use such beneficial properties of isogeometric analysis and to make exact validations with analytic results, some assumptions have been made for the beam model.

Modeling assumptions of the present work are as follows;

- Geometrical non-linearity
- Linear isotropic material properties
- Slender Beam Consideration

An arched beam modeled as a NURBS curve and required variables to calculate its potential energy functional are illustrated in Figure 4.1. According to the figure ξ is the parametric coordinate, dS is the differential arc length and $\underline{r}(\xi_i)$ is the position vector for a parametric location ξ_i on the beam.

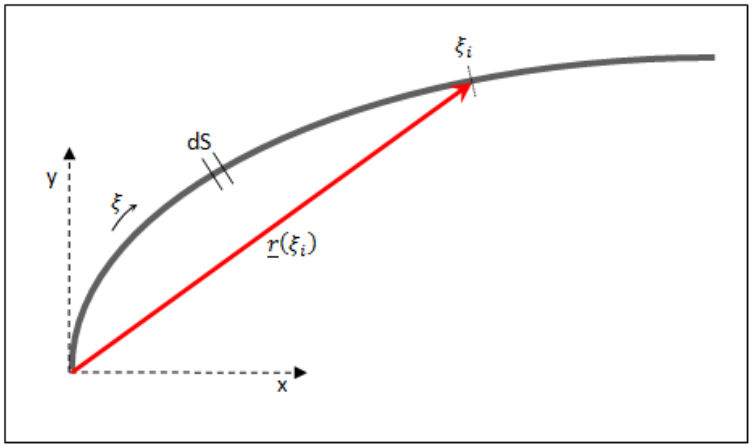

Figure 4.1 : Illustration of an arched beam as a NURBS curve and the required variables to calculate the potential energy functional.

The total potential energy functional of an arbitrary conservative system is the sum of the elastic strain energy stored in the deformed body and the potential energy of applied forces. So it can be written as;

$$\Pi = U + V \tag{4.1}$$

Since a slender beam can be considered as an Euler-Bernoulli beam, strain energy functional and the potential energy of applied external forces can be formulated as follows;

$$U(\tilde{u}) = \frac{1}{2}\int \left[EA\varepsilon^2 + EI\rho^2 \right] dS_0 \tag{4.2}$$

$$V(\tilde{u}) = -\int \left[p_0 \underline{n}^T \tilde{u} + \underline{q}_0{}^T \tilde{u} \right] dS_0 - \underline{f}^T \tilde{u} \tag{4.3}$$

where $\tilde{u}$ denotes the continuous displacement field and the terms p_0, $\underline{n}$, $\underline{q}_0$, and $\underline{f}$ in (eq. 4.3) denotes the scalar value of the pressure load, the normal vector of the NURBS curve, the vector of distributed loads per unit length, and the vector of concentrated loads, respectively.

A function code is developed to calculate the strain energy functional. The algorithm for this code is described as follows:

I) Computation of gauss points and weights for the problem

II) Looping over knot spans

   a) Non-zero knot span check

b) Computation of numerical jacobian

c) Evaluating the integration points

d) Looping over integration points

   i) Computation of relative strain measures (see chapter 4.1.1)

   ii) Computing dS_0 for the integration

   iii) Updating strain energy value

Although strain energy functional is not directly used in main analysis code (as seen in chapter 4.2, first and second derivatives are employed in the main code), it is used for finite difference check to verify its first and second derivatives' calculations and for relative strain measures' calculations which is described in the following sub-chapter.

4.1.1 Calculation of relative strain measures

In order to calculate strain energy function, beside material and cross-section oriented variables (E, I and A) there are two more integrant unknowns which need to be calculated. They are ε and ρ which referred to as relative strain measures. ε is the rate of change in differential arc length and ρ is the rate of change in curvature relative to undeformed configurations. Figure 4.2 illustrates the stretch and curvature change in an elastic rod. Unlike in Figure 4.1, here in Figure 4.2, R denotes not the position vector but the radius of curvature.

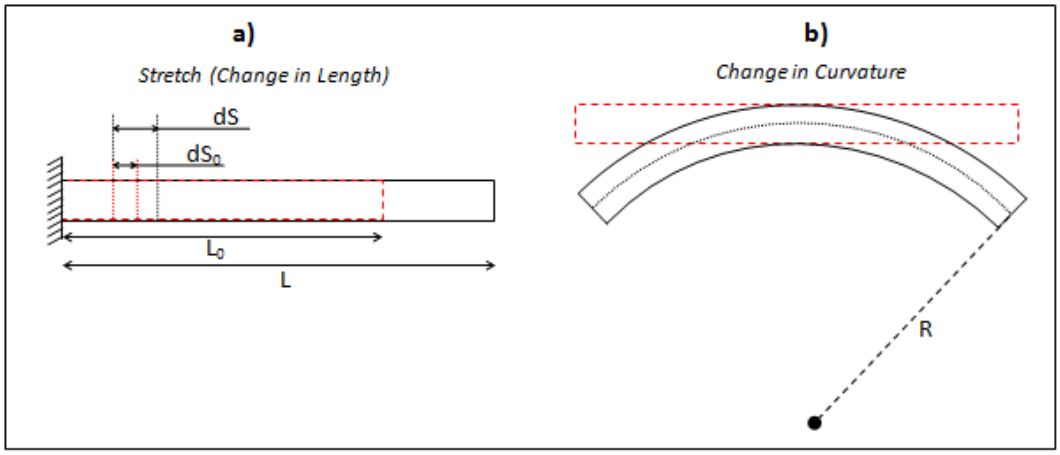

Figure 4.2 : Stretch and change in curvature in an elastic rod.

ε and ρ can be obtained by[24];

$$\varepsilon = \frac{dS - dS_0}{dS_0} \tag{4.4}$$

$$\rho = \left(\kappa - \kappa_0\right)\frac{dS}{dS_0} \tag{4.5}$$

where;

$$dS = \left\| \frac{\partial \underline{r}}{\partial \xi} \right\| \qquad dS_0 = \left\| \frac{\partial \underline{r}_0}{\partial \xi} \right\| \tag{4.6}$$

and

$$\kappa = \frac{\underline{r}' \times \underline{r}''}{\left\| \underline{r}' \right\|^3} \qquad \kappa_0 = \frac{\underline{r}_0' \times \underline{r}_0''}{\left\| \underline{r}_0' \right\|^3} \tag{4.7}$$

All derivatives of the position vectors are evaluated by successive differentiations with respect to ξ.

A subroutine is developed to calculate the relative strain measures in the strain energy function. This subroutine employs curve information (which is stored in a MATLAB structure contains the knot vector, number of control points and their co-ordinates etc.), discrete displacement matrix of control points and concerned parametric location on the curve as its inputs and brings the relative strain measures as its outputs. The algorithm for relative strain measures for a parametric location can be described as:

I) Computation of the first and second derivative of initial position vector

II) Computation of the first and second derivative of deformed position vector.

   a) Computation of the block diagonal matrices of basis function derivatives

      i) Computation the first and second derivatives of all non-zero rational basis functions with respect to ξ at the concerned parametric location.

      ii) Construction of block diagonal matrices for first and second derivatives of the basis functions

   b) Creating the d.o.f. vector

      i) Detection of the knot span which contains concerned parametric location

ii) Reshaping the selected (according to the detected knot span) part of discrete displacement matrix of control points to construct a $2(p+1)\times 1$ d.o.f. vector.

c) Multiplication of d.o.f. vector and block-diagonal matrices for the computation of first and second derivative of the displacement vector

d) Summation of the derivatives of initial position and displacement vectors to get the deformed position vector derivatives.

III) Computation of the change in length (ε) according to **(4.4)**

IV) Computation of the change in curvature (ρ) according to **(4.5)**

4.2 Stiffness Matrix and External Force Vector Calculation for 1D Application

In order to set a linear solution for the beam analysis, right and the left side terms should satisfy the equilibrium that is the potential energy functional has to be stationary for the diverse allowable displacement configurations. In addition, under the assumption of static elastic problem, the total potential energy functional is not only stationary but also preserve a global minimum [25]. Therefore, the solution can be simplified by an approach of the minimization of the total potential energy for relevant constraints.

As it is explained in the previous chapters, isoparametric concept employs the same rational basis functions both to define the geometry and to approximate the displacement field, hence

$$\underline{\tilde{u}} = \underline{\underline{R}}.\underline{u} \qquad \textbf{(4.8)}$$

where $\underline{u}$ denotes displacement of the control point coordinates and $\underline{\underline{R}}$ is the interpolation matrix which contains non-zero basis function values at concerned parametric location.

Thus (eq. 4.8) can be restated as follows;

$$\underline{\tilde{u}}(\xi)=\begin{bmatrix} R_{0,p}(\xi) & 0 & R_{1,p}(\xi) & 0 & \cdots\cdots R_{n,p}(\xi) & 0 \\ 0 & R_{0,p}(\xi) & 0 & R_{1,p}(\xi)\cdots\cdots & 0 & R_{n,p}(\xi) \end{bmatrix}\begin{Bmatrix} \Delta x_0 \\ \Delta y_0 \\ \Delta x_1 \\ \Delta y_1 \\ \vdots \\ \Delta x_n \\ \Delta y_n \end{Bmatrix} \tag{4.9}$$

Relying on linearly isotropic constitutive law and geometrically non-linear structural response, internal force vector and stiffness matrix can be generated by successive derivation of the strain energy functional with respect to the vector of control point displacements (d.o.f. vector) as

$$f_i\left(\underline{u}\right)=\frac{\partial U}{\partial \underline{u}}=\int \underline{D}^T \underline{\underline{C}}\underline{G}\, dS_0 \tag{4.10}$$

$$K\left(\underline{u}\right)=\frac{\partial^2 U}{\partial \underline{u}}=\int \underline{D}^T \underline{\underline{C}}\underline{D}\, dS_0+\int\left[EA\varepsilon\frac{\partial^2\varepsilon}{\partial \underline{u}^2}+EI\,\rho\frac{\partial^2\rho}{\partial \underline{u}^2}\right]dS_0 \tag{4.11}$$

where;

$$C=\begin{bmatrix} EA & 0 \\ 0 & EI \end{bmatrix} \tag{4.12}$$

$$D=\begin{Bmatrix} \dfrac{\partial\varepsilon}{\partial \underline{u}} \\ \dfrac{\partial\rho}{\partial \underline{u}} \end{Bmatrix} \tag{4.13}$$

$$G=\begin{Bmatrix} \varepsilon \\ \rho \end{Bmatrix} \tag{4.14}$$

A subroutine is developed to calculate the first and second derivatives of ε and ρ to be employed in stiffness matrix and internal force vector codes. Derivatives of ε and ρ are evaluated by hand calculation then the eventual expressions are used in the subroutine as follows;

$$\frac{\partial\varepsilon}{\partial \underline{u}}=\frac{\partial(dS)}{\partial \underline{u}}\cdot\frac{1}{2\cdot dS_0} \tag{4.15}$$

$$\frac{\partial\rho}{\partial \underline{u}}=\frac{\partial(\kappa-\kappa_0)}{\partial \underline{u}}\cdot\frac{dS}{dS_0}+\frac{\kappa-\kappa_0}{dS_0}\cdot\frac{\partial(dS)}{\partial \underline{u}} \tag{4.16}$$

(Eq.4.15) and (eq.4.16) are derived once more with respect to d.o.f vector $\underline{u}$ and second derivatives are defined as follows;

$$\frac{\partial^2 \varepsilon}{\partial \underline{u}^2} = \frac{\partial^2 (dS)}{\partial \underline{u}^2} \cdot \frac{1}{2 \cdot dS_0} \tag{4.17}$$

$$\frac{\partial^2 \rho}{\partial \underline{u}^2} = \left[\frac{\partial^2 (\kappa - \kappa_0)}{\partial \underline{u}^2} \cdot dS + \frac{\partial (\kappa - \kappa_0)}{\partial \underline{u}} \cdot \frac{\partial (dS)}{\partial \underline{u}} + \frac{\partial^2 (dS)}{\partial \underline{u}^2} \cdot (\kappa - \kappa_0) + \frac{\partial (dS)}{\partial \underline{u}} \cdot \frac{\partial (\kappa - \kappa_0)}{\partial \underline{u}} \right] \Big/ dS_0 \tag{4.18}$$

A finite difference method code is developed and used to validate the derived expressions in eq. 4.17 and eq. 4.18. Exact match of the results have been achieved between finite difference results and hand calculated derivatives for both first and second derivative of ε and ρ. A separate finite difference method code is also developed to validate entire derivation of strain energy functional. Results of hand calculated internal force vector (first derivative of strain energy functional) and stiffness matrix (second derivative of strain energy functional) expressions are perfectly matched with each other. Thus these expressions were ready to be implemented in the main analysis code to construct the global internal force vector and the stiffness matrix.

Similarly, computing the first derivative of potential energy of applied forces results in the external force vector, i.e.

$$f_e(\underline{u}) = \frac{\partial V}{\partial \underline{u}} = -\int \left[p_0 \underline{R}^T \underline{n} + \underline{R}^T \underline{q}_0 \right] dS_0 - \underline{R}^T f \tag{4.19}$$

This expression also attached by a subroutine to the main code. In this subroutine, $\underline{R}^T$ is constructed as a block diagonal matrix consists of basis functions. The normal vector $\underline{n}$ is computed as a unit vector at the concerned parametric location.

The internal and external force vectors and the stiffness matrix are computed locally in each knot span by using Gaussian quadrature. These local vectors and matrixes are assembled to construct the global internal and external force vectors and the global stiffness matrix. This process is quite analogous to standard FEA assembly procedure. However, it is remarkable that highest order basis functions, i.e. higher order local support of the interpolation functions yields much more overlapped

entities of local arrays belong to adjacent knot spans. Eventually global arrays with a characteristic size of $2(n+1)$ are constructed by the local arrays with a characteristic size of $2(p+1)$

4.3 Stress Recovery for 1D Applications

The non-linear equilibrium equation for the discrete model can be formulated as

$$f_i = f_e \tag{4.20}$$

Linearized form of equilibrium equation at the undeformed configuration yields

$$K\Big|_{\underline{u}=0} \cdot \underline{u} = f_e \tag{4.21}$$

In the main analysis code global arrays for the stiffness matrix and internal and external force vector are constructed. Then a linear static solver employed under defined boundary conditions to evaluate the displacements. Evaluation of the displacements in control points allow to plot a new NURBS curve which is actual deformed geometry. Since $\underline{u}$ is known at this level in the analysis, it is possible to calculate the total stress at a distance to the neutral axis. This stress contains bending and membrane stress components defined as

$$\sigma_{total} = \sigma_m + \sigma_b \tag{4.22}$$

σ_m and σ_b denote bending stress and membrane stress components respectively which are defined as

$$\sigma_m = \frac{\partial \varepsilon}{\partial \underline{u}}\Bigg|_{\underline{u}=0} \cdot \underline{u} \cdot E \tag{4.23}$$

$$\sigma_b = \frac{\partial \rho}{\partial \underline{u}}\Bigg|_{\underline{u}=0} \cdot \underline{u} \cdot E \cdot y \tag{4.24}$$

where y is the distance from the neutral axis.

4.4 Stiffness Matrix and External Force Vector Calculation for 2D Application

In order to calculate the stiffness matrix for the two-dimentional applications in this study, the equation below is used;

$$\underline{\underline{K}} = \int \underline{\underline{D}}^T \underline{\underline{C}} \underline{\underline{D}} \, dA = \iint \underline{\underline{D}}^T \underline{\underline{C}} \underline{\underline{D}} \, dxdy \tag{4.25}$$

where C is the stiffess tensor for the relevant coordinate in the surface where continous stiffness matrix is being integrated. Since stiffness matrix only depends on the material properties, it can be reduced according to the boundary conditions and the loading case. In isotropic two dimensional beam analysis applications C matrix has the same values during the integration as the material properties does not change along the beam thickness or longtitude. However, for the composite beam analysis case this matrix is particularly constructed for the elements depending on the layer that they lay within. D matrix, which contains strain values, is constructed as follows;

$$D = \begin{Bmatrix} \dfrac{\partial \underline{\underline{\tilde{u}}}}{\partial x} & 0 \\ 0 & \dfrac{\partial \underline{\underline{\tilde{v}}}}{\partial y} \\ \dfrac{\partial \underline{\underline{\tilde{u}}}}{\partial y} & \dfrac{\partial \underline{\underline{\tilde{v}}}}{\partial x} \end{Bmatrix} \tag{4.26}$$

Here $\underline{\tilde{u}}$ and $\underline{\tilde{v}}$ are the continous displacements along the longitude and the thickness directions. Using **(4.8)** in **(4.26)** yields;

$$D = \begin{Bmatrix} \dfrac{\partial \underline{\underline{R}} \underline{u}}{\partial x} & 0 \\ 0 & \dfrac{\partial \underline{\underline{R}} \underline{v}}{\partial y} \\ \dfrac{\partial \underline{\underline{R}} \underline{u}}{\partial y} & \dfrac{\partial \underline{\underline{R}} \underline{v}}{\partial x} \end{Bmatrix} \tag{4.27}$$

Here $\underline{u}$ and $\underline{v}$ are discrete displacements. Since the derivations in the elements of D are not convenient to evaluate, chain rule is applied.

$$\frac{\partial \underline{\underline{R}} \underline{u}}{\partial x} = \frac{\partial \underline{\underline{R}} \underline{u}}{\partial \xi} \frac{\partial \xi}{\partial x} \tag{4.28}$$

$$\frac{\partial \underline{\underline{R}} \underline{v}}{\partial y} = \frac{\partial \underline{\underline{R}} \underline{v}}{\partial \eta} \frac{\partial \eta}{\partial y} \tag{4.29}$$

$$\frac{\partial \underline{\underline{R}} \underline{u}}{\partial y} = \frac{\partial \underline{\underline{R}} \underline{u}}{\partial \eta} \frac{\partial \eta}{\partial y} \tag{4.30}$$

$$\frac{\partial \underline{\underline{R}} \underline{v}}{\partial x} = \frac{\partial \underline{\underline{R}} \underline{v}}{\partial \xi} \frac{\partial \xi}{\partial x} \tag{4.31}$$

Hence $\partial \underline{R}/\partial x$ and $\partial \underline{R}/\partial x$ are the only terms to construct the B matrix. In order to create these terms in the analysis code, a jacobian matrix, which is used to make the transformation from the physical domain to parametric domain, is created as follows;

$$J_1 = \begin{Bmatrix} \dfrac{\partial x}{\partial \xi} & \dfrac{\partial y}{\partial \xi} \\ \dfrac{\partial x}{\partial \eta} & \dfrac{\partial y}{\partial \eta} \end{Bmatrix} \tag{4.32}$$

Then required transformation is done as shown below;

$$\begin{Bmatrix} \dfrac{\delta \underline{R}}{\delta x} \\ \dfrac{\delta \underline{R}}{\delta y} \end{Bmatrix} = \underline{\underline{J}}_1^{-1} . \begin{Bmatrix} \dfrac{\delta \underline{R}}{\delta \xi} \\ \dfrac{\delta \underline{R}}{\delta \eta} \end{Bmatrix} \tag{4.33}$$

Thus the B matrix of the analysis is created as shown in **(4.34)**

$$\underline{\underline{B}} = \begin{bmatrix} \partial \underline{R}_1/\partial x & 0 & \partial \underline{R}_2/\partial x & 0 & \cdots\cdots & \partial \underline{R}_n/\partial x & 0 \\ 0 & \partial \underline{R}_1/\partial y & 0 & \partial \underline{R}_2/\partial y & \cdots\cdots & 0 & \partial \underline{R}_n/\partial y \\ \partial \underline{R}_1/\partial y & \partial \underline{R}_1/\partial x & \partial \underline{R}_2/\partial y & \partial \underline{R}_2/\partial x & \cdots\cdots & \partial \underline{R}_n/\partial y & \partial \underline{R}_n/\partial x \end{bmatrix} \tag{4.34}$$

In the integration of stiffness matrix through the gauss points in an element, another jacobian matrix is needed to realize the transformation from parametric domain to element coordinate system. This jacobian is stated as;

$$J_2 = \begin{Bmatrix} \dfrac{\partial \xi}{\partial \hat{\xi}} & \dfrac{\partial \eta}{\partial \hat{\xi}} \\ \dfrac{\partial \xi}{\partial \hat{\eta}} & \dfrac{\partial \eta}{\partial \hat{\eta}} \end{Bmatrix} = \begin{Bmatrix} \dfrac{\xi_{i+1} - \xi_i}{2} & 0 \\ 0 & \dfrac{\eta_{i+1} - \eta_i}{2} \end{Bmatrix} \tag{4.35}$$

Since the jacobian for the transformation from physical domain to parametric domain and the jacobian for the transformation from parametric domain to element coordinate system are stated, local stiffness integration for an element can be stated as

$$\underline{\underline{K}}_e = \int \underline{\underline{B}}^T \underline{\underline{C}} \underline{\underline{B}} \ \det(\underline{\underline{J}}) \approx \sum_{i=1}^{m} w_i \underline{\underline{B}}^T \underline{\underline{C}} \underline{\underline{B}} \det(\underline{\underline{J}}) \tag{4.36}$$

where;

$$\underline{\underline{J}} = \underline{\underline{J}}_1 \cdot \underline{\underline{J}}_2 \tag{4.37}$$

Local external force vectors on the edges which has a load applied is calculated as follows;

$$Fe_e = \int \underline{\underline{R}}_{loc} \underline{q}_{loc} \; dS \; J_{1D} \approx \sum_{i=1}^{m} w_i' \underline{\underline{R}}_{loc} \underline{q}_{loc} \; dS \; J_{1D} \tag{4.38}$$

where;

$$J_{1D} = \frac{\xi_{i+1} - \xi_i}{2} \quad \text{or} \quad J_{1D} = \frac{\eta_{i+1} - \eta_i}{2} \tag{4.39}$$

and

$$dS_0 = \left\| \frac{\partial \underline{r}_0}{\partial \xi} \right\| \quad \text{or} \quad dS_0 = \left\| \frac{\partial \underline{r}_0}{\partial \eta} \right\| \tag{4.40}$$

and $\underline{\underline{R}}_{loc}$ is the block-diagoal matrix containing the shape functions. Calculation of J_{1D} and dS_0 depends on the edge where local external force vector is integrated. If the load is applied on an edge along the length, ξ is used because the knot vectors used on the edges along the length are defined by the parameter ξ while the knot vectors used on the edges along thickness defined by the parameter η.

4.5 Stress Recovery for 2D Applications

Diagonal B matrix in 4.34, which contains bivariate derivatives of shape functions, is used to calculate strain distribution along the surface. This diagonal matrix is multiplied by discrete displacement vector of relevant control points. Hence the strain distribution is obtained as follows,

$$\underline{\varepsilon} = \underline{\underline{B}} \cdot \underline{u}_{2D} \tag{4.41}$$

In open form;

$$\underline{\varepsilon} = \begin{bmatrix} \partial \underline{R}_1/\partial x & 0 & \partial \underline{R}_2/\partial x & 0 & \cdots\cdots & \partial \underline{R}_n/\partial x & 0 \\ 0 & \partial \underline{R}_1/\partial y & 0 & \partial \underline{R}_2/\partial y & \cdots\cdots & 0 & \partial \underline{R}_n/\partial y \\ \partial \underline{R}_1/\partial y & \partial \underline{R}_1/\partial x & \partial \underline{R}_2/\partial y & \partial \underline{R}_2/\partial x & \cdots\cdots & \partial \underline{R}_n/\partial y & \partial \underline{R}_n/\partial x \end{bmatrix} \cdot \begin{Bmatrix} \Delta x_0 \\ \Delta y_0 \\ \Delta x_1 \\ \Delta y_1 \\ \vdots \\ \Delta x_n \\ \Delta y_n \end{Bmatrix} \quad \textbf{(4.42)}$$

Then the stress values are evaluated from the strain values by multiplying with relevant local stiffness tensor. In isotropic two dimensional beam analysis applications C matrix has the same values during the integration as the material properties does not change along the beam thickness or longtitude. However, for the composite beam analysis case this matrix is particularly constructed for the elements depending on the material properties of the layer that they lay within.

Thus stress equation used in 2D codes can be described as;

$$\underline{\sigma} = \underline{\varepsilon} \cdot E_{layer} \quad \textbf{(4.43)}$$

5. 1D APPLICATIONS AND RESULTS

In this section, the applications of isogeometric analysis on a straight slender beam with two different boundary conditions are firstly presented. The results computed with developed code are compared with analytic results. Then a half circle slender arch application and finally an application on a free formed slender arch also performed. For the half circle and free formed slender arch applications, stress at extreme fibers and displacement results compared with a commercial structural analysis package (ABAQUS).

5.1 Application 1

5.1.1 Application 1:Problem description

Structural analysis of a straight beam with a circular cross section of radius r is considered. The beam is modeled as a cantilevered beam. Rotationless nature of the clamped root of the beam ensured by setting the vertical co-ordinates of the first two control points equal to zero. In addition, the horizontal co-ordinates of the control points set as zero regarding small angle deflection assumption. A distributed load is applied on the beam on –y direction. Geometrical and material constants are as seen in the computational model given in Figure 5.1.

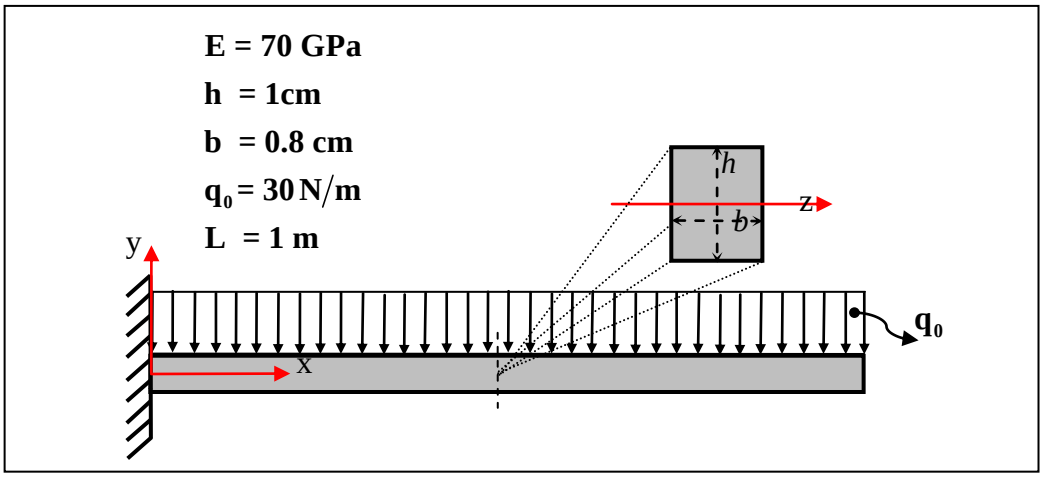

Figure 5.1 : Computational model of the rectangular cross sectional cantilevered beam under uniform distributed load.

5.1.2 Application 1:Results

Maximum deflection at the free end of the beam is observed for different characteristic mesh sizes. Although the ratio between numerical and analytical value is enough high for even five elements, according to Figure 5.2 a characteristic mesh size of 0,025 which is achieved by 40 elements can be considered as the convergence limit for the analysis.

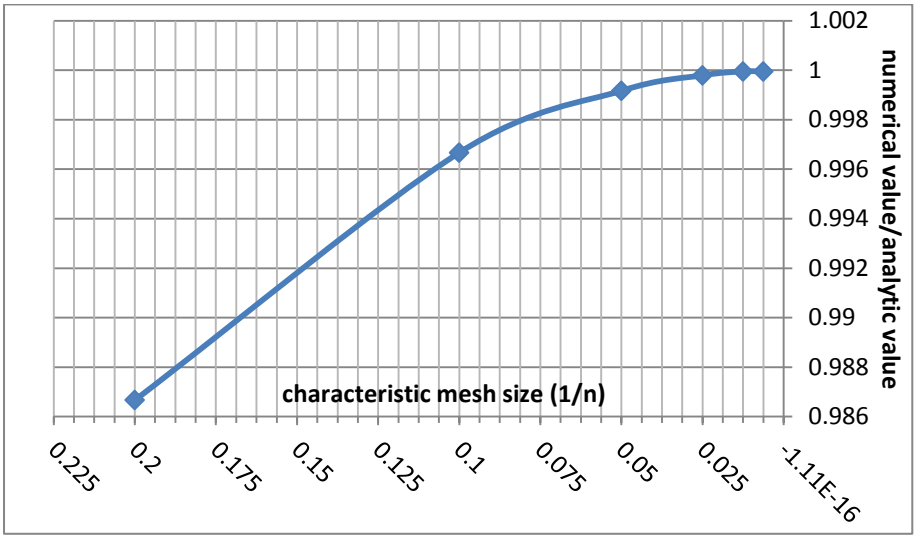

Figure 5.2 : Convergance curve of max. displacement.

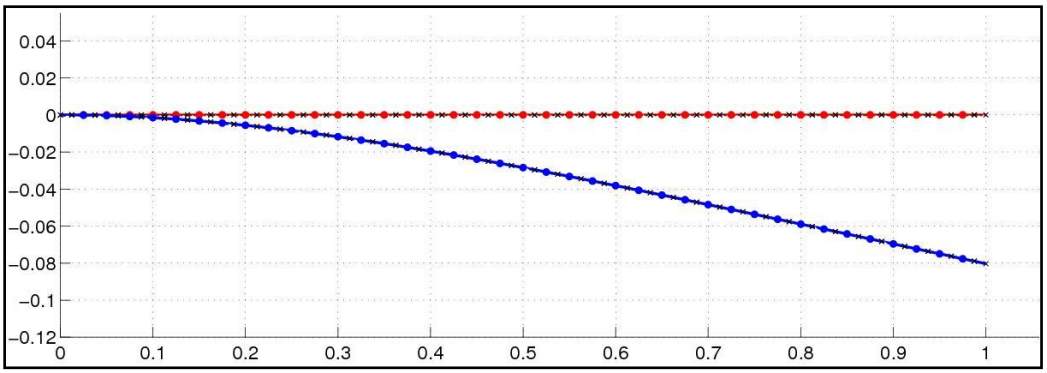

Figure 5.3 : Deformed and initial beam geometry produced by NURBS structure.

Deflection results of the isogeometric analysis performed with quadratic basis functions and 40 elements returns exact match with the analytic results as seen in Figure 5.4

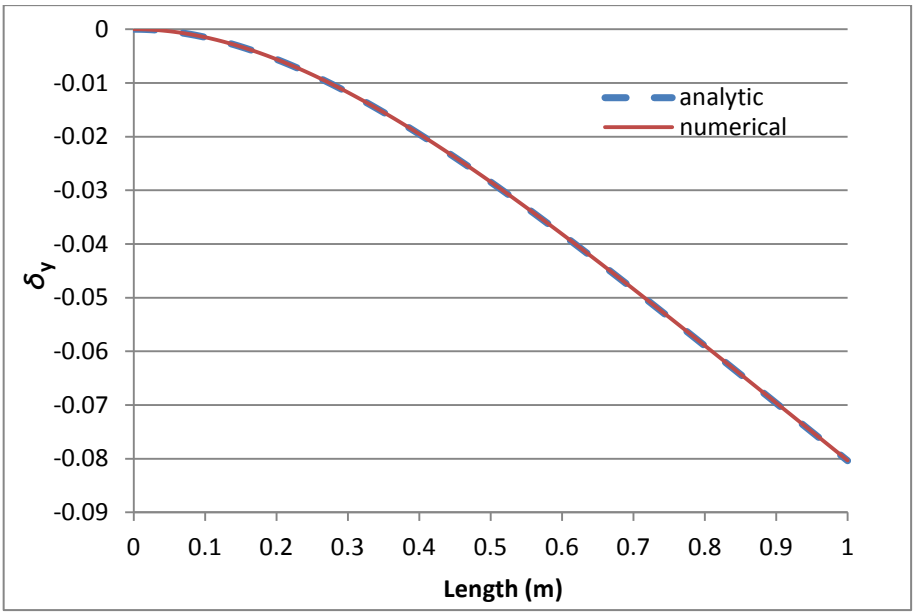

Figure 5.4 : Analytic and isogeometric numerical analysis results for displacement.

Analysis repeated with a single element and third order basis functions yields very close results with the analytic solution results. However, boundary condition definition in the analysis causes a small difference. It is a fact that there is only three control points used to define the geometry. For that reason, second control point, which is used to ensure cantilevered boundary condition, is not close enough to the root.

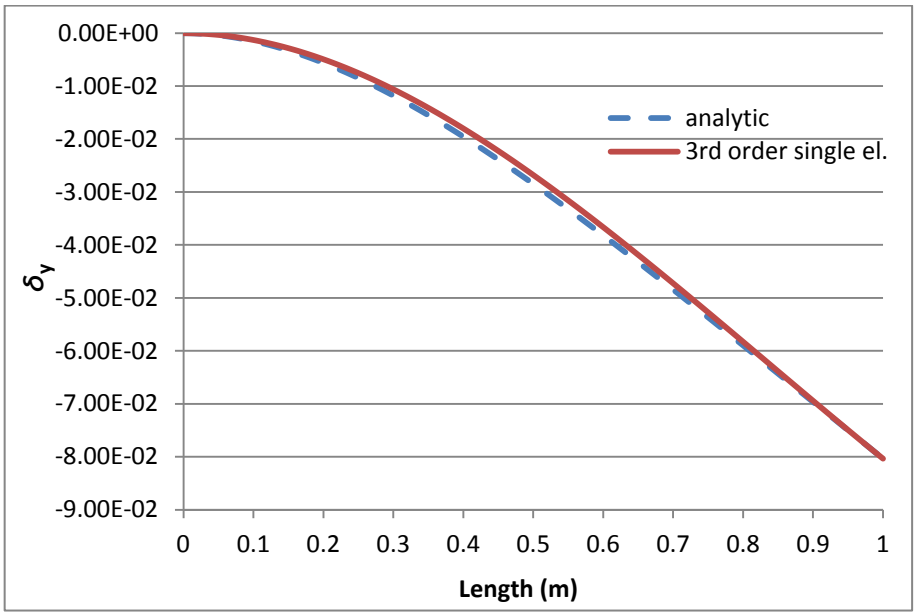

Figure 5.5 : Isogeometric numerical results for single third order element.

Stress values in the beam are computed as described in chapter 3.3. Figure 5.6 shows the analysis results for total stress at the extreme fibers.

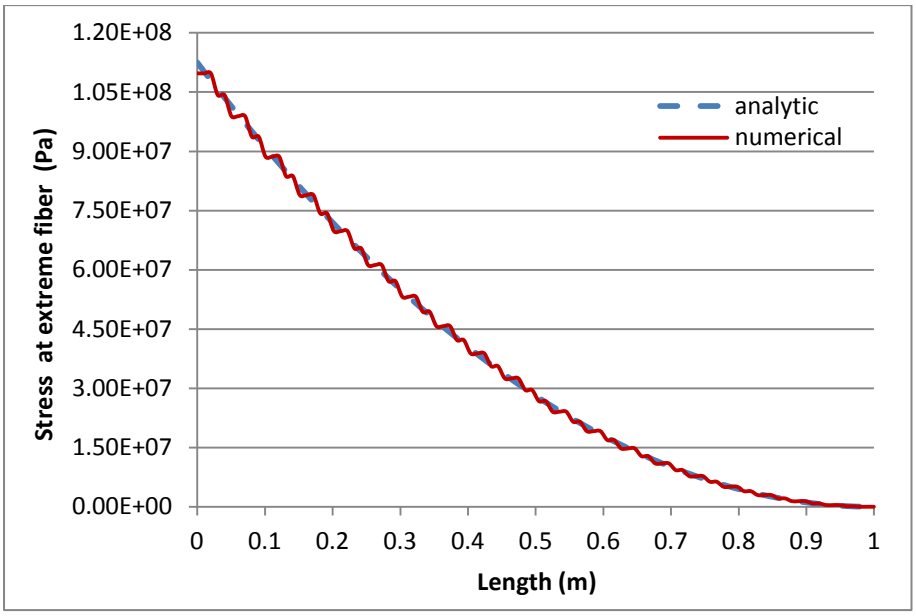

Figure 5.6 : Stress results at extreme fiber with quadratic basis functions (n_{el}=40).

Oscillation around the analytical results in Figure 5.6 can be easily smoothed out by order elevation of the analysis basis functions. Order elevation allows reducing element number in the analysis as well. Results achieved with higher order basis functions by using less element number yields smooth and precise results as seen in Figure 5.7.

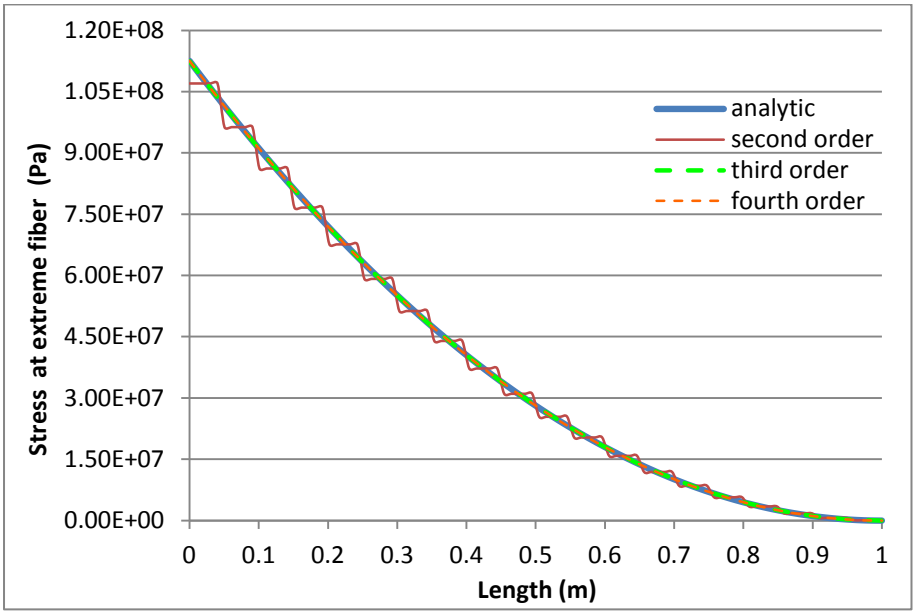

Figure 5.7 : Stress results at extreme fiber for several basis orders (n_{el}=20).

5.2 Application 2

5.2.1 Application 2:Problem description

Structural analysis of a straight beam with a rectangular cross section is considered. The beam is simply supported at one end and attached with a sliding support at the other end. At the left end, boundary condition fixed the horizontal and vertical entities of the control point to zero which does not allow displacement in any direction but rotation. On the right end, the support condition is ensured by setting the vertical coordinate zero. In addition, relying on small deflection assumption the horizontal co-ordinate is also set to zero. A distributed load is applied along the beam length on –y direction. Geometrical and material constants are as seen in the computational model given in Figure 5.8.

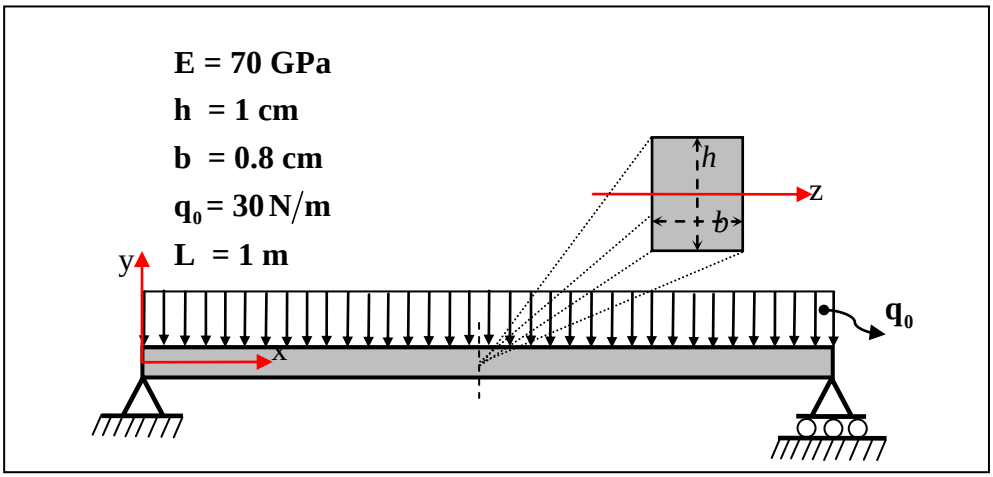

Figure 5.8 : Computational model of simply supported beam under uniform distributed load.

5.2.2 Application 2:Results

Maximum deflection at the mid-length of the beam is observed for different characteristic mesh sizes. Similarly, the ratio between numerical and analytical value is also quite high even for high characteristic mesh sizes. Figure 5.9 shows convergence curve for the maximum displacement. For this application, characteristic mesh size of 0.025 is also convenient for the analyses.

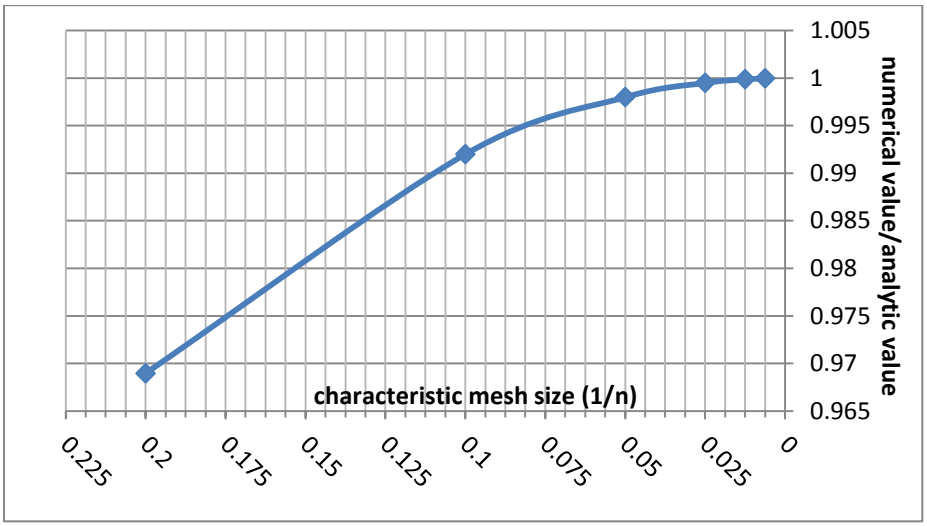

Figure 5.9 : Convergence curve of max. displacement.

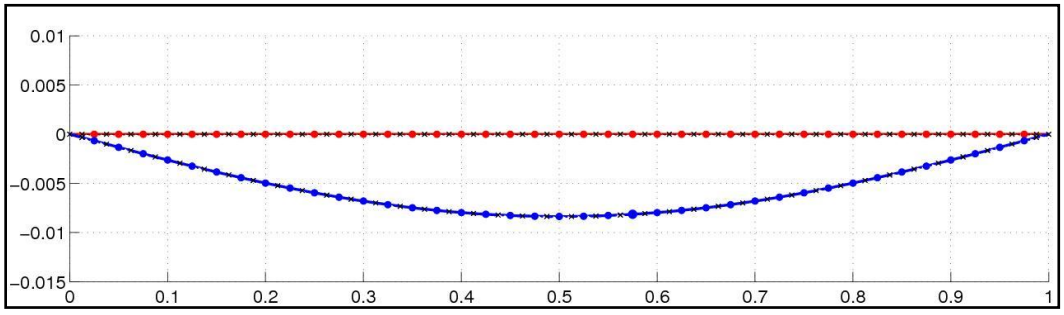

Figure 5.10 : Deformed and initial beam geometry produced by NURBS structure.

Deflection results of the isogeometric analysis performed with quadratic basis functions and 40 elements and singe third order element isogeometric analysis return exact matches with the analytic results as seen in Figure 5.11 and Figure 5.12.

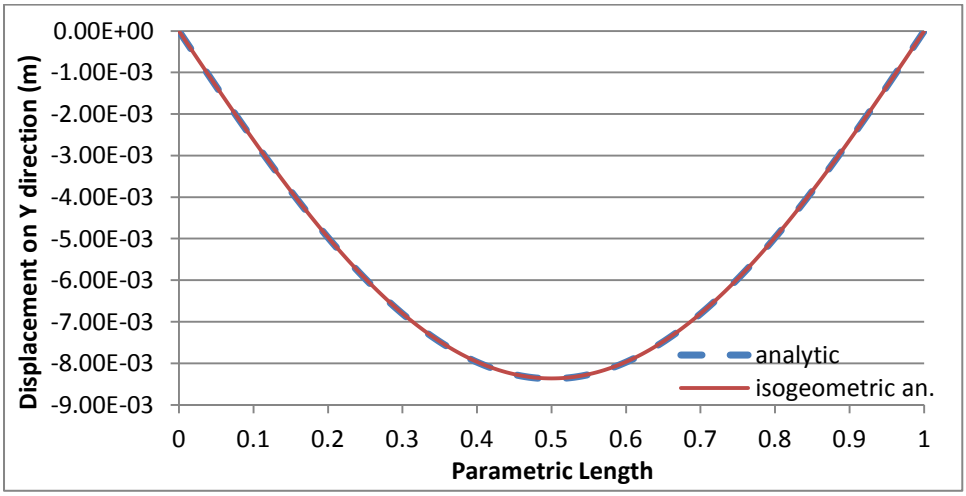

Figure 5.11 : Analytic and isogeometric numerical analysis results for displacement.

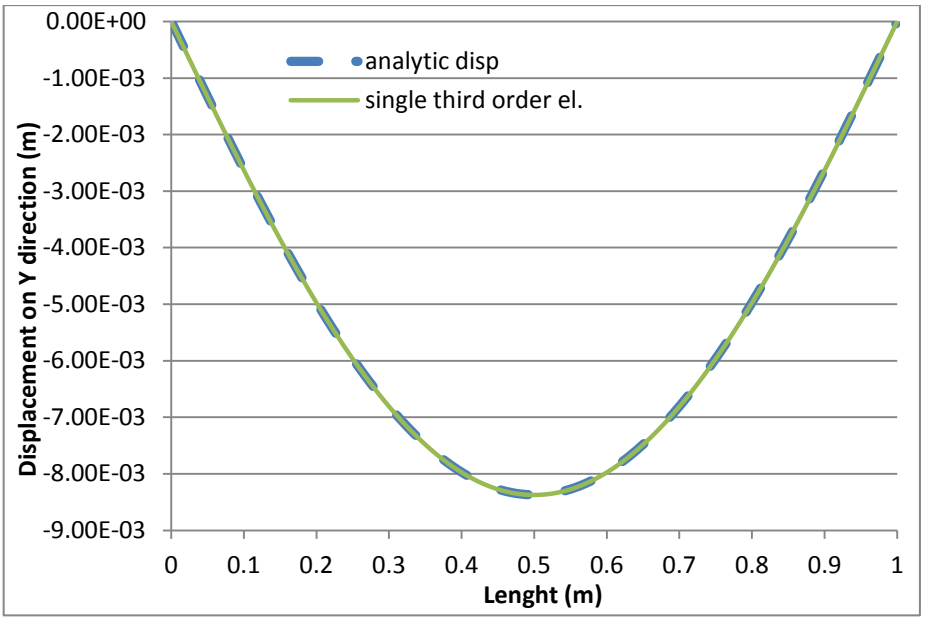

Figure 5.12 : Single third order element result for displacement.

Stress values in the beam are computed as described in chapter 3.3. Figure 5.13 shows the analysis results for total stress at the extreme fibers.

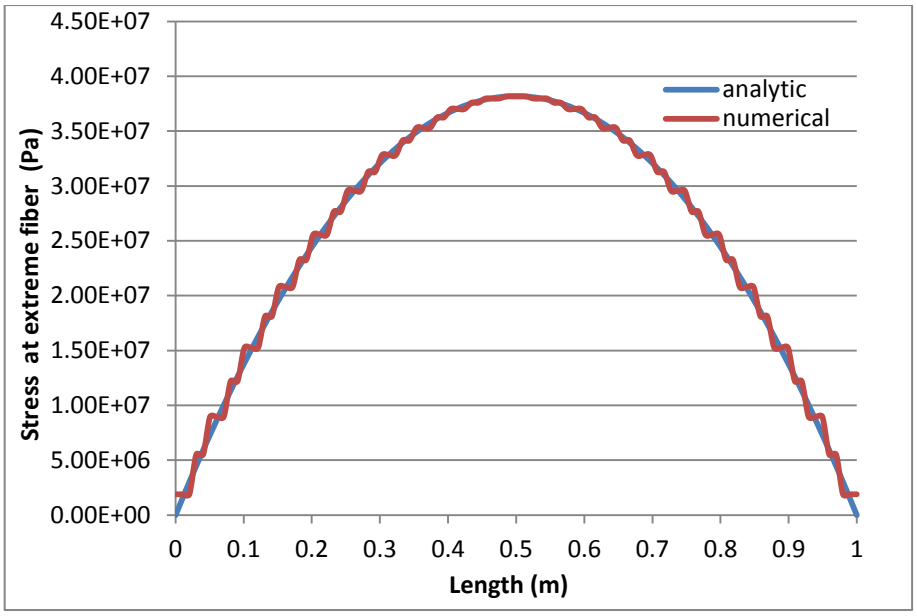

Figure 5.13 : Stress results at extreme fiber with quadratic basis functions (n_{el}=40).

Oscillation in the numerical results is smoothed out by order elevation of the analysis basis functions. Results achieved with higher order basis functions by using less element number yields smooth and precise results like in the previous application. Figure 5.14 shows the stress results at extreme fibers for several basis function orders by using 20 elements.

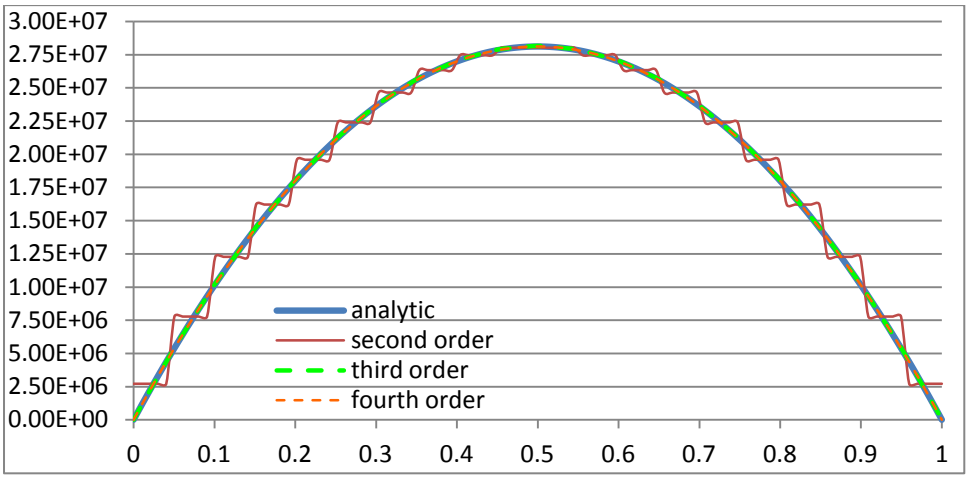

Figure 5.14 : Stress results at extreme fibers for several basis orders (n_{el}=20).

5.3 Application 3

5.3.1 Application 3:Problem description

Isogeometric structural analysis of an arched beam with a circular cross section of radius r is considered. Boundary condition at both ends does not allow displacements in any direction but rotation. This boundary condition ensured by setting both horizontal and vertical coordinates of the control points to zero at the ends of the beam. A pressure load is applied along the beam length. Since this is a 2D example, pressure load has been applied as a line load with the unit of N/m. The code developed for this problem allows application of concentrated loads as well. Geometrical and material constants are as seen in the computational model of the arched beam shown in Figure 5.15.

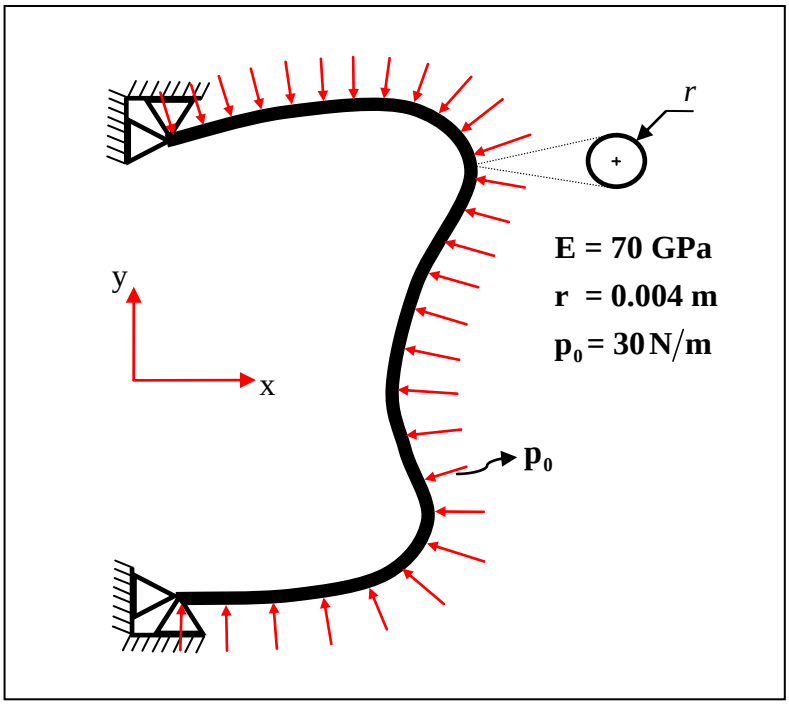

Figure 5.15 : Computational model of the circular cross sectional arched beam under preassure load.

5.3.2 Application 3:Results

Since it is not so convenient to get an analytic solution in this problem, isogeometric analysis results has been compared with a structural analysis package ABAQUS. In the ABAQUS analysis, using 200 elements is found fine enough to maintain precise results and to get a realistic geometric representation. The isogeometric analysis code results in x and y deflections and stress values at extreme fibers successfully matched with ABAQUS results in this application as well.

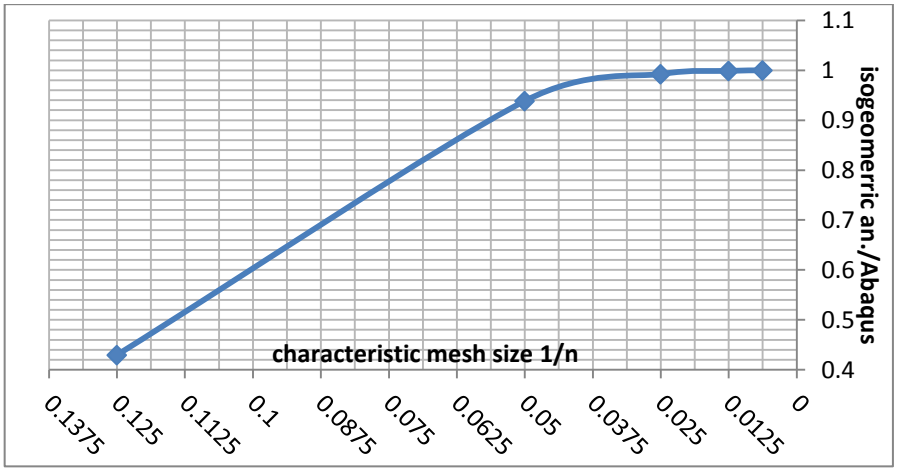

Figure 5.16 : Convergance curve for the maximum displacement.

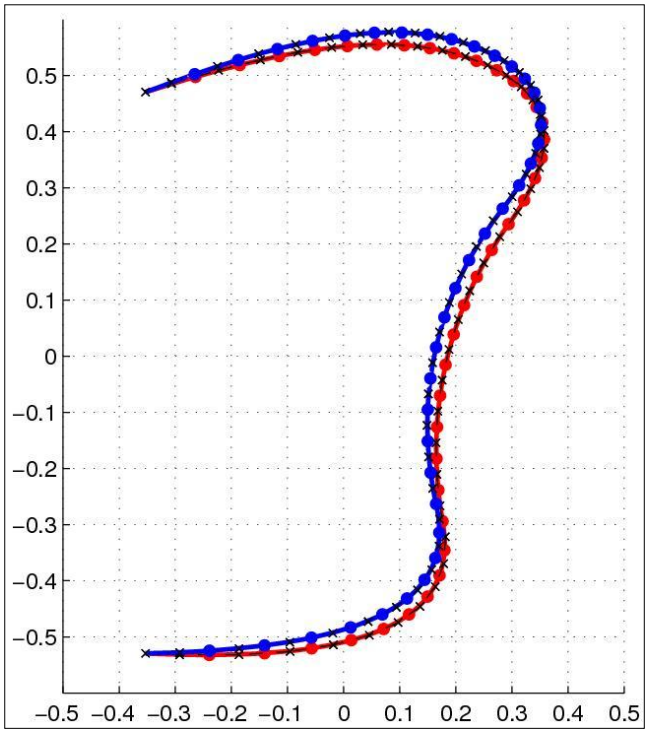

Figure 5.17 : Initial and deformed beam geometry produced by NURBS structure.

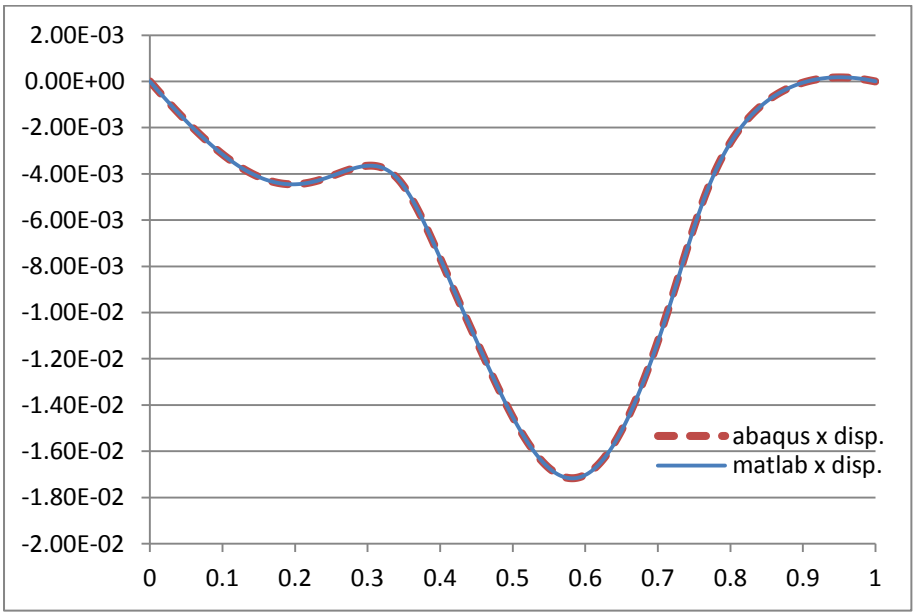

Figure 5.18 : Benchmark results with ABAQUS for the displacement on x direction.

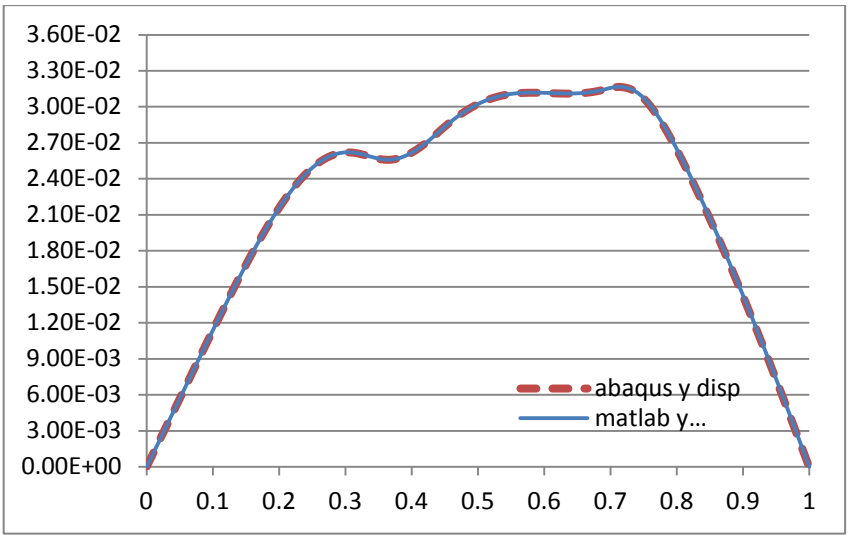

Figure 5.19 : Benchmark results with ABAQUS for the displacement on y direction.

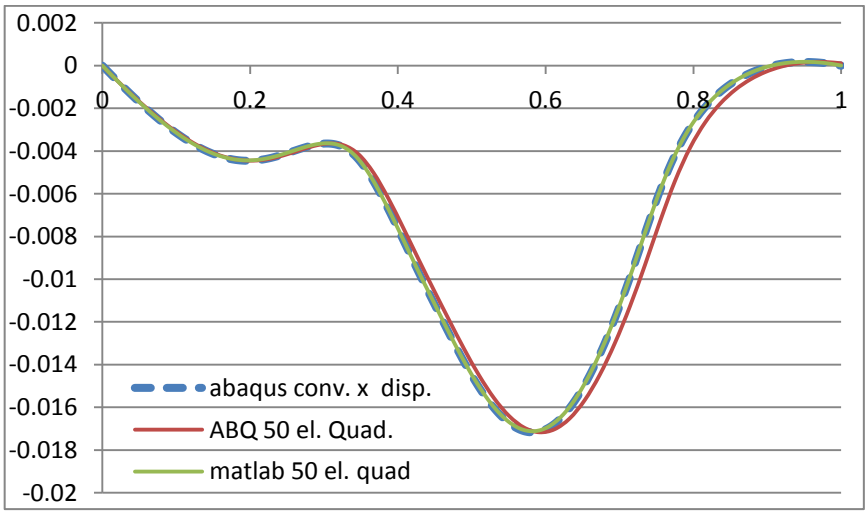

Figure 5.20 : Benchmark results with ABAQUS for 50 elements.

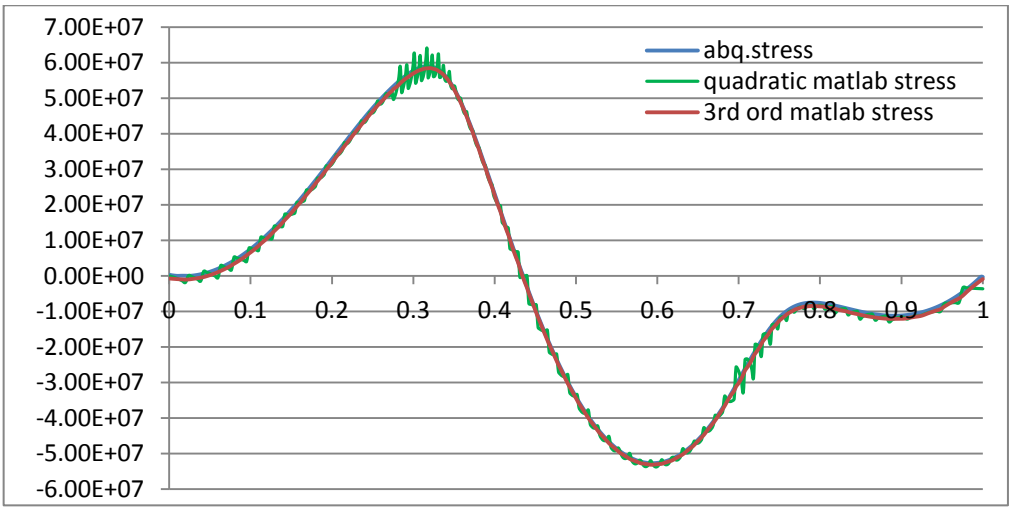

Figure 5.21 : Stress benchmark results with ABAQUS results.

6. 2D APPLICATIONS AND RESULTS

6.1 Isotropic Beam Applicatons

Isogeometric structural analyses of isotropic thick beams are realized for different boundary conditions and load cases. A stretch case is carried out initially to verify the accuracy of Poisson effect and axial displacements. Subsequently two bending analysis with distributed and concentrated load are accomplished. Contrary to one-dimensional applications in the fifth chapter, in these two applications shear effects are also taken into account. That is Timoshenko beam theory is considered and cross-section on x-z plane of the beam is no longer perpendicular to the neutral axis under deformation.

Mesh structure in Figure 6.1 is used for all three isotropic cases. As seen in the figure, four elements have been used through the thickness while eight elements used along the beam length. Red lines correspond to knot vectors that define the elements and black lines are the control points net. All the two dimensional applications in this chapter has been realized with a beam geometry that has an aspect ratio of 4.

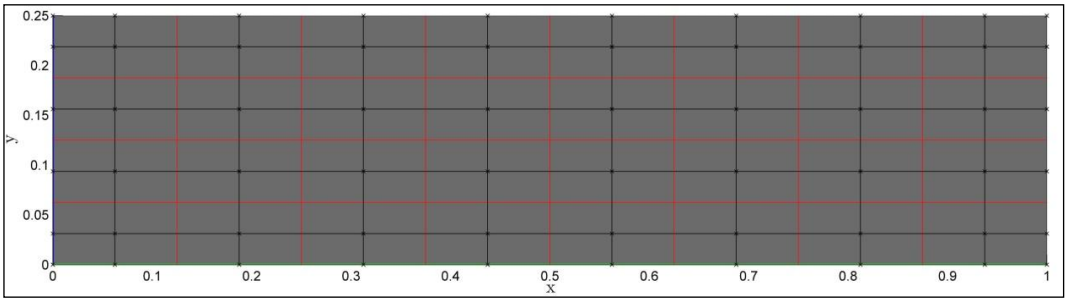

Figure 6.1 : Control points net (black) and mesh structure (red)

6.1.1 Application 1

6.1.1.1 Application 1:Problem description

Isogeometric structural analysis of a beam under stretch is considered in this application. As seen in the computational model in Figure 6.2, lower left corner is clamped and lower right end is clamped with a slider. In addition, left edge is

constraint on x direction while all the control points on this edge is free to move on y direction. Therefore, beam is stretched under the load applied on the right edge on x direction and because of the Poisson effect there is also a contraction along the thickness.

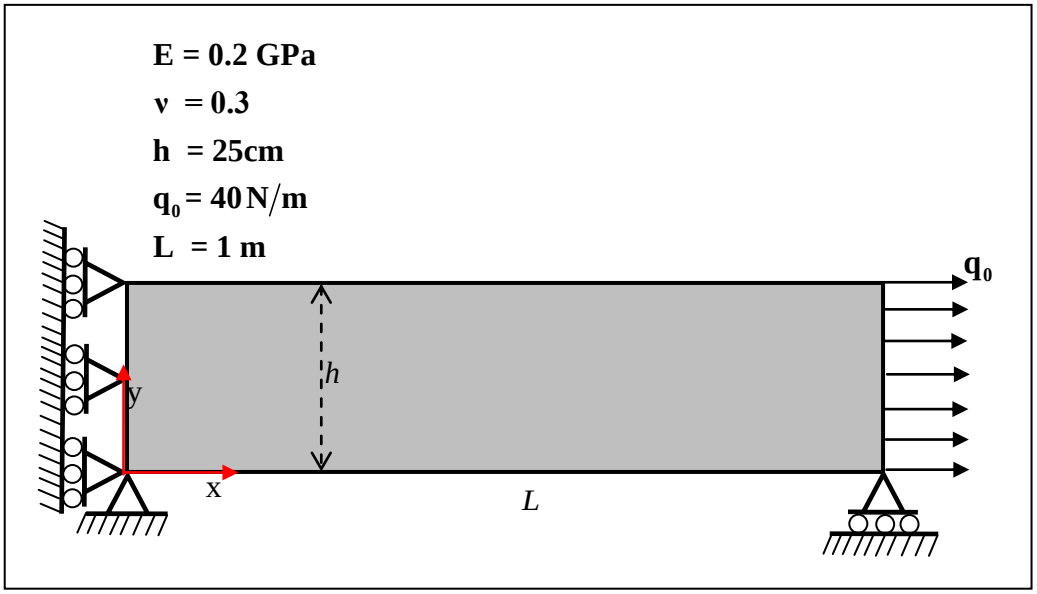

Figure 6.2 : Computational model for stretch analysis

In order to maintain a realistic stretch case, distributed stretch load in this application is simulated with a concentrated load on the lover right corner with a magnitude of 10N. This magnitude is equal to a distributed load of 40N/m for this edge. Then multi point constraint applied on x direction on this free edge. Applying this multi point constraint, since all the points on the right edge deformed equally while they are free for contraction, stretch case is properly simulated.

6.1.1.2 Application 1:Results

In order to have a benchmark, same geometry is created in ABAQUS. Later on boundary conditions, load and multi point constraint applied in isogeometric code is applied in the same way in the ABAQUS analysis. ABAQUS analysis is realized with a high number of elements to maintain reliable results to compare with isogeometric results. Isogeometric contour plots are matched with ABAQUS plots for both stretch and contraction values as seen in Figure 6.3 and Figure 6.4. In these figures ABAQUS results has a deformation scale factor of 10^3 while isogeometric deformation is scaled with 10^5.

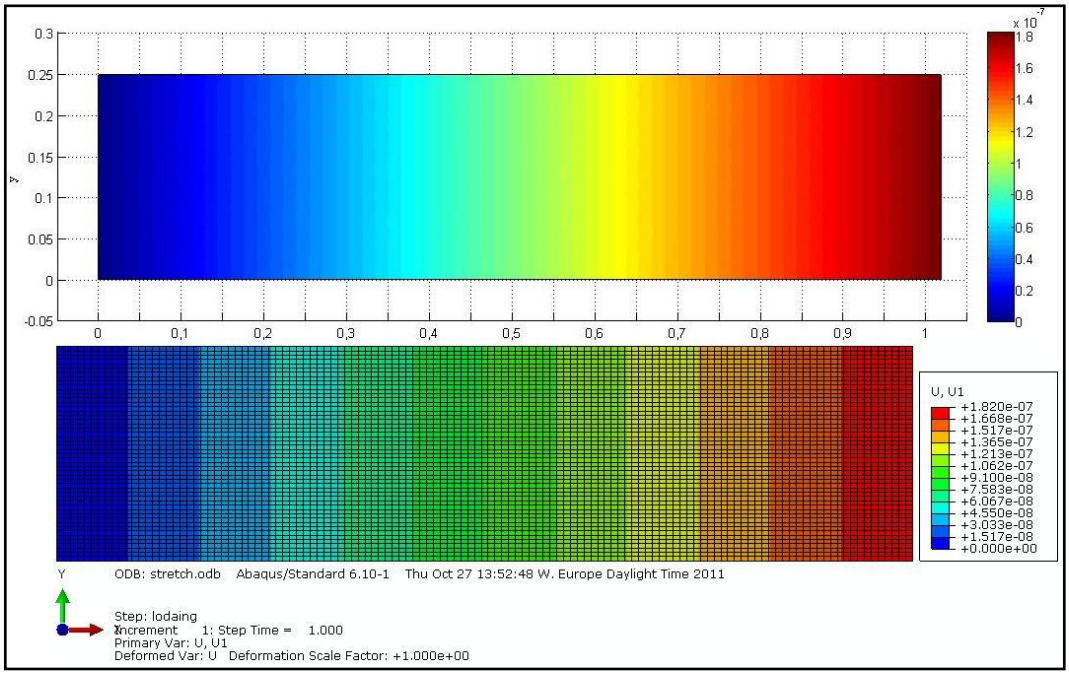

Figure 6.3 : Isogeometric (upper) and ABAQUS (lower) results for displacement on x direction.

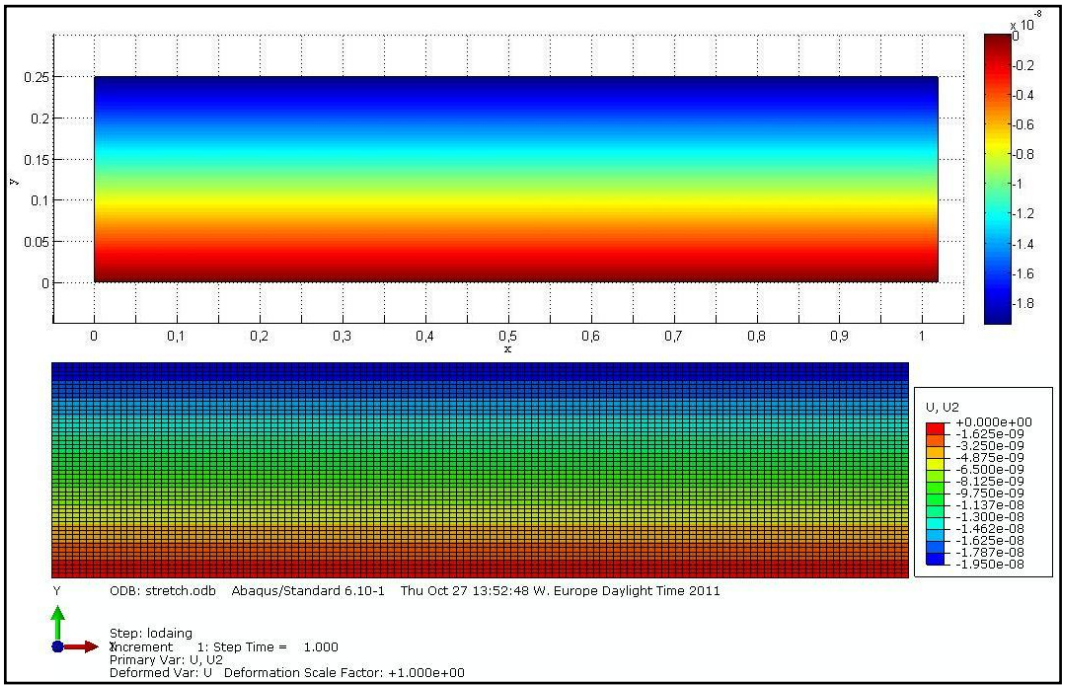

Figure 6.4 : Isogeometric (upper) and ABAQUS (lower) results for displacement on y direction.

Displacement results through the beam thickness are shown in Figure 6.5. Since this application is a stretch case, displacemet on x direction is constant along the thickness for a given position on the beam length as expected. Therewithal contraction results in Figure 6.5 are quite meaningful as they matched perfectly with

ABAQUS results. Since beam is constrained on the y direction at lover corners, contraction is at the maximum on the top edge of the beam and linearly decreases to zero.

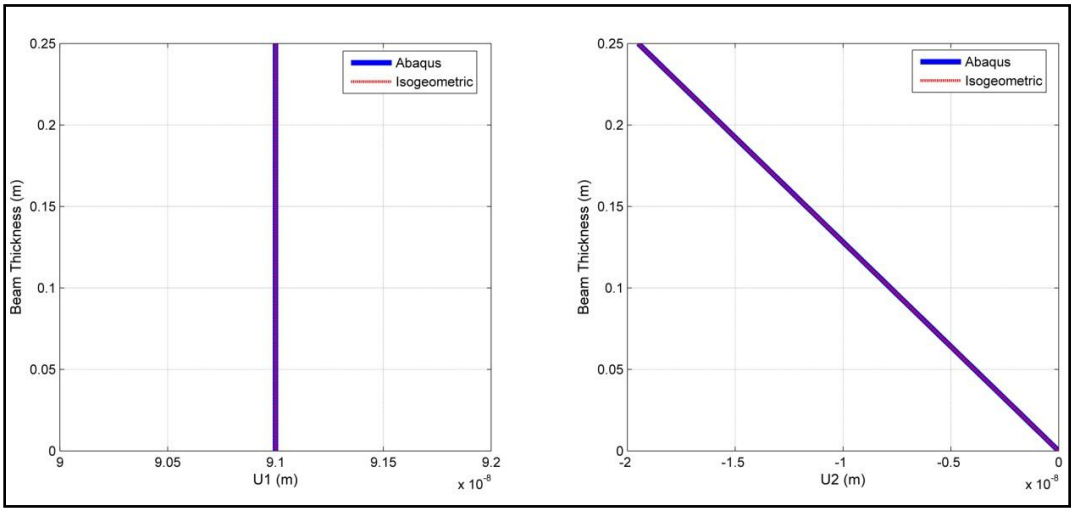

Figure 6.5 : Isogeometric and ABAQUS results for displacements on x (left) and y (right) direction through the thickness at mid-length.

Constant axial stress result is identical with the results obtained from ABAQUS. In addition, as the beam is only exposed to an axial load on this application stress values through the thickness is zero at any location in the beam. However, there is a very small numerical noise in both isogemetric and ABAQUS results, which can be neglected as seen on the right in Figure 6.6.

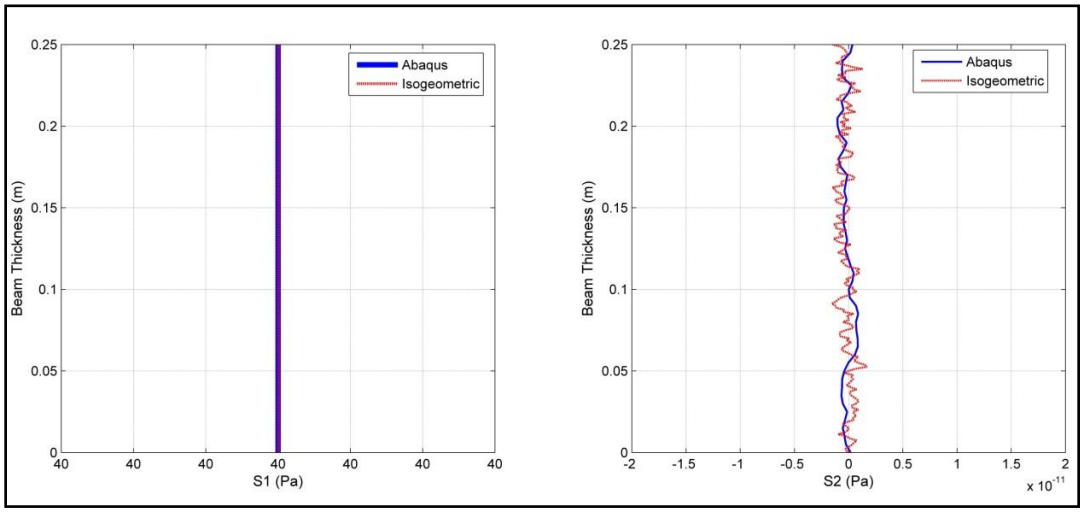

Figure 6.6 : Isogeometric and ABAQUS results for stress results through the thickness on x (left) and y (right) direction at mid-length.

6.1.2 Application 2

6.1.2.1 Application 2:Problem description

Isogeometric structural analysis of a simply supported thick beam under a distributed load considered in this application. Contrary to the slender beam applications in the fifth chapter, in this application stress distribution is non-linaear through the thickness. For that reason, in order to get accurate deformation and stress results through the beam thickness, shear effects are taken into account.

Distributed load on the top edge of the beam is applied by integrating the load magnitude among the points defined on the knot vector, which lays on the top edge. This integration is shown in **(4.38)** in element level.

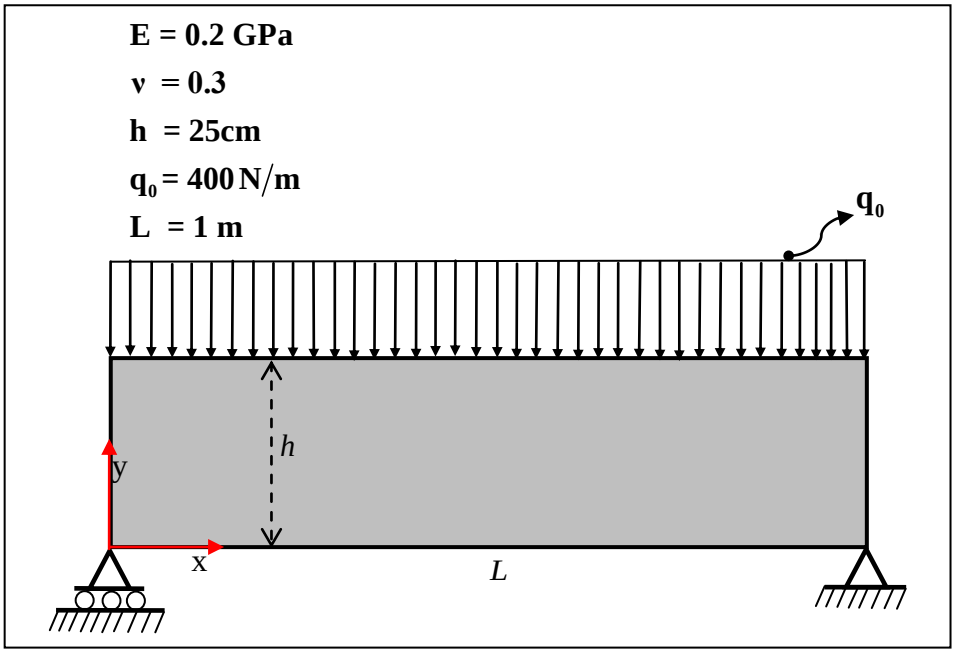

Figure 6.7 : Computational model for distributed load case.

6.1.2.2 Application 2: Results

As seen in in Figure 6.8 and Figure 6.9 displacement and stress contour results of isogeometric analysis very well match with the contour plot outputs of ABAQUS. Lower left corner of the beam is constrained vertically while it slides horizontally as seen in Figure 6.8. For that reason deformation under a distributed load also yields a small amount of stress in x direction plotted in Figure 6.10. As the problem geometry is simply supported, a symmetric deflection on y direction is observed in contour plots as seen in Figure 6.9.

Due to the plot in Figure 6.11 it can be said that isogeometric displacement plot through the thickness has less than $0.1x10^{-5}$m difference than ABAQUS results, which can be considered accurate enough.

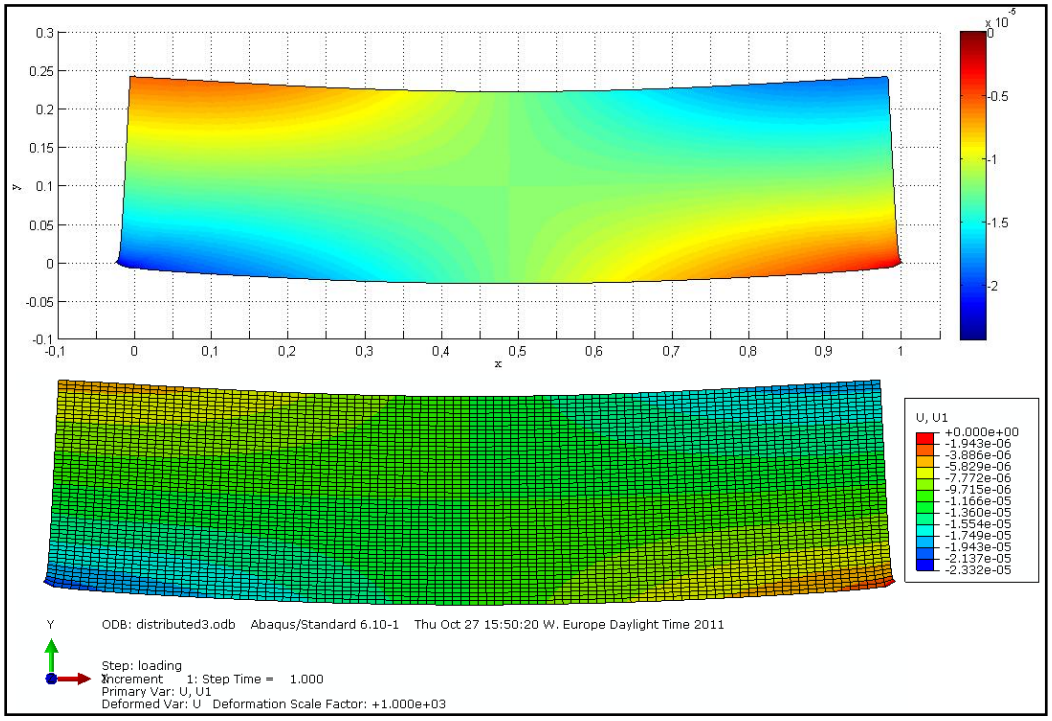

Figure 6.8 : Isogeometric (upper) and ABAQUS (lower) results for displacement on x direction.

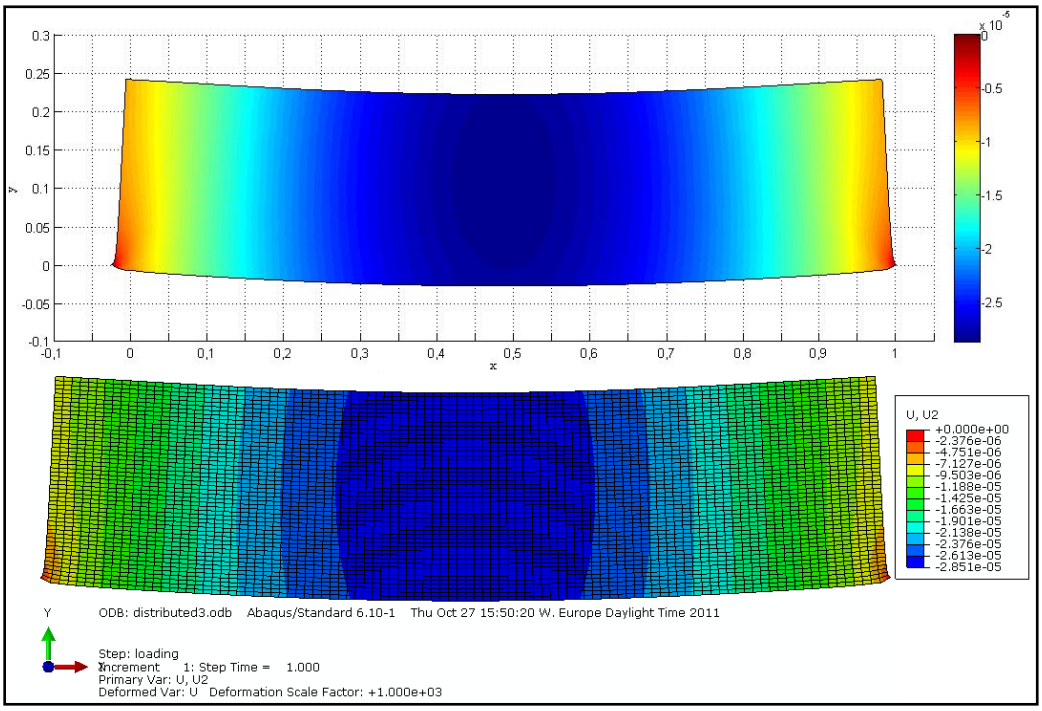

Figure 6.9 : Isogeometric (upper) and ABAQUS (lower) results for displacement on y direction.

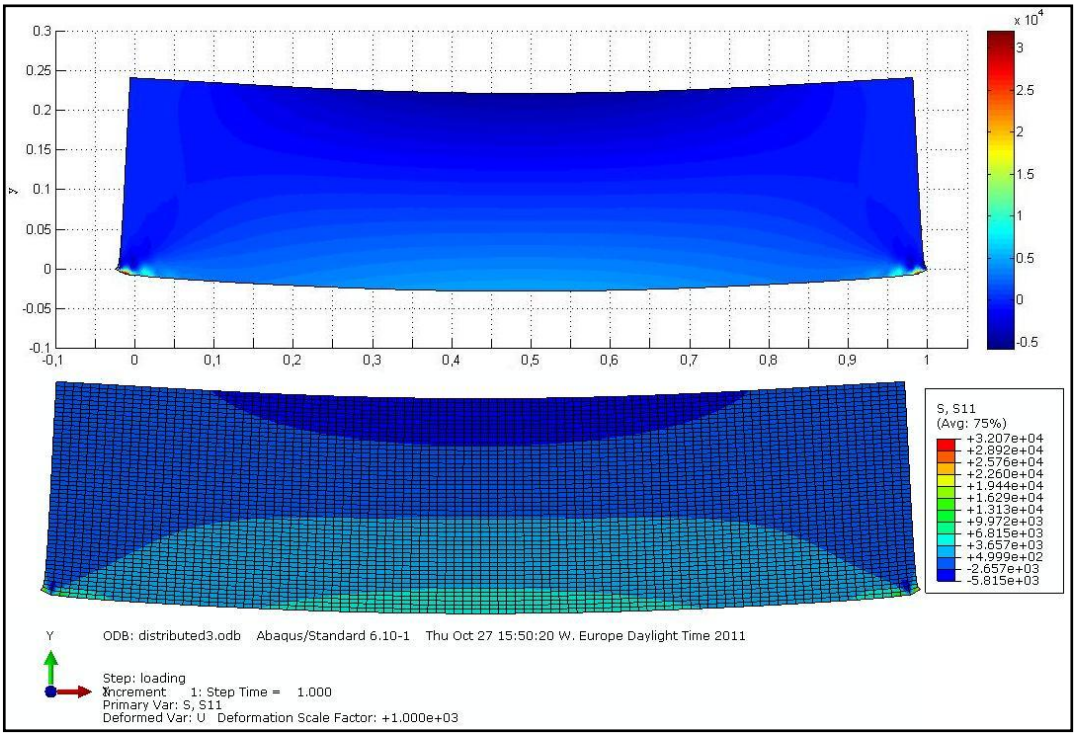

Figure 6.10 : Isogeometric (upper) and ABAQUS (lower) results for the stress on x direction

Beside deformation results, stress results through the thickness has perfect match with ABAQUS results and non-linear stress distribution on y direction is remarkable in Figure 6.12. At the top and lower edge of the beam, a small jump for the stress values on y direction is observed in ABAQUS results while isogeometric analysis values starts with zero at the lower edge and ends at the 400 Pa which is applied distributed force on the top edge of the beam as expected.

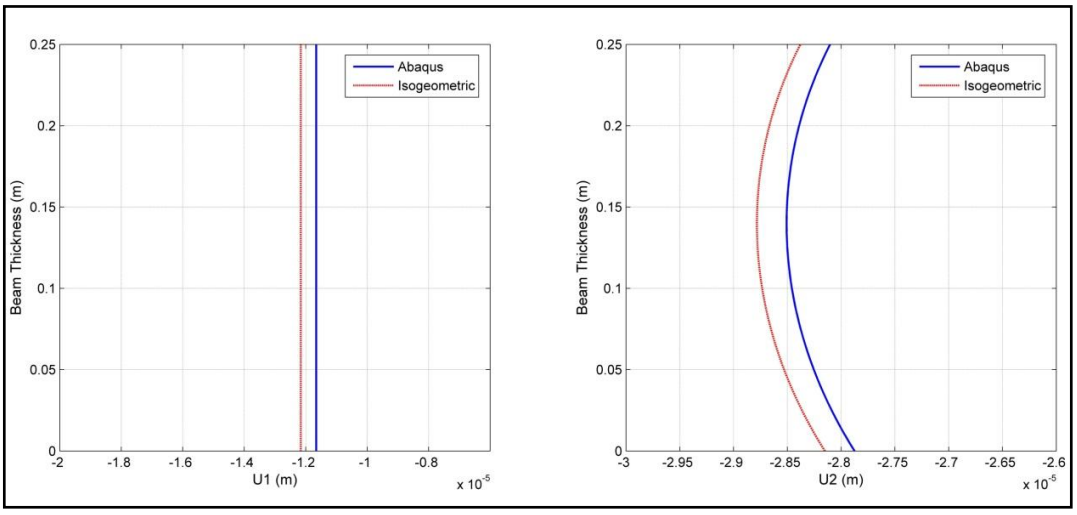

Figure 6.11 : Isogeometric and ABAQUS displacement results through the thickness on x (left) and y (right) direction at mid-length.

Since the case is symmetric, shear stress value through the thickness at the mid-length should be zero. Plot in Figure 6.13 shows that shear stress results oscilates around zero while isogeometric analysis results are constant at zero. This proves that isogeometric analysis has less noise than ABAQUS results for the stress distribution through thickness in a thick beam analysis.

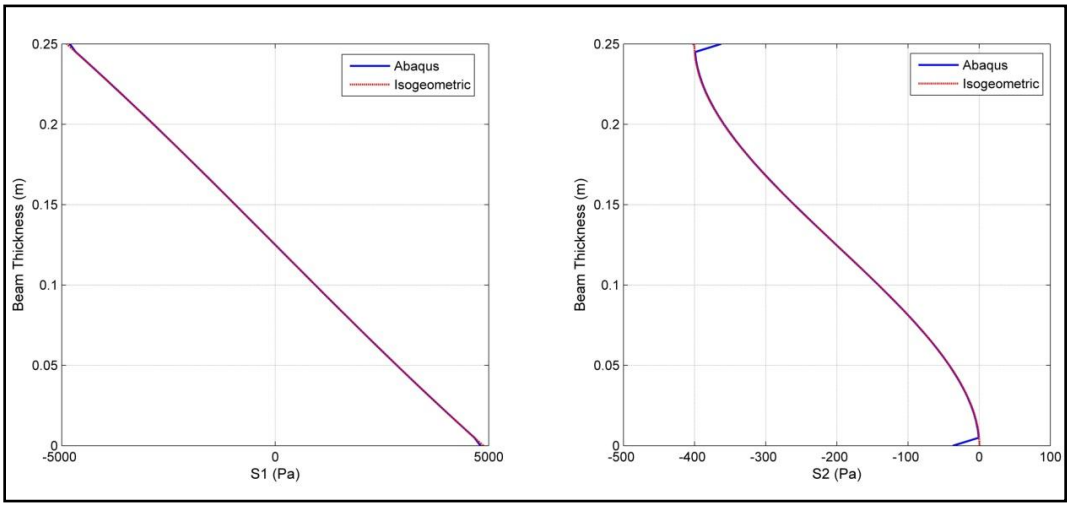

Figure 6.12 : Isogeometric and ABAQUS stress results through the thickness on x (left) and y (right) direction at mid-length.

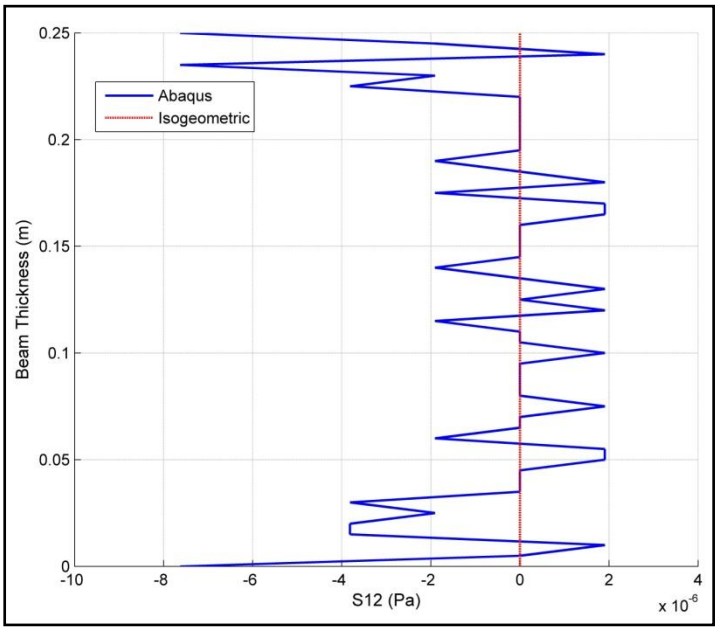

Figure 6.13 : Isogeometric and ABAQUS shear stress noise comparison through the thickness at mid-length.

6.1.3 Appplication 3

6.1.3.1 Application 3:Problem description

Isogeometric structural analysis of a simply supported thick beam under a concentrated load at its mid-length is considered in this application. In this application shear effects are taken into account as in the previous example.

Concentrated load on the top edge of the beam is applied by defining the parameterized position of the load on the knot vector at the top edge border of the beam. During element external force vector integration, isogeometric code checks the edges for the existence of a concentrated load. If there is a concentrated load, the corresponding knot span that includes the load is found then the contribution of this concentrated load is added to the relevant element external force vector.

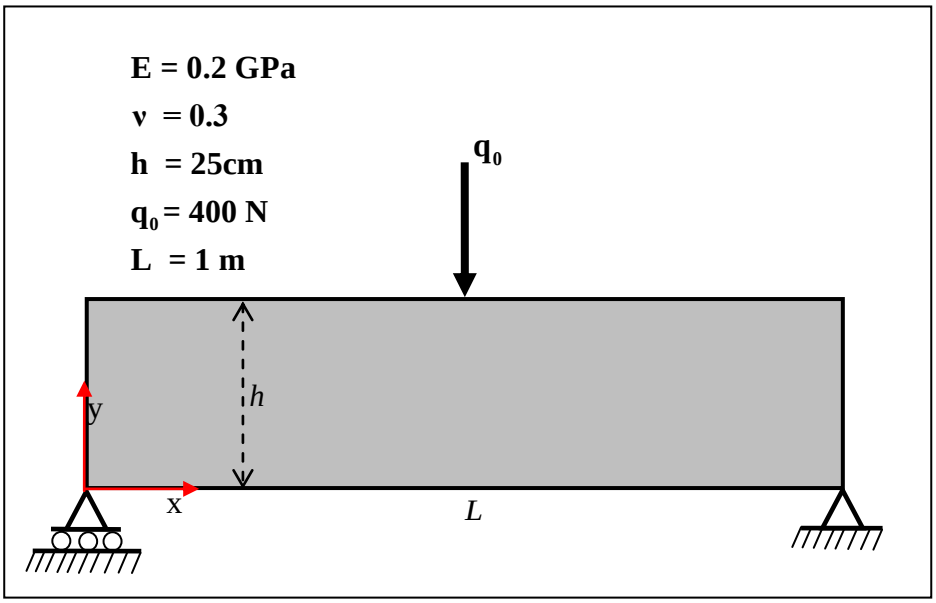

Figure 6.14 : Computational model for distributed load case.

6.1.3.2 Application 3: Results

Figure 6.15 and Figure 6.16 indicates the benchmark of displacement contour results of isogeometric analysis with ABAQUS results. As seen in the figures, these results also have a meaningful match as in the previous applications. Due to the concentrated load, a local deflection can be seen at the mid-length on the top edge of the beam in both isogeometric and ABAQUS plots. Because of the simply supported boundary conditions, a symmetric vertical deflection is observed in the contour plots as seen in Figure 6.16.

Isogeometric horizontal displacement plot in Figure 6.18 has a difference than ABAQUS results around $0.5x10^{-6}$ m, which can be considered accurate enough.

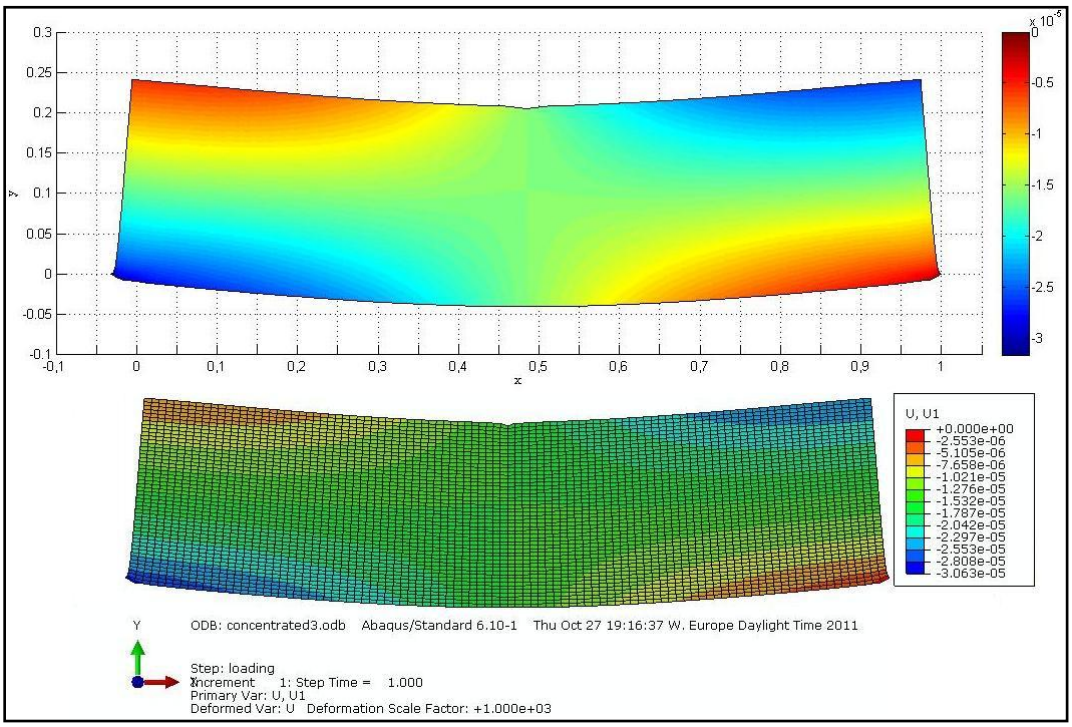

Figure 6.15 : Isogeometric (upper) and ABAQUS (lower) results for displacement on x direction.

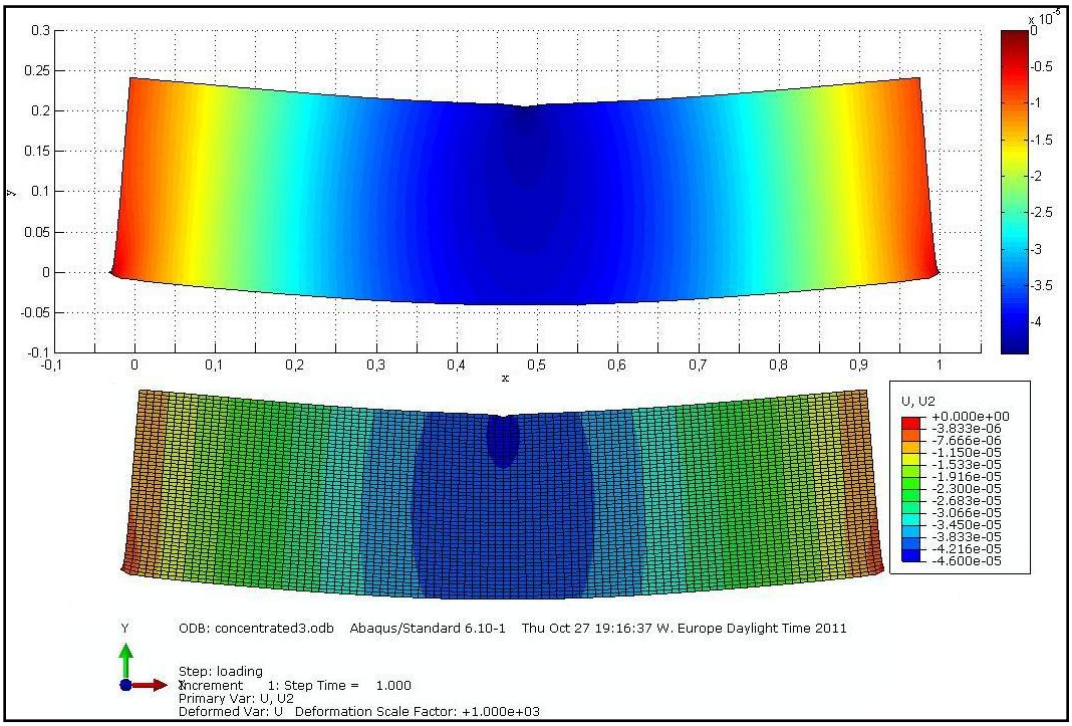

Figure 6.16 : Isogeometric (upper) and ABAQUS (lower) results for displacement on y direction.

However, as seen in the Figure 6.17 vertical displacement results have a 0.2x10-5m difference on the top edge at the mid-length where the concentrated load is applied. Most probably, the local deflections are the reason of this higher difference. This difference can be eliminated by using higher number of elements in the isogeometric analysis code.

In Figure 6.18 this local difference also can be observed on stress values. As seen in the figure, isogeometric and ABAQUS results match clearly through the thickness but on the locations closer to the top edge some difference is observed.

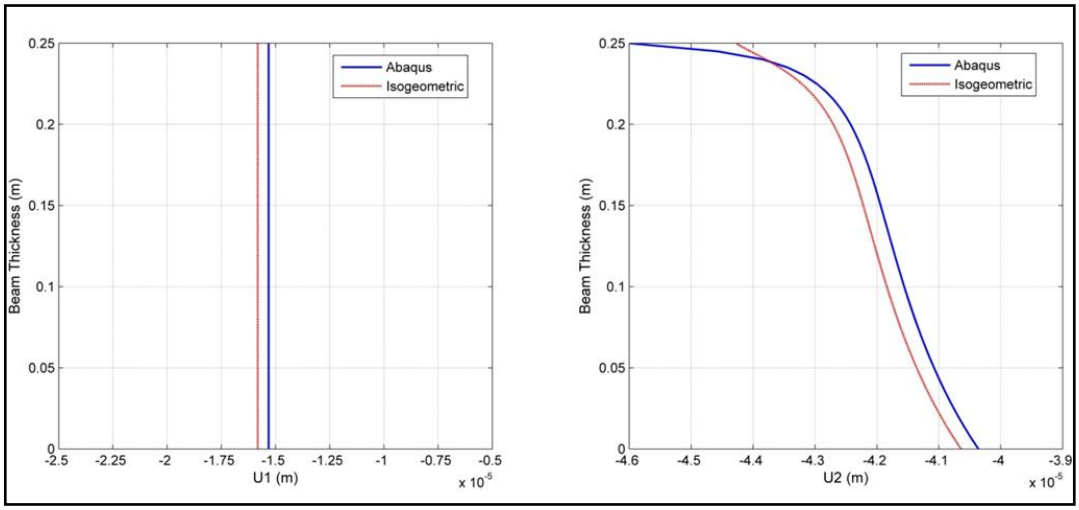

Figure 6.17 : Isogeometric and ABAQUS displacement results through the thickness on x (left) and y (right) direction at mid-length.

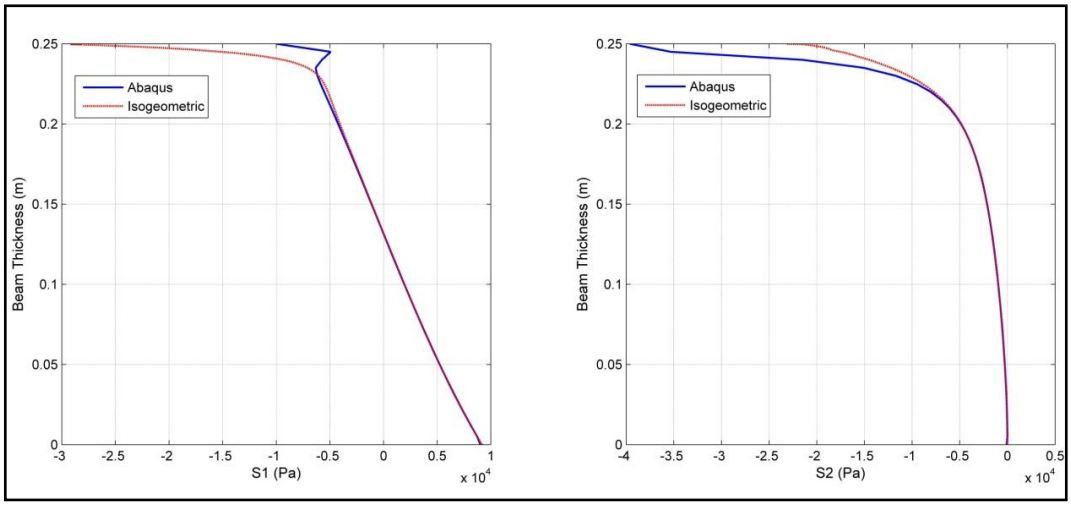

Figure 6.18 : Isogeometric and ABAQUS stress results through the thickness on x (left) and y (right) direction at mid-length.

6.2 Composite Beam Applications

Isogeometric structural analyses of composite thick beams under cylindrical bending are realized for two different stacking sequences. A general computational model is presented in Figure 6.19. The layers of the laminated beam have the same material properties but different fiber directions. Cases for 0/90 and 0/90/0 are carried out and the results for each case are presented at the end of each sub-chapter. For each layup, different combinations of basis orders and element numbers are employed along the thickness and length. Complete lists of cases for each layup are presented in Table 6.1 and Table 6.2.

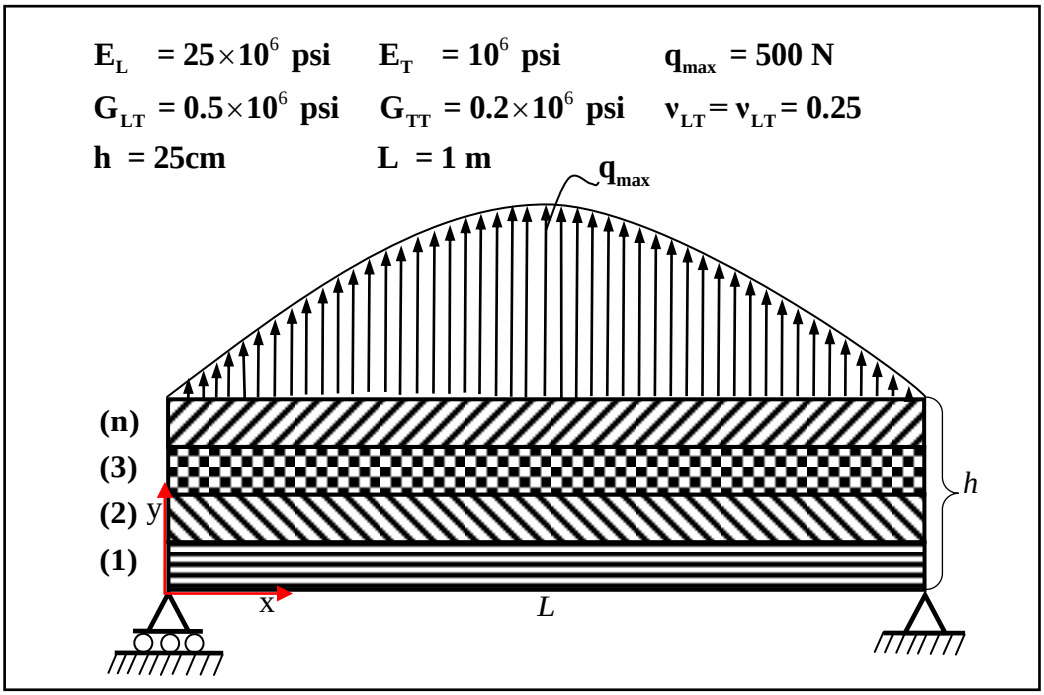

Figure 6.19 : Computational model for cylindrical bending of a composite beam.

Contrary to isotropic analyses in the sub-chapter 6.1, in these composite cases basis functions used through the beam thickness has discontinuities. These discontinuities are located on the layer interfaces and maintained by knot repetition as shown in the second chapter in Figure 2.2. Knot repetition yields an increase in the number of control points as explained in the second chapter. Increase of the control points around the layer interface can be observed in Figure 6.20 and Figure 6.30. Since several analyses with different number of elements have been carried out for each stacking sequence, the mesh structures in the Figure 6.20 and Figure 6.30 are shown

only to indicate the difference of the mesh structure than the ones used in isotropic cases.

Table 6.1 : List of cases carried out for 0/90 stacking sequence.

Case no.	eL	eW^L	AR_el	p	q		
1	4	2	4	1	1	2	3
2	4	4	8	1	1	2	3
3	4	2	4	2	1	2	3
4	4	4	8	2	1	2	3
5	8	2	2	1	1	2	3
6	8	4	4	1	1	2	3
7	8	8	8	1	1	2	3
8	8	2	2	2	1	2	3
9	8	4	4	2	1	2	3
10	8	8	8	2	1	2	3
11	16	2	1	1	1	2	3
12	16	4	2	1	1	2	3
13	16	8	4	1	1	2	3
14	16	16	8	1	1	2	3
15	16	2	1	2	1	2	3
16	16	4	2	2	1	2	3
17	16	8	4	2	1	2	3
18	16	16	8	2	1	2	3

The beam geometry in all the composite cases has an aspect ratio of 4. Thus these analyses are also thick beam analyses where shear effects are taken into account. Cylindrical bending is applied with a static distributed load in a shape of half sinus wave. In order to integrate this load over the top edge of the beam, a subroutine is developed to calculate the magnitude of the load for a desired location on the edge. Then the contribution of the calculated magnitude for each knot span is added to the relevant element external force vector.

Table 6.2 : List of cases carried out for 0/90/0 stacking sequence.

Case no.	eL	eW^L	AR_el	p	q		
1	4	2	6	1	1	2	3
2	4	4	12	1	1	2	3
3	4	2	6	2	1	2	3
4	4	4	12	2	1	2	3
5	8	2	3	1	1	2	3
6	8	4	6	1	1	2	3
7	8	8	12	1	1	2	3
8	8	2	3	2	1	2	3
9	8	4	6	2	1	2	3
10	8	8	12	2	1	2	3
11	16	2	1.5	1	1	2	3
12	16	4	3	1	1	2	3
13	16	8	6	1	1	2	3
14	16	16	12	1	1	2	3
15	16	2	1.5	2	1	2	3
16	16	4	3	2	1	2	3
17	16	8	6	2	1	2	3
18	16	16	12	2	1	2	3

Since local stiffness values are different for the layers in the composite cases, a subroutine is developed to call the right stiffness values for the corresponding elements. During the integration of element stiffness matrices, these right stiffness values are used. In addition, these stiffness values also used for the stress recovery process as explained in **(4.43)**.

In these composite applications, isogeometric analysis results are compared with analytic elasticity solutions. An analytic elasticity solution code is developed referring to the calculations in a study of N.J Pagano.[24] This analytic code is called in the main isogeometric analysis and realize the analytic elasticity solution then stores the result data. Thus, analytic and isogeometric results are plotted together for the benchmark results.

6.2.1 Application 1: Analysis for 0/90 stacking sequence

Isogeometric structural analysis of a simply supported, composite, thick beam with a stacking sequence of 0/90 under a cylindrical bending is considered in this application. Figure 6.20 shows an example mesh structure for 0/90 stacking sequence. As seen in the figure, there is a populated number of control points at the mid-thickness of the beam. This is because of the knot repetition as explained in the previous sub-chapter.

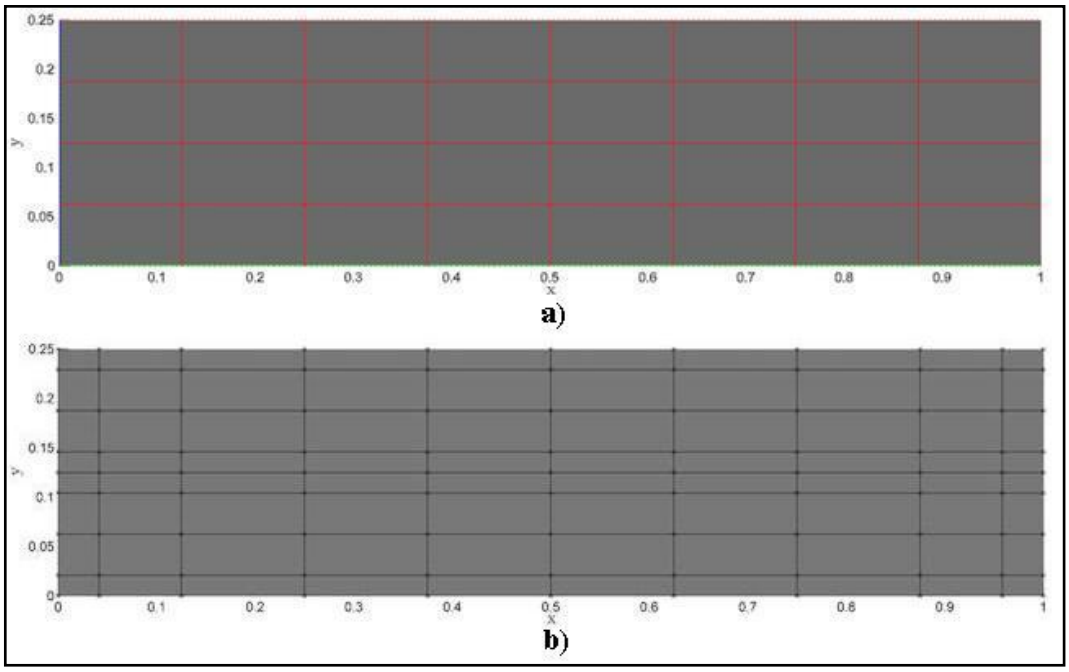

Figure 6.20 : a) Mesh structure **b)** Control points net for 0/90 stacking sequence

6.2.1.1 Application 1:Problem description

6.2.1.2 Application 1:Results

Contour plots of displacement results in Figure 6.21 and Figure 6.22 are quite reasonable for the bending case. Because of the simply supported boundary conditions and symmetrical load, a symmetric vertical deflection is observed in the contour plots as seen in Figure 6.22.

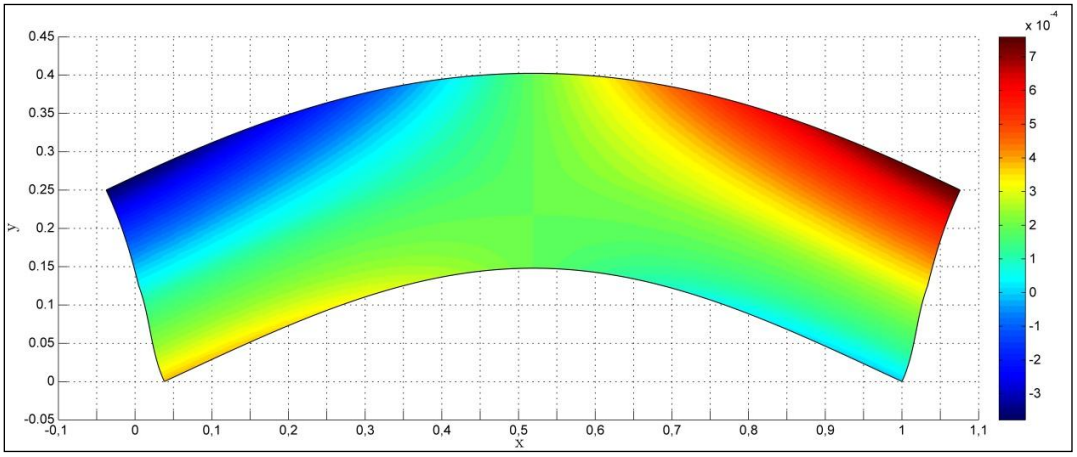

Figure 6.21 : Isogeometric displacement results on x direction.

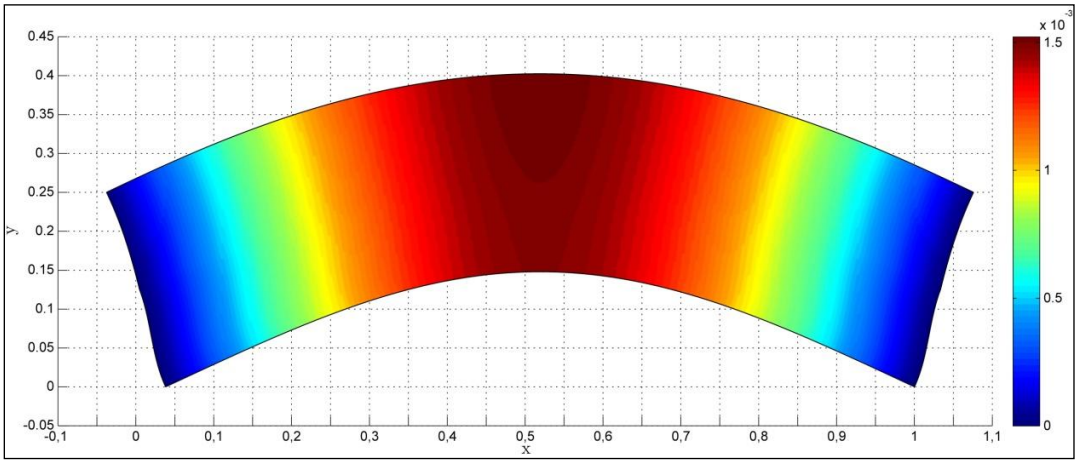

Figure 6.22 : Isogeometric displacement results on y direction.

Contour plot of the stress on x direction in Figure 6.23 indicates the layers significantly. Since the top layer has a fiber orientation of 90 degrees, the lower layer handles the stress on x direction. Furthermore, as it is expected there is a tensile stress on the top of lower layer and a negative stress at the bottom.

Similarly, as seen in the Figure 6.24 the maximum stress on y direction is observed in the mid-length at the top edge where the load is applied. The magnitude of this stress is equal to the maximum value of the load. Therefore Figure 6.24 proves that the load is integrated properly and the stress recovery process is done properly by the isogeometric code.

In adition, Figure 6.25 shows shear stress distribution on xy plane. As it is expected, maximum absolute shear stress values are also observed in bottom layer which has a fiber orientation on the direction of beam length

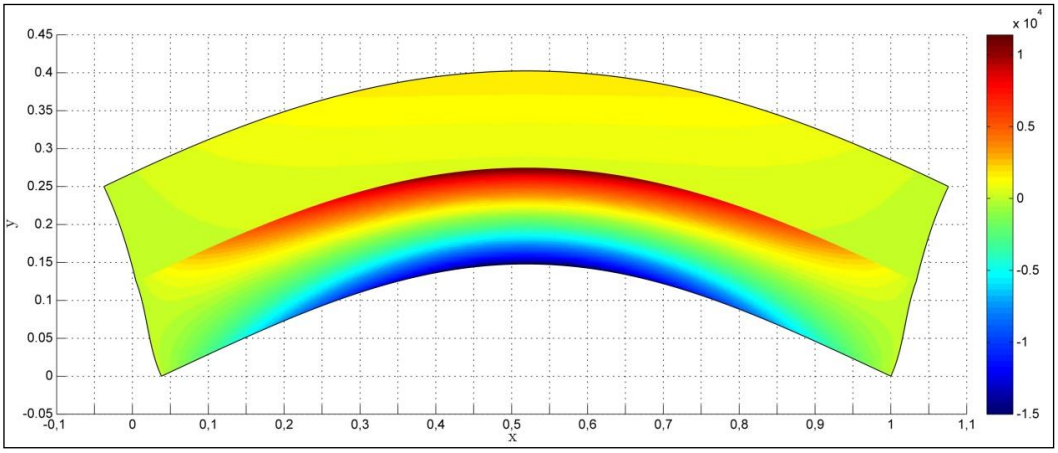

Figure 6.23 : Isogeometric stress results on x direction.

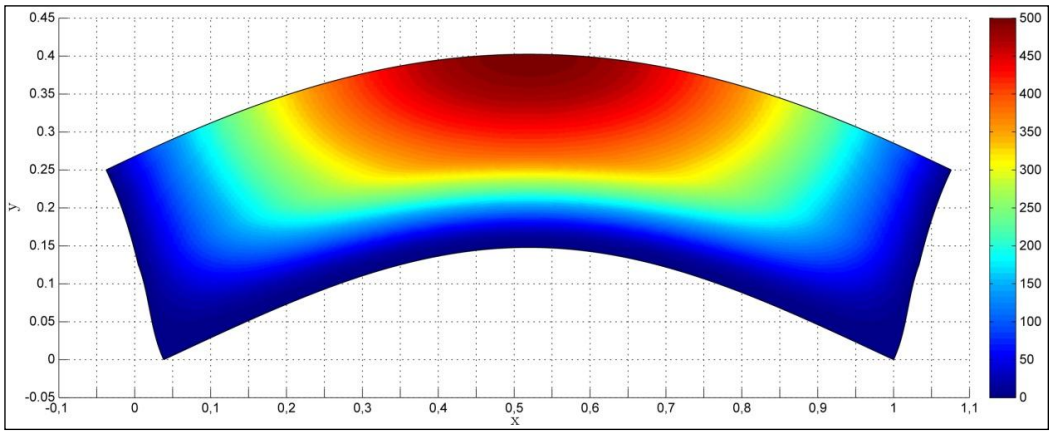

Figure 6.24 : Isogeometric stress results on y direction.

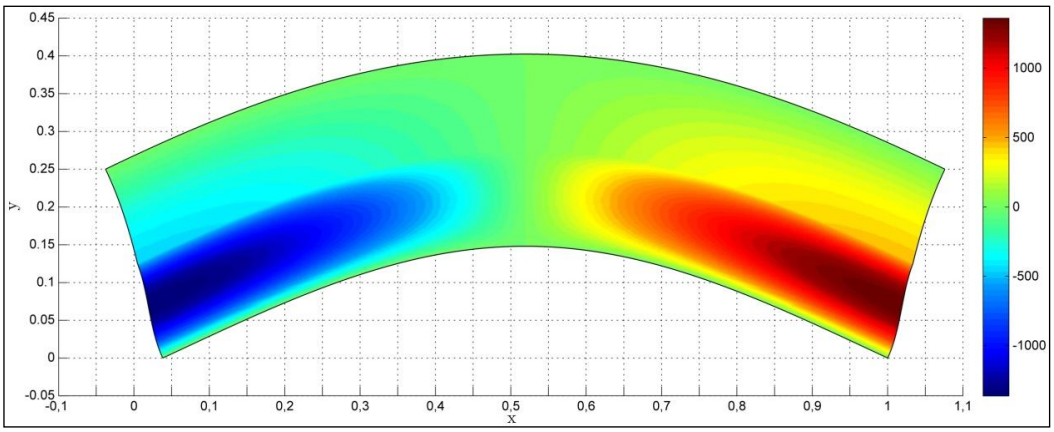

Figure 6.25 : Isogeometric shear stress results.

After general observation of the stress distribution over contour plots, stress values along the thickness are plotted with the analytic results. This plots are compared for different mesh structures and for different polynomial degrees of basis functions in the following figures. In these plots, stress data on the x and y directions are derived

on the mid length of the beam while shear values are derived on the free end of the bea where x=0. In Figure 6.26 and in Figure 6.27 since the mesh structure is quite coarse, shear stress values has a signicant difference with analytic values.

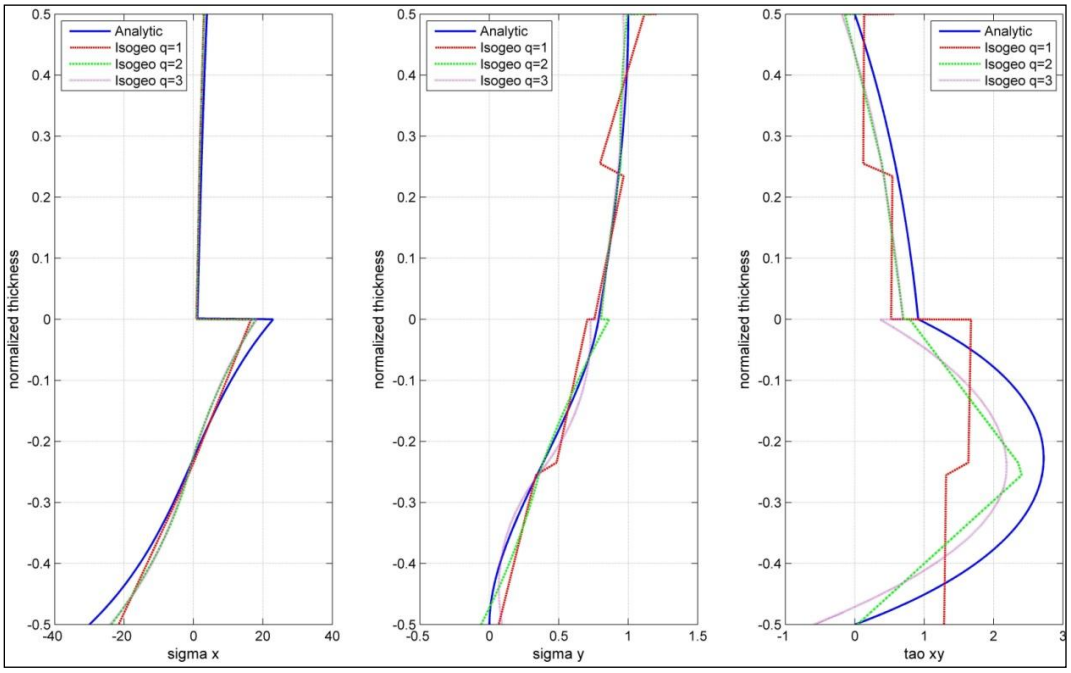

Figure 6.26 : Stress results for 4 elements along the length and 2 elements per layer by using linear basis functions along the length.

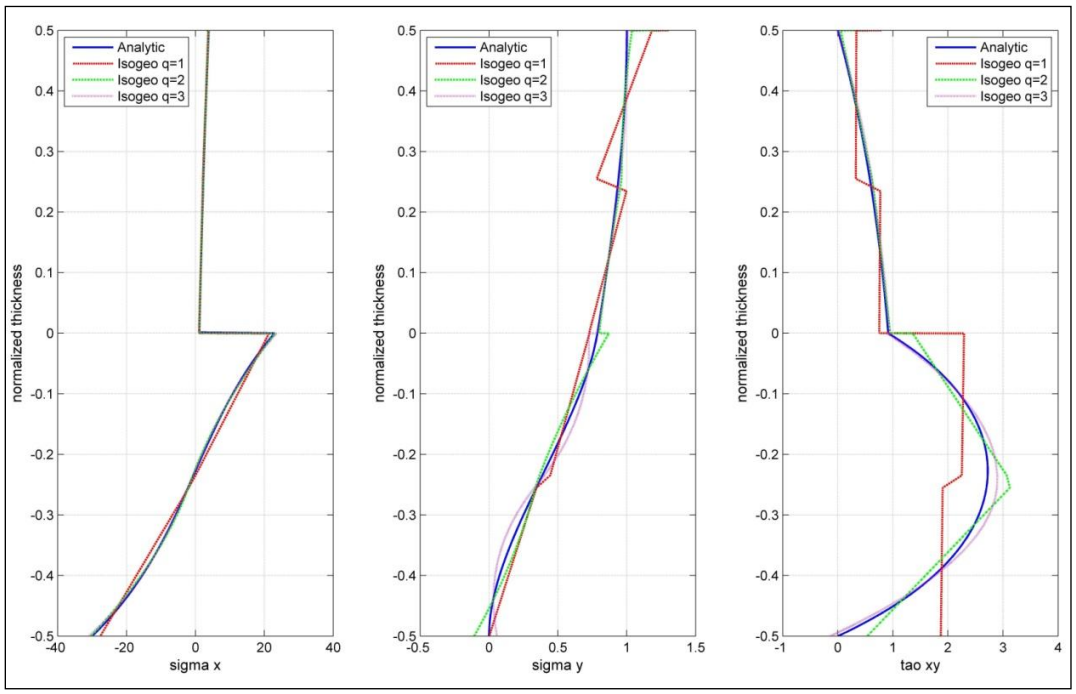

Figure 6.27 : Stress results for 8 elements along the length and 2 elements per layer by using quadratic basis functions along the length.

However, as seen in Figure 6.28 and Figure 6.29, isogeometric results for cubic basis functions along the thickness leads smoother and more accurate results than the results derived with quadratic basis functions for finer mesh structures.

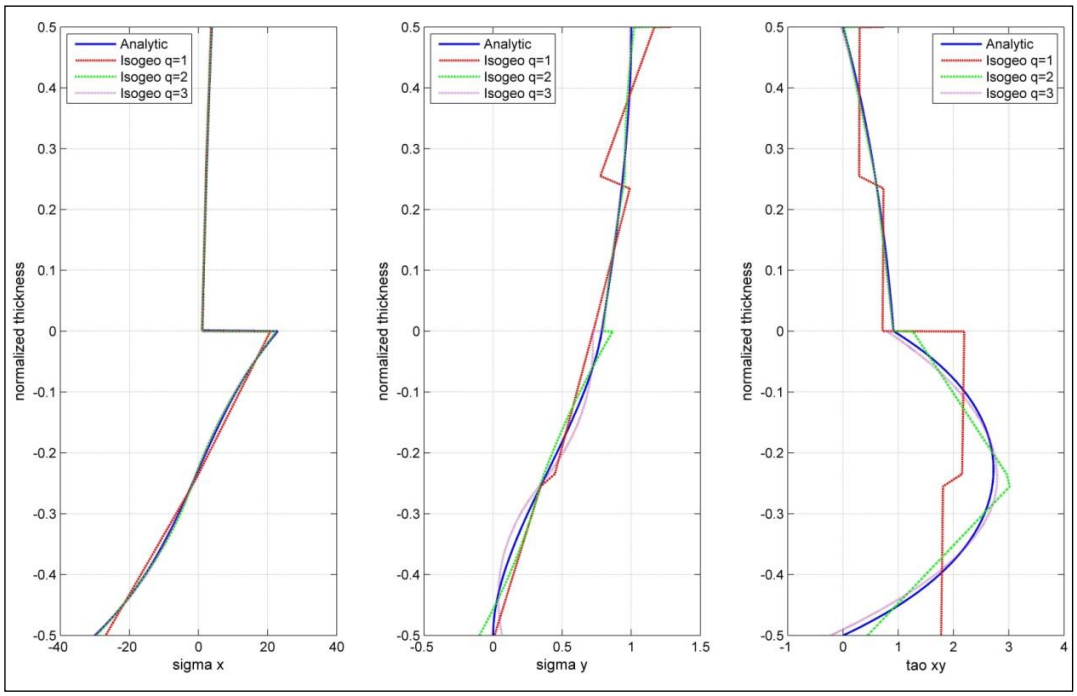

Figure 6.28 : Stress results for 16 elements along the length and 2 elements per layer by using linear basis functions along the length.

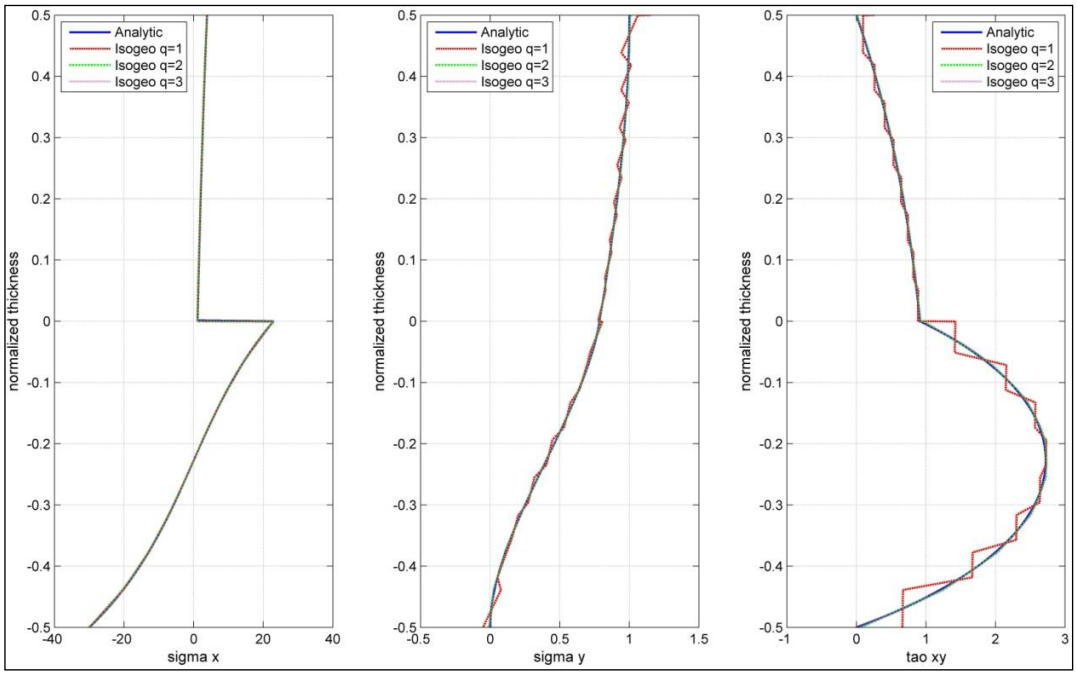

Figure 6.29 : Stress results for 16 elements along the length and 8 elements per layer by using quadratic basis functions along the length.

In the stress plots along the thickness, the results derived with quadratic basis functions can be obtained with the current FEM packages. Since isogeometric analysis allows using higher order basis functions through the thickness; for the case in Figure 6.28, isogeometric results for cubic basis functions introduce the superiority over classical FEM.

6.2.2 Application 2: Analysis for 0/90/90 stacking sequence

Isogeometric structural analysis of a simply supported, composite, thick beam with a stacking sequence of 0/90/0 under a cylindrical bending is considered in this application. Figure 6.30 shows an example mesh structure for 0/90/0 stacking sequence. As seen in the figure, there is a populated number of control points at two layer interface in thickness direction. As it is explained in the previous application this is also because of the knot repetition on that locations.

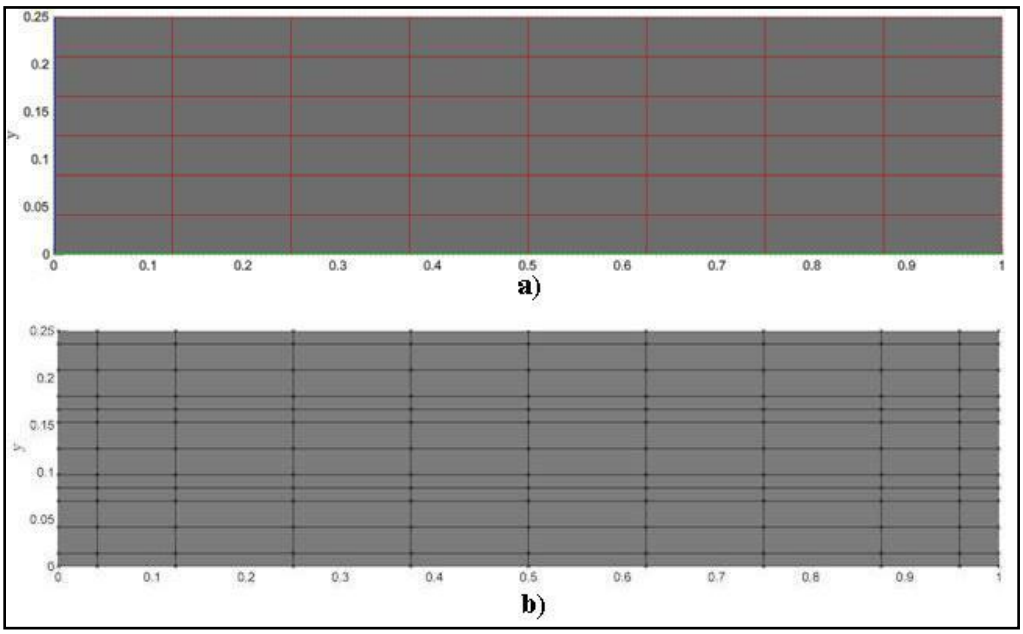

Figure 6.30 : a) Mesh structure **b)** Control points net for 0/90/0 stacking sequence

6.2.2.1 Application 2:Problem description

6.2.2.2 Application 2:Results

Contour plots of displacement results in Figure 6.31 and Figure 6.32 are also reasonable for this bending case as it is in the previous application. Because of the simply supported boundary conditions and symmetrical load, a symmetric vertical deflection is observed in the contour plots as seen in Figure 6.32.

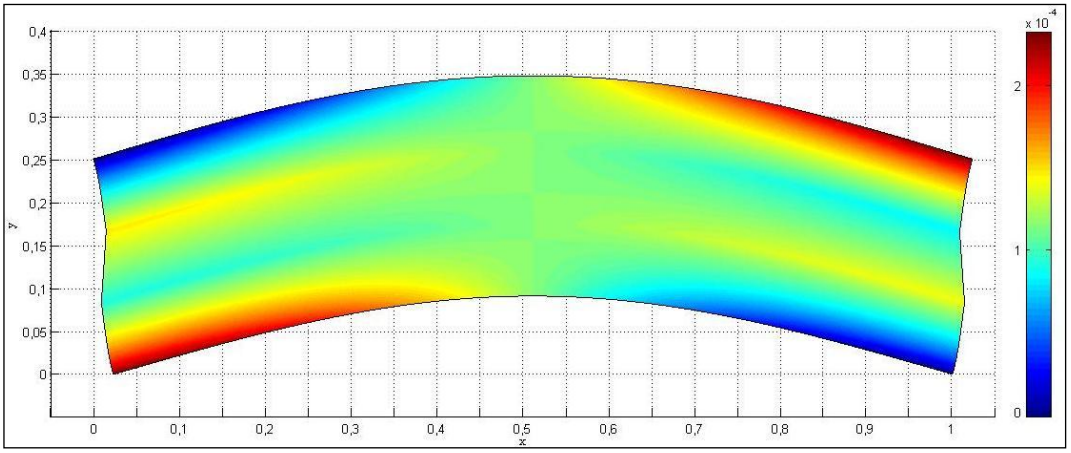

Figure 6.31 : Isogeometric displacement results on x direction.

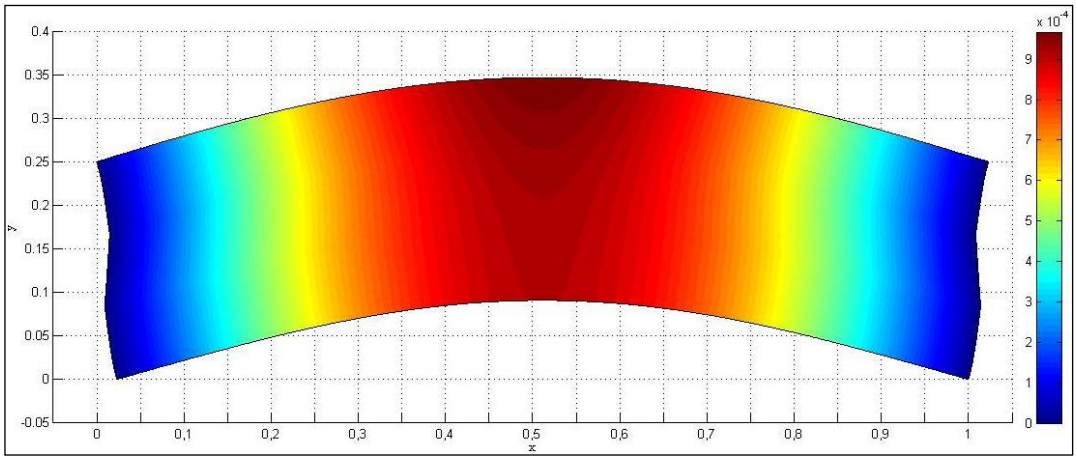

Figure 6.32 : Isogeometric displacement results on y direction.

Layers of the beam can be easily seen in the contour plot of the stress on x direction in Figure 6.33. Since the mid layer has a fiber orientation of 90 degrees, the bottom and top layers handle the stress on x direction. Furthermore, as it is expected there is a tensile stress on the top of lower layer and a negative stress at the bottom.

In the Figure 6.34, maximum stress on y direction is observed in the mid-length at the top edge where the load is applied. The magnitude of this stress is equal to the maximum value of the load. Therefore, Figure 6.34 proves that the load is integrated properly and the stress recovery process is done properly by the isogeometric code.

Figure 6.35 shows shear stress distribution on xy plane. As it is expected, also the maximum absolute shear stress values are observed in the bottom and top layers which have a fiber orientation on the direction of beam length.

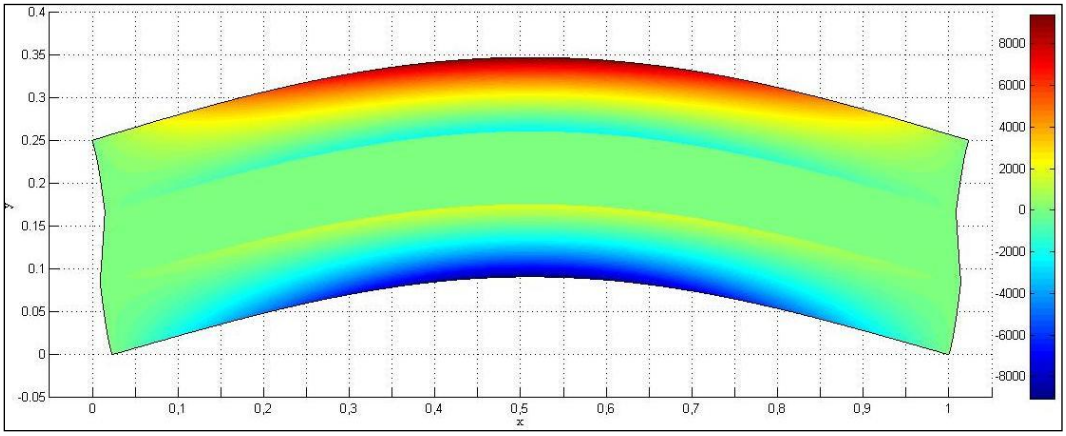

Figure 6.33 : Isogeometric stress results on x direction.

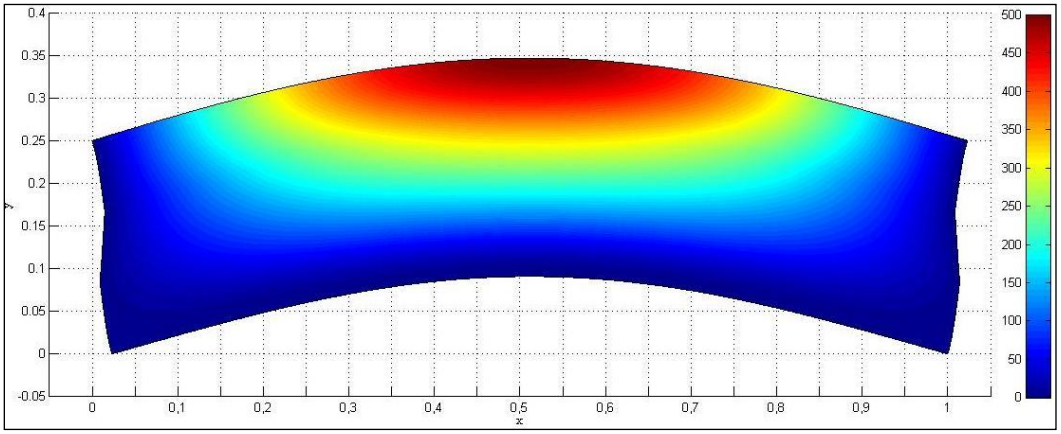

Figure 6.34 : Isogeometric stress results on y direction.

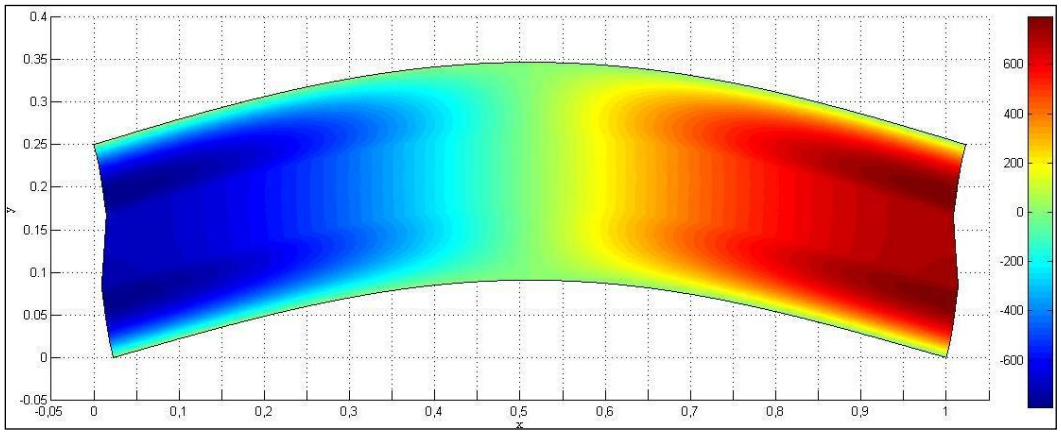

Figure 6.35 : Isogeometric shear stress results.

After general observation of the stress distribution over contour plots, stress values along the thickness are plotted with the analytic results. This plots are compared for different mesh structures and for different polynomial degrees of basis functions as it is done in the previous application. In Figure 6.36 and in Figure 6.37 since the mesh structure is quite coarse, shear stress values has a signicant difference with analytic values.

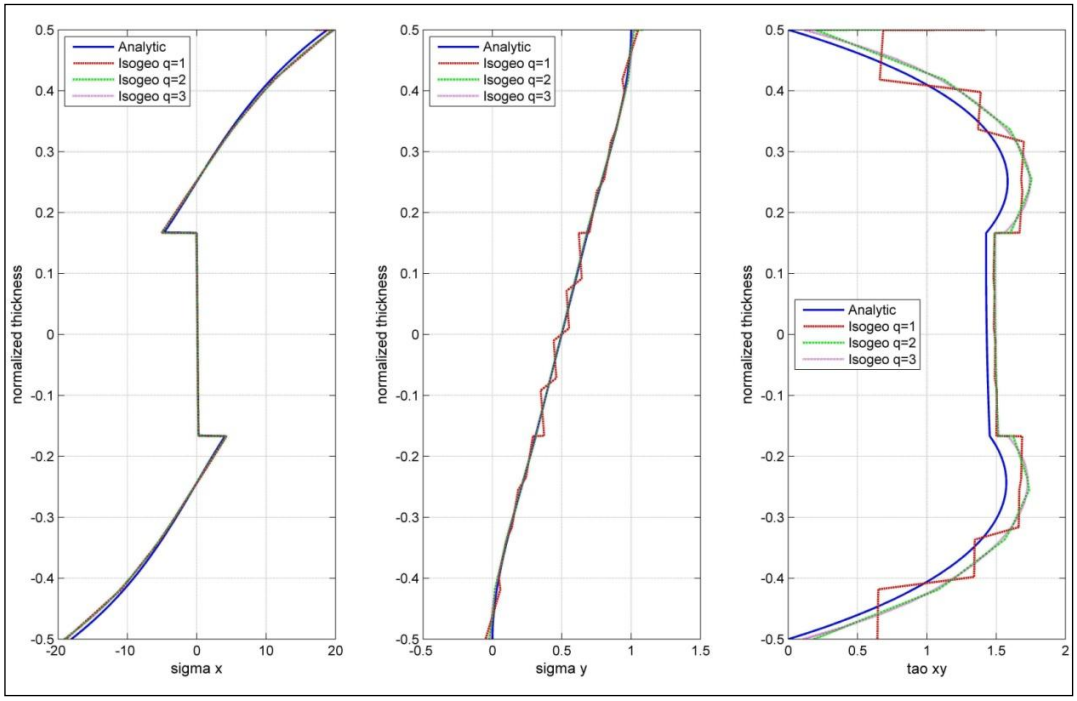

Figure 6.36 : Stress results for 4 elements along the length and 4 elements per layer by using quadratic basis functions along the length.

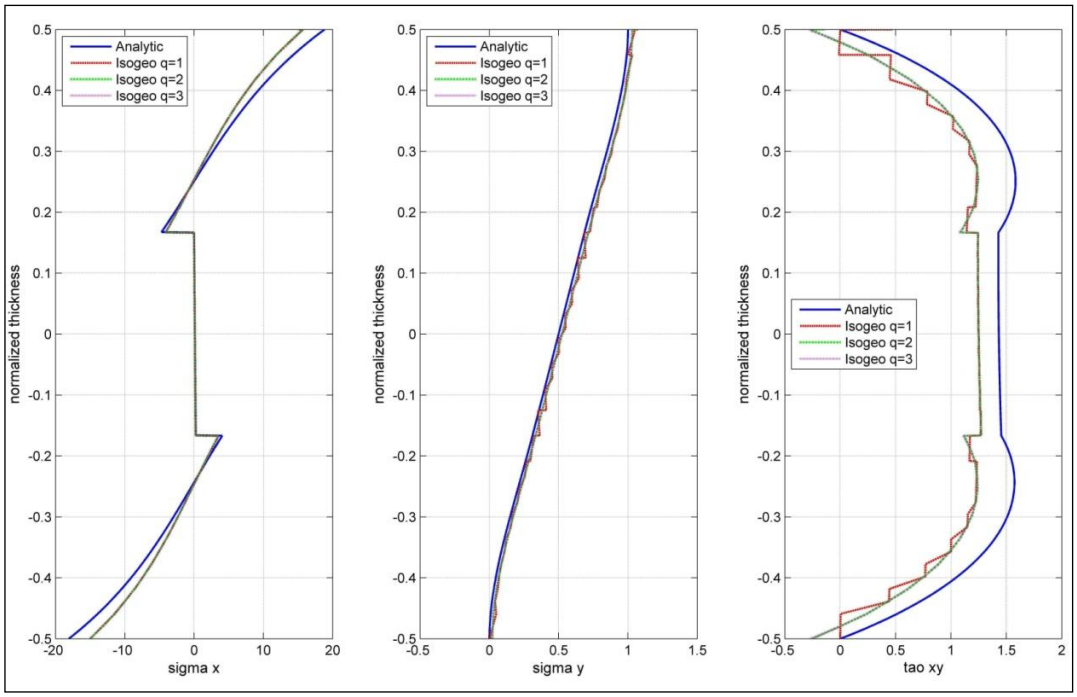

Figure 6.37 : Stress results for 4 elements along the length and 8 elements per layer by using linear basis functions along the length.

However, as seen in Figure 6.38 and Figure 6.39, isogeometric results for cubic basis functions along the thickness introduce smoother and more accurate results than the results derived with linear and quadratic basis functions for finer mesh structures.

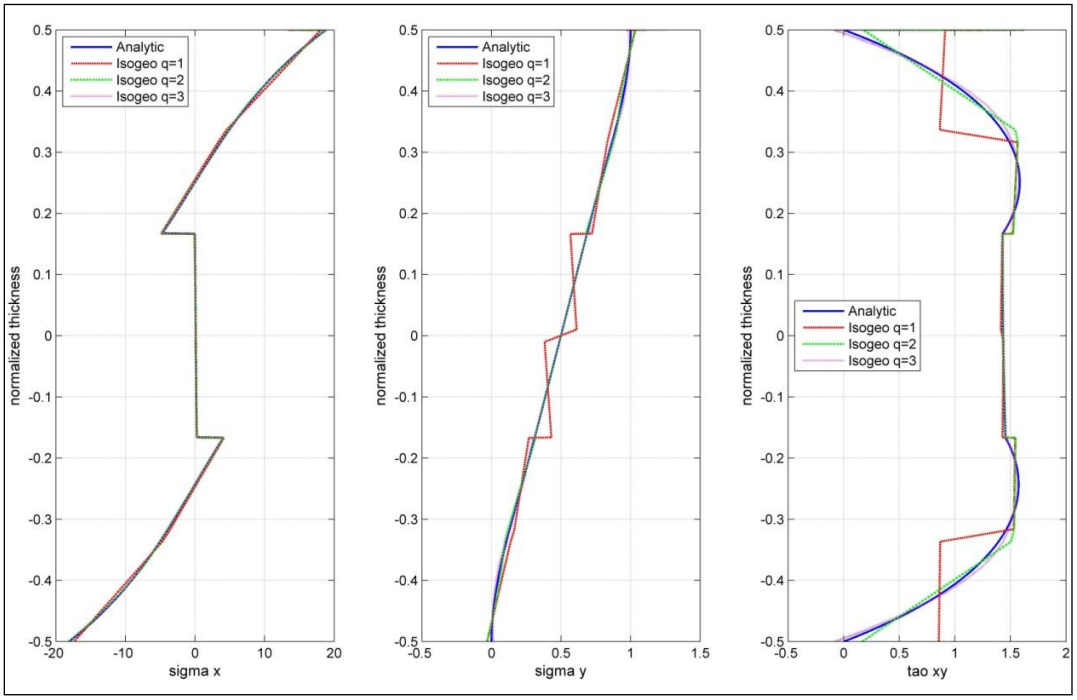

Figure 6.38 : Stress results for 16 elements along the length and 2 elements per layer by using quadratic basis functions along the length.

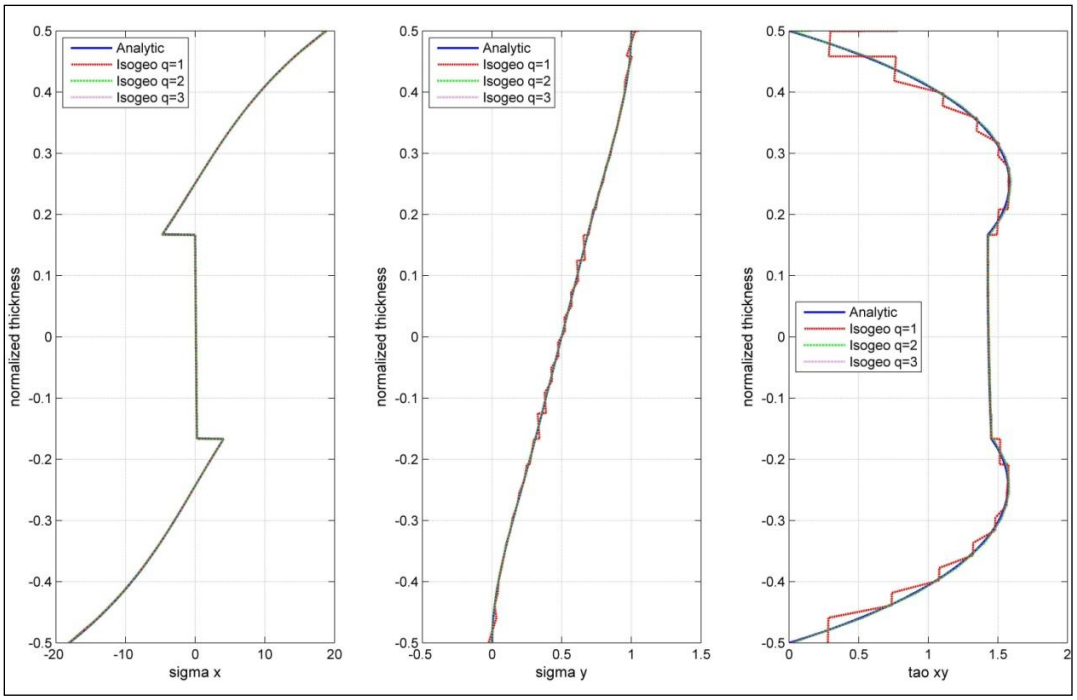

Figure 6.39 : Stress results for 16 elements along the length and 8 elements per layer by using quadratic basis functions along the length.

As same as in the previous application; since isogeometric analysis allows using higher order basis functions through the thickness, for the analysis case in Figure 6.38, isogeometric results for cubic basis functions introduce the superiority over the results of quadratic solutions. Hence, by using higher order basis functions, results

that are more accurate can be obtained with less number of elements that is with less number of degrees of freedom.

Stress plots through the thickness indicate that, by using higher number of elements, stress results on x direction can be approximated easier than the results on y direction. On the other hand, for a certain mesh structure shear stress results has the least accuracy when compared with the stress results on x and y direction. This seems natural when more sophisticated formulation of shear stress calculation is taken into account. However, using higher order basis functions along the length allows maintaining accurate results even with coarse mesh structures. For that reason, it can be stated that; isogeometric analysis introduces a significant advantage especially for shear stress calculations in cylindrical bending of thick beams.

Stress plots for different mesh structures also indicate that, not only the element number along the thickness but also the element number along the length has an effect on the accuracy of the stress results through the thickness.

7. CONCLUSIONS

Isogeometric analysis, a new approach for structural analysis, and its advantages over standard finite element method have been studied. This new method has been validated for some test-cases dealing with structural analysis of slender beams in 1D based on Euler-Bernoulli theory . Then isotropic thick beams are analysed for several boundary conditions and load options with a coding structure which are also contains shear effects. Finally a code framework has been created which is able to analyse comosite thick beams under cylindrical bending for any desired stacking sequence and compares the results with elasticity solution.

As an alternative to conventional finite element method, successful isogeometric analysis applications on structural analysis of beams yield the following comments:

- Although isogeometric analysis includes some fragments of classical FEM framework isogeometric analysis have significant differences and advantages. Using high order NURBS basis functions which may have C1 and higher continuity instead of employing C0 continuous classical Lagrange polynomials as shape functions, and using control points as degrees of freedom which can be outside of the actual geometry are the most outstanding features.
- Perfect geometrical representation with coarsest mesh structure is possible for most of the cases whatever the number of degrees of freedom. This prevents unnecessary mesh refinements for geometrical representation. Thus, number of degrees of freedom is risen only for the solution accuracy.
- High-order solutions mentioned in the first entry are employed without extra coding work, thanks to the features of NURBS functions.
- A combined refinement process (k-refinement) is applicable which allows increased inter-element regularity i.e. covering the same element domain with fewer number of basis functions while maintaining the level of continuity.

- Since degrees of freedom are defined on control points, at a given location they cannot be assumed as the solution values while degrees of freedom is interpreted as the solution values in classical FEM.
- Identical data structure for geometry and solution domain eliminates many extra lines of code. Therefore, the coding framework is created much easier.

Results of straight beam analyses have maintained perfect match with analytical solutions in both displacement and stress plots. Accurate results can be obtained with even single elements with higher order basis functions. Displacement and stress results for arched beam had some difference with the results of structural analysis software package, ABAQUS in the initial analysis. Then it is recognized that this is caused by different parameterization fashion of the curve. In curved beam analysis the parametrical coordinate is not directly proportional with the curve length as it is in straight beam. So in curved beam analysis the parametric coordinate is transferred to curve length as in ABAQUS plots. Thus matched plots of displacement and stress are obtained eventually.

In isotropic and composite thick beam cases, deflection and stress countour plots are perfectly matched with the plots obtained from a commerical analysis package, ABAQUS. Deflection and stress comparison through the beam thickness also yields satisfactory results.

The most significant acquisition of this research is the stress results through the thickness of a composite beam under cylindrical bending. This is a novel application for isogeometric analysis. In this application, isogeometric analysis allows using high order basis functions which is able to provide much more accurate results than conventional FEM packages. While isogeometric analysis allows this higer order solutions, conventional FEM packages (such as ABAQUS,ANSYS etc.) can employ second order shape fuctions at best.

REFERENCES

[1] **Zienkiewicz, O. C.,** 1989. The Finite Element Method in Engineering Science (second ed.). London: McGraw-Hill.

[2] **Luo, X.-J., M. S. Shephard, and J.-F. Remacle,** 2001. Influence of geometric approximation on the accuracy of higher order methods. Technical Report 1, SCOREC.

[3] **Munoz, J. J.,** 2008. Modelling unilateral frictionless contact using the null-space method and cubic B-Spline interpolation. *Comput. Methods Appl. Mech. Engrg.* 197 (9-12), 979–993.

[4] **Kagan, P. A. Fischer, and P. Z. Bar-Yoseph,** 1998. New B-spline finite element approach for geometrical design and mechanical analysis. *Internat. J. Numer. Methods Engng.* 41, 435–458.

[5] **Hughes, T. J. R., J. A. Cottrell, and Y. Bazilevs,** 2005. Isogeometric analysis: CAD, finite elements, NURBS, exact geometry and mesh refinement. *Comput. Methods Appl. Mech. Engrg.* 194 (39–41), 4135–4195.

[6] **Cottrell, J., Hughes, T., and Reali, A.** 2007. Studies of refinement and continuity in isogeometric analysis. *Computer Methods in Applied Mechanics and Engineering*, 196, 4160–4183.

[7] **Dorfel, M., Juttler, B., and Simeon, B.** 2009. Adaptive isogeometric analysis by local h-refinement with t-splines. *Computer Methods in Applied Mechanics and Engineering***.**

[8] **J.A. Cottrell, A. Reali, Y. Bazilevs, T.J.R. Hughes,** 2006. Isogeometric analysis of structural vibrations. *Comput. Meth. Appl. Mech. Eng.* 195**,** 5257–5296.

[9] **Nagy, A. P., Mostafa M. Abdalla, Zafer Gurdal,** 2010. Isogeometric sizing and shape optimisation of beam structures. *Comput. Methods Appl. Mech. Engrg.* 199 1216-1230

[10] **Bazilevs, Y., de Veiga, L. B., Cottrell, J., Hughes, T., and Sangalli., G.** 2006. Isogeometric analysis: approximation, stability and error estimates for refined meshes. *Mathematical Models and Methods in Applied Sciences*, 6 1031–1090.

[11] **Y.J. Zhang, Y. Bazilevs, S. Goswami, C.L. Bajaj, T.J.R. Hughes,** 2007. Patient-specific vascular NURBS modeling for isogeometric analysis of blood flow. *Comput. Meth. Appl. Mech. Eng.* 196 2943–2959.

[12] **D.J. Benson, Y. Bazilevs, M.C. Hsu, T.J.R. Hughes,** 2010. Isogeometric shell analysis: the Reissner–Mindlin shell. *Comput. Meth. Appl. Mech. Eng.* 199 276–289.

[13] **H. Gómez, V.M. Calo, Y. Bazilevs, T.J.R. Hughes,** 2008**.** Isogeometric analysis of the Cahn–Hilliard phase-fieldmodel. *Comput. Meth. Appl. Mech. Eng.* 197 4333–4352.

[14] **R. Echter, M. Bischoff, Numerical,** 2010. Efficiency, locking and unlocking of NURBS finite elements**.** *Comput. Meth. Appl. Mech. Eng.* 199 374–382.

[15] **S. Lipton, J.A. Evans, Y. Bazilevs, T. Elguedj, T.J.R. Hughes,** 2010**.** Robustness of isogeometric structural discretizations under severe mesh distortion. *Comput. Meth. Appl. Mech. Eng.* 199 357–373.

[16] **H.J. Kim, Y.D. Seo, S.K. Youn,** 2010. Isogeometric analysis for trimmed CAD Surfaces. *Comput. Meth. Appl. Mech. Eng.* 198 2982–2995.

[17] **J. Lu,** 2009**.** Circular element: isogeometric elements of smooth boundary. *Comput. Meth. Appl. Mech. Eng.* 198 2391–2402.

[18] **R. Sevilla, S. Fernandez-Mendez, A. Huerta,** 2008. NURBS-enhanced finite element method**.** *Int. J. Numer. Meth. Eng.* 76 56–83.

[19] **A. Shaw, D. Roy,** 2008. NURBS-based parametric mesh-free methods. *Comput. Meth. Appl. Mech. Eng.* 197 1541–1567**.**

[20] **Carl de Boor,** 1978. A Practical Guide to Splines. Springer-Verlag. pp. 113–114.

[21] **Cox, M.G.,** 1971. The numerical evolution of B-Splines. Technical report, National Physics Laboratory

[22] **D.F. Rogers,** 2001. Introduction to NURBS With Historical Perspective, Academic Press, San Diego, CA,

[23] **J.A. Cottrell, T.J.R. Hughes, Y. Bazilevs,** 2009. Isogeometric Analysis Toward Integration of CAD and FEA

[24] **N.J. Pagano,** 1969. Exact Solutions for Composite Laminates in Cylindrical Bending. *Journal of Composite Materials 3: 398*

APPENDICES

APPENDIX A : Stress results for the 0/90 layup with the mesh structures in Table 6.1

APPENDIX B : Stress results for the 0/90/0 layup with mesh structures in Table 6.2

APPENDIX A Stress results for the 0/90 layup with the mesh structures in Table 6.1. Cases which is not presented here, is already in the text.

APPENDIX A.1

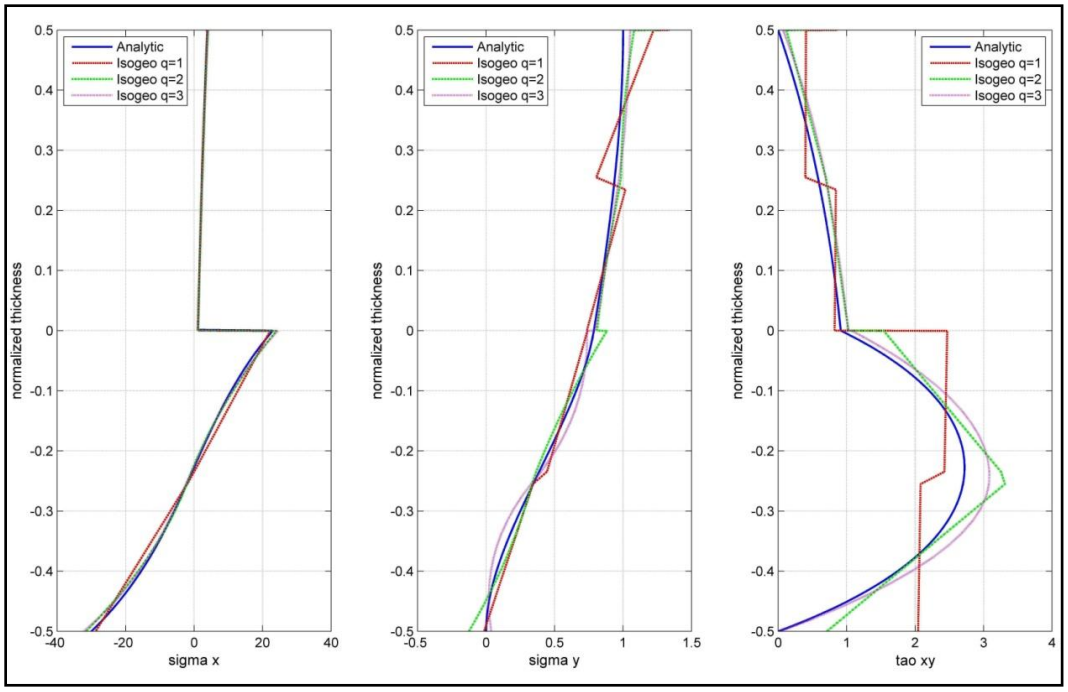

Figure A.1 : Stress results for 4 elements along the length and 2 elements per layer by using quadratic basis functions.

APPENDIX A.2

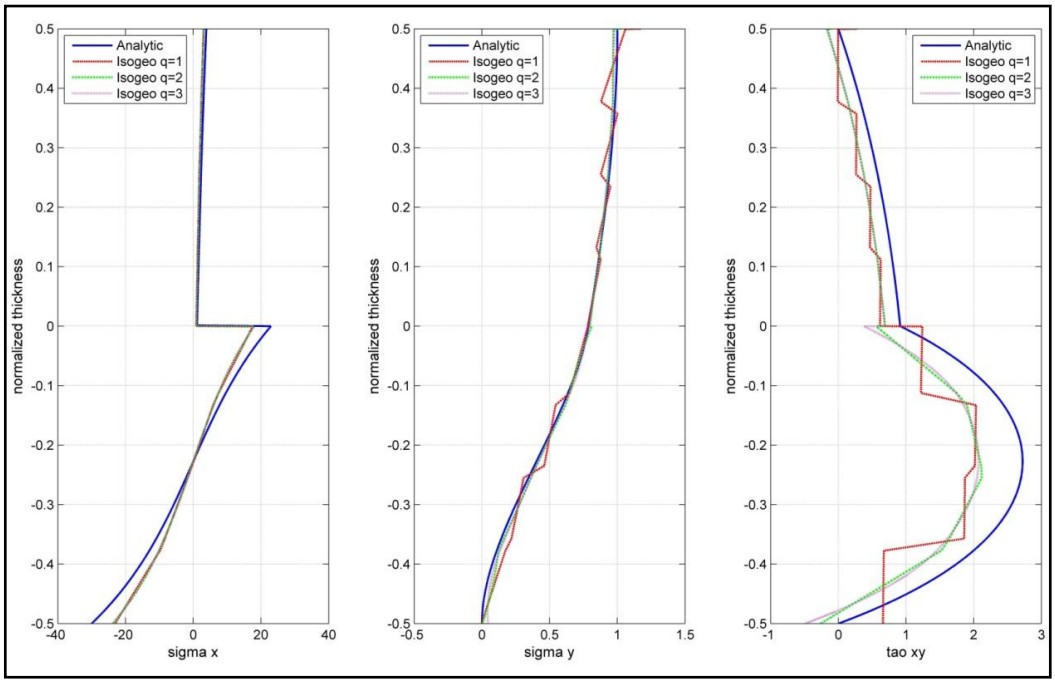

Figure A.2 : Stress results for 4 elements along the length and 4 elements per layer by using linear basis functions.

APPENDIX A.3

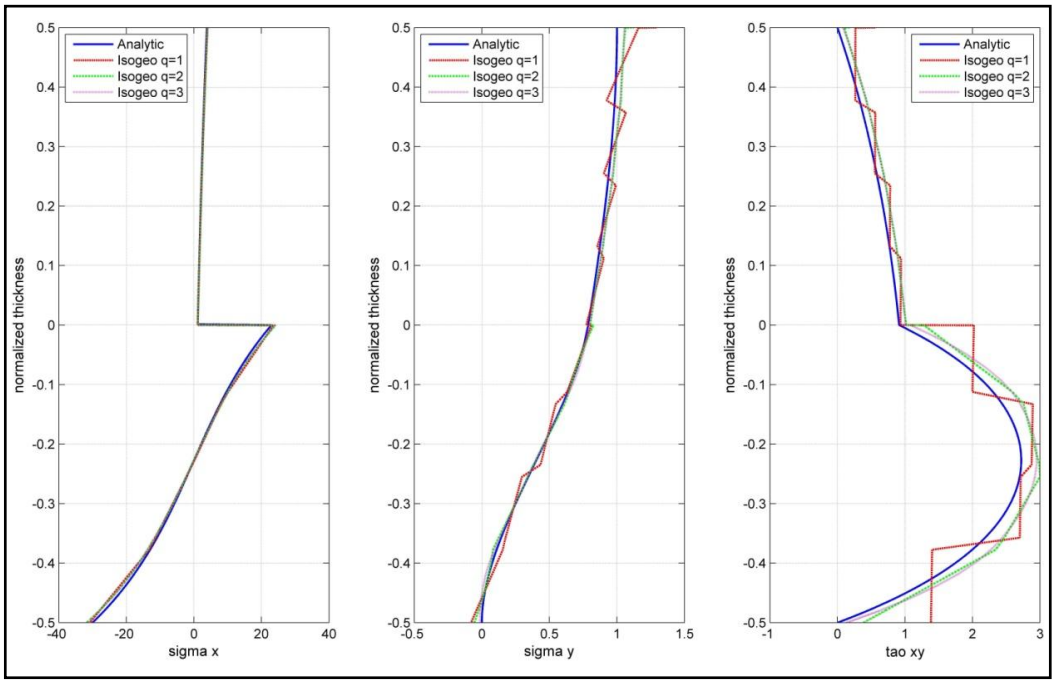

Figure A.3 : Stress results for 4 elements along the length and 8 elements per layer by using linear basis functions.

APPENDIX A.4

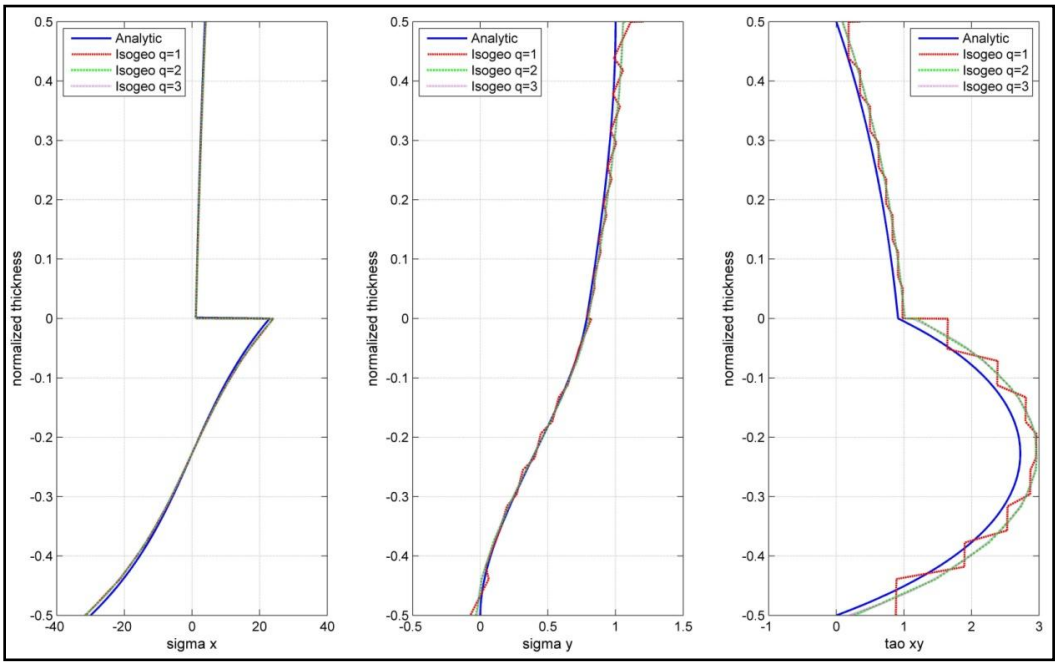

Figure A.4 : Stress results for 4 elements along the length and 8 elements per layer by using quadratic basis functions.

APPENDIX A.5

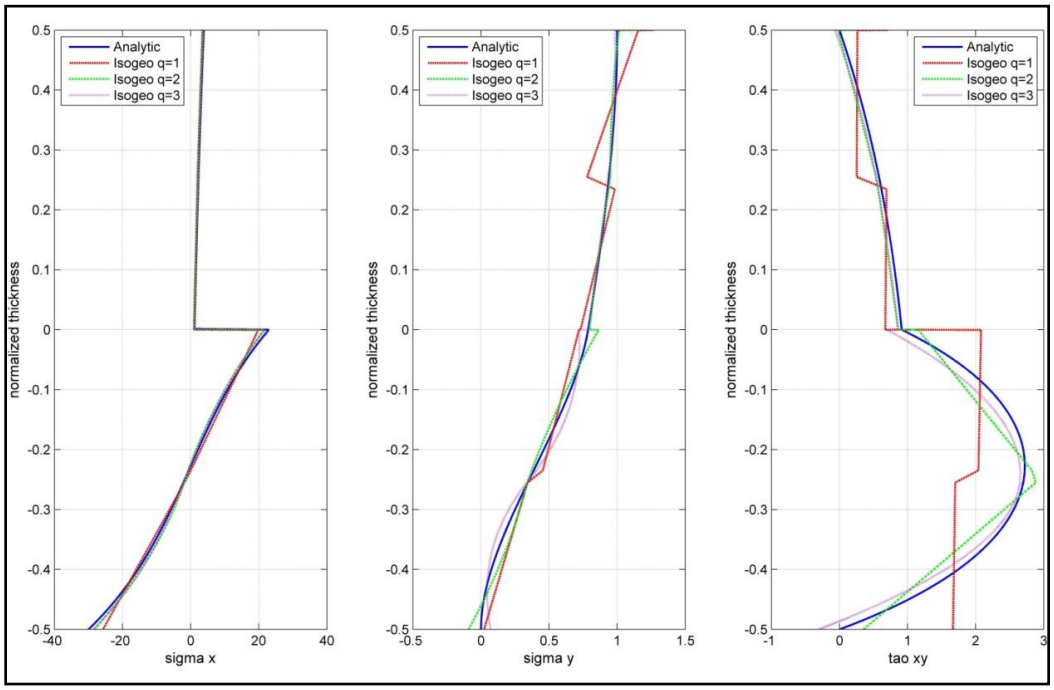

Figure A.5 : Stress results for 8 elements along the length and 2 elements per layer by using linear basis functions.

APPENDIX A.6

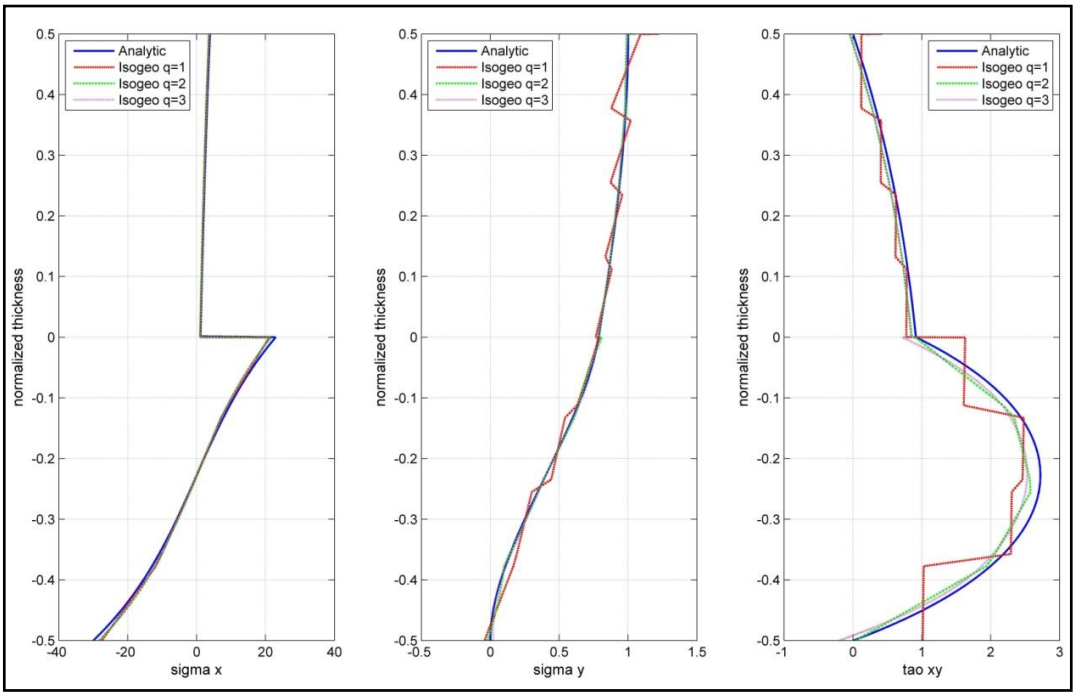

Figure A.6 : Stress results for 8 elements along the length and 4 elements per layer by using linear basis functions.

APPENDIX A.7

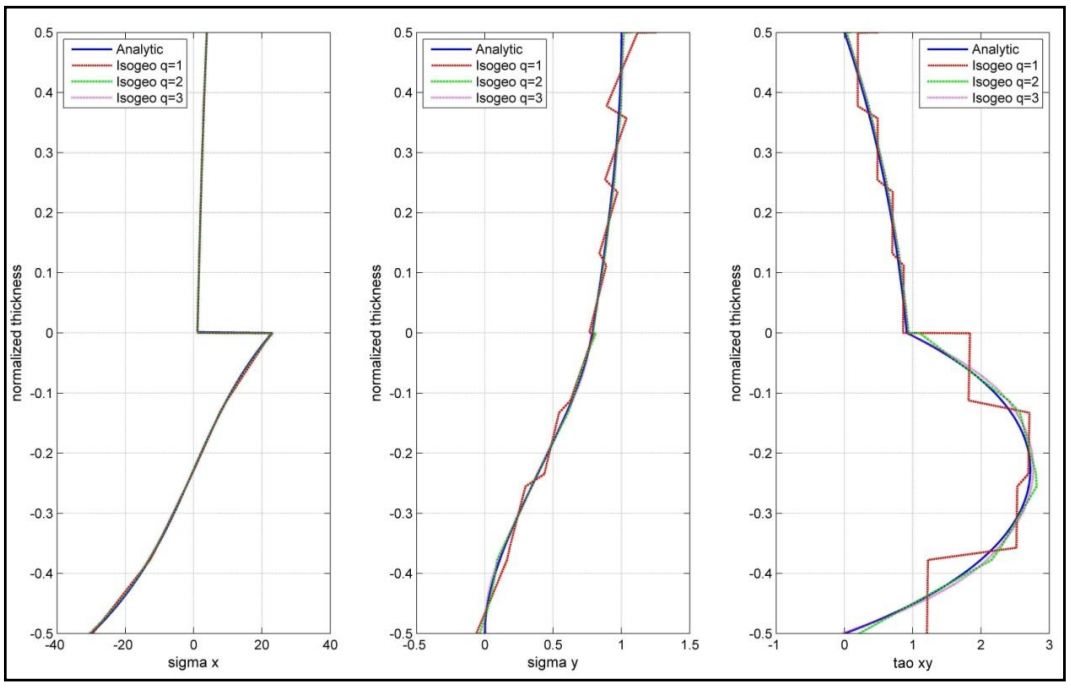

Figure A.7 : Stress results for 8 elements along the length and 4 elements per layer by using quadratic basis functions.

APPENDIX A.8

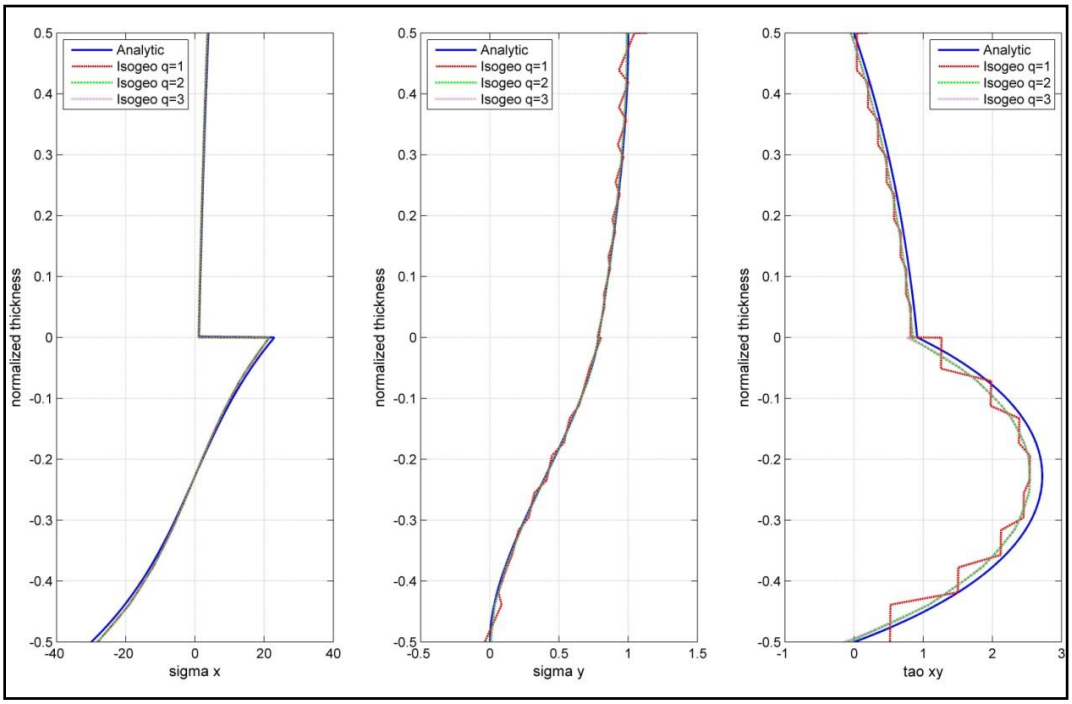

Figure A.8 : Stress results for 8 elements along the length and 8 elements per layer by using linear basis functions.

APPENDIX A.9

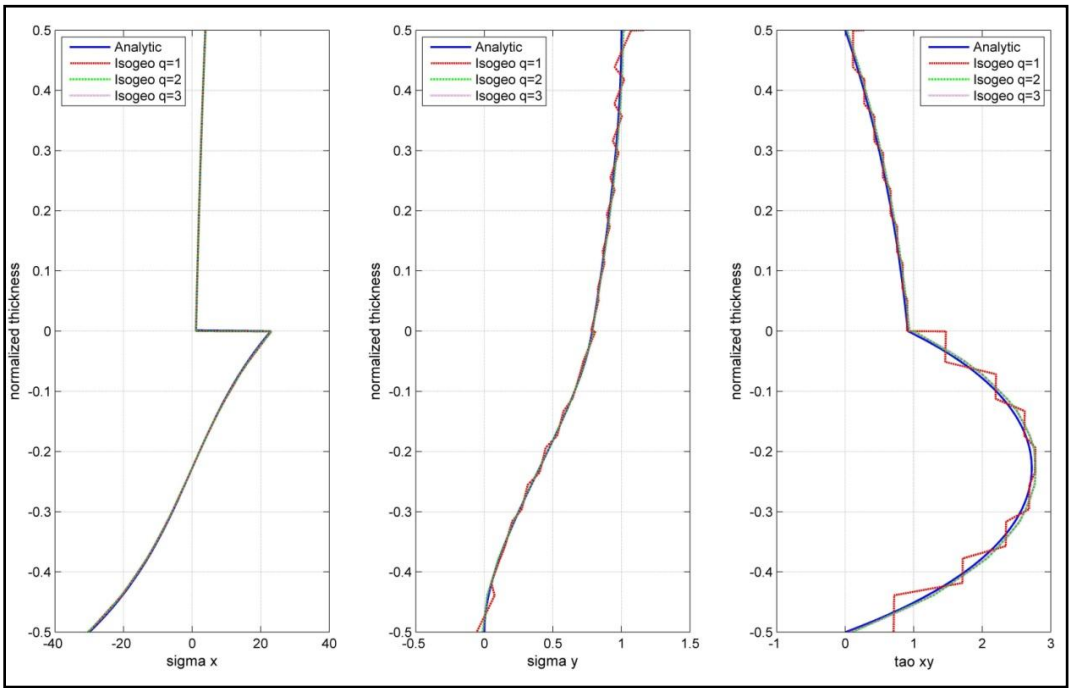

Figure A.9 : Stress results for 8 elements along the length and 8 elements per layer by using quadratic basis functions.

APPENDIX A.10

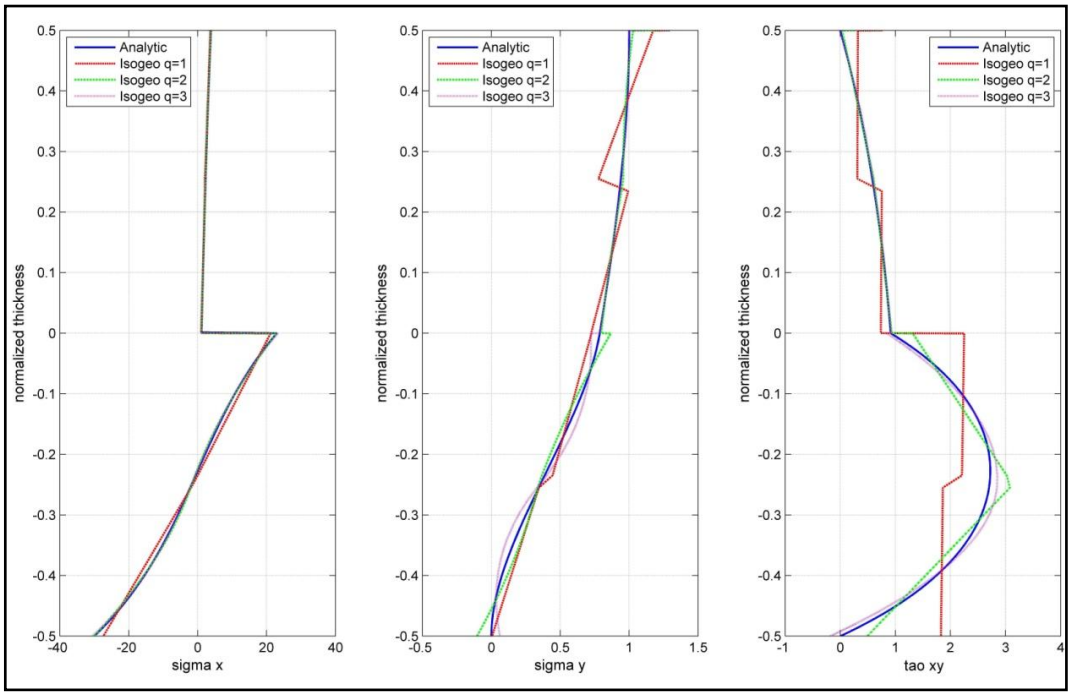

Figure A.10 : Stress results for 16 elements along the length and 2 elements per layer by using quadratic basis functions.

APPENDIX A.11

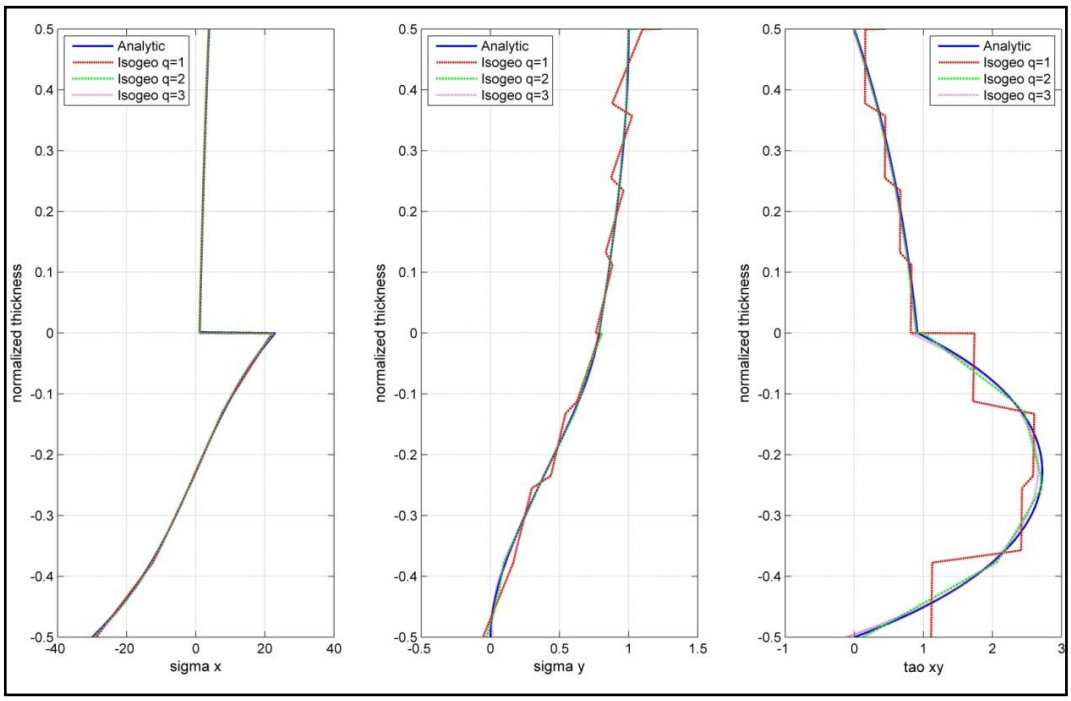

Figure A.11 : Stress results for 16 elements along the length and 4 elements per layer by using linear basis functions.

APPENDIX A.12

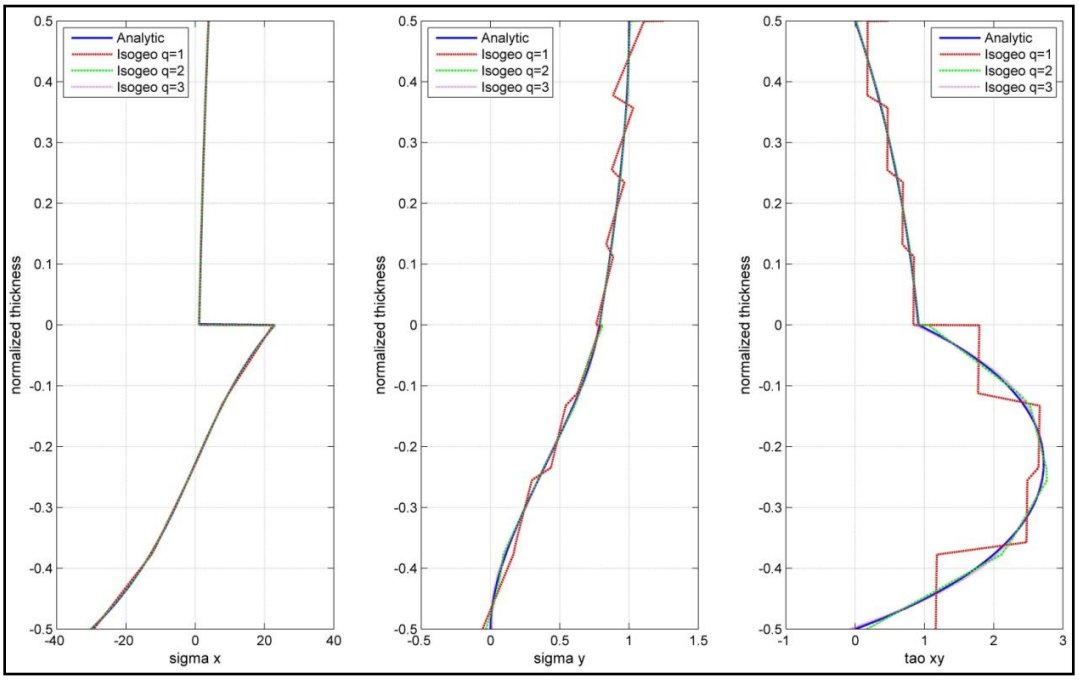

Figure A.12 : Stress results for 16 elements along the length and 4 elements per layer by using quadratic basis functions.

APPENDIX A.13

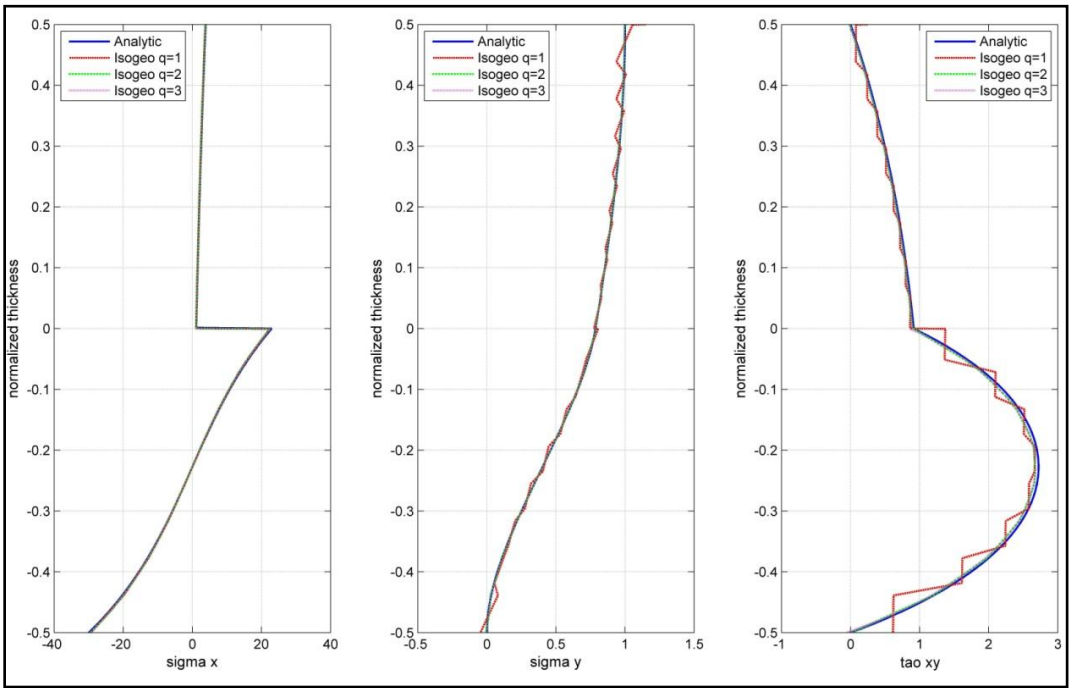

Figure A.13 : Stress results for 16 elements along the length and 8 elements per layer by using linear basis functions.

APPENDIX B Stress results for the 0/90/0 layup with the mesh structures in Table 6.2. Cases which is not presented here, is already in the text.

APPENDIX B.1

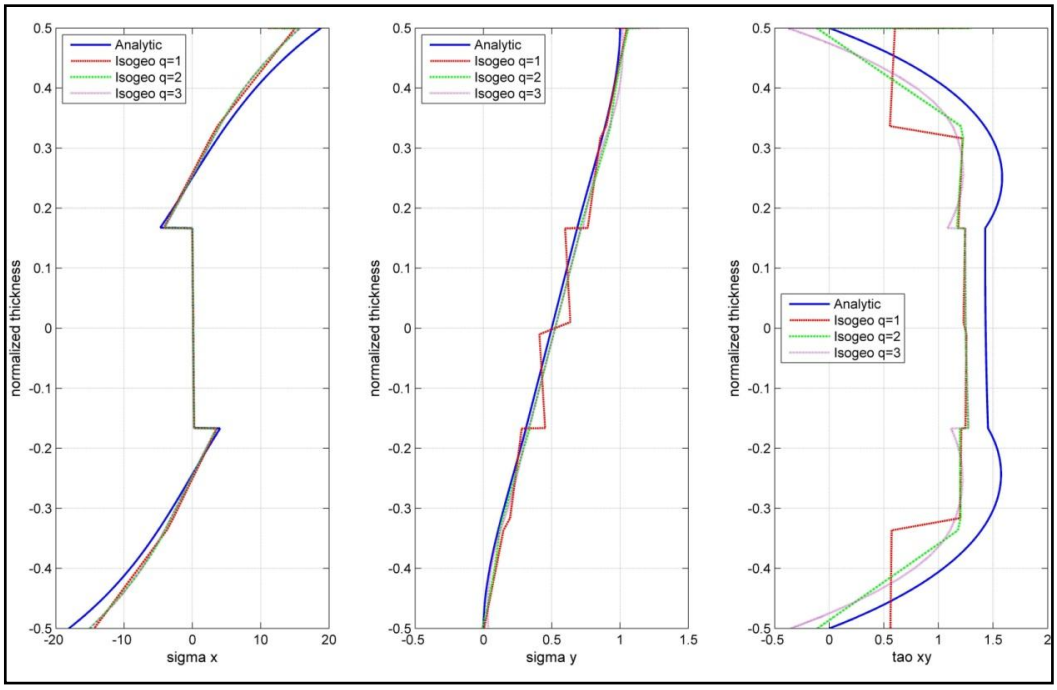

Figure B.1 : Stress results for 4 elements along the length and 2 elements per layer by using linear basis functions.

APPENDIX B.2

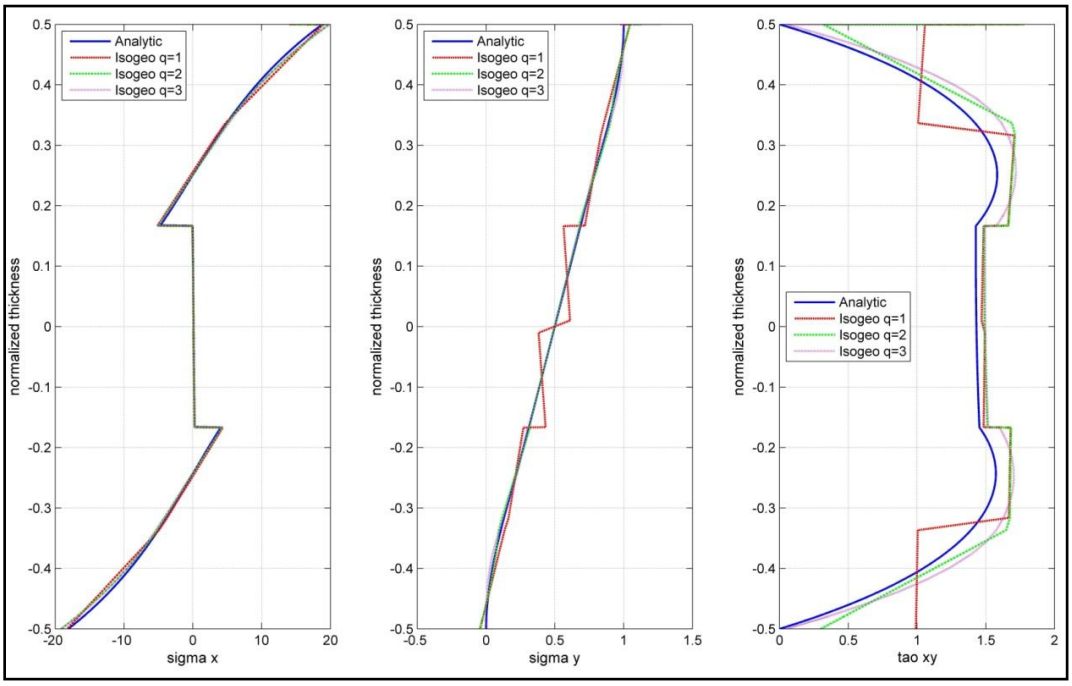

Figure B.2 : Stress results for 4 elements along the length and 2 elements per layer by using quadratic basis functions.

APPENDIX B.3

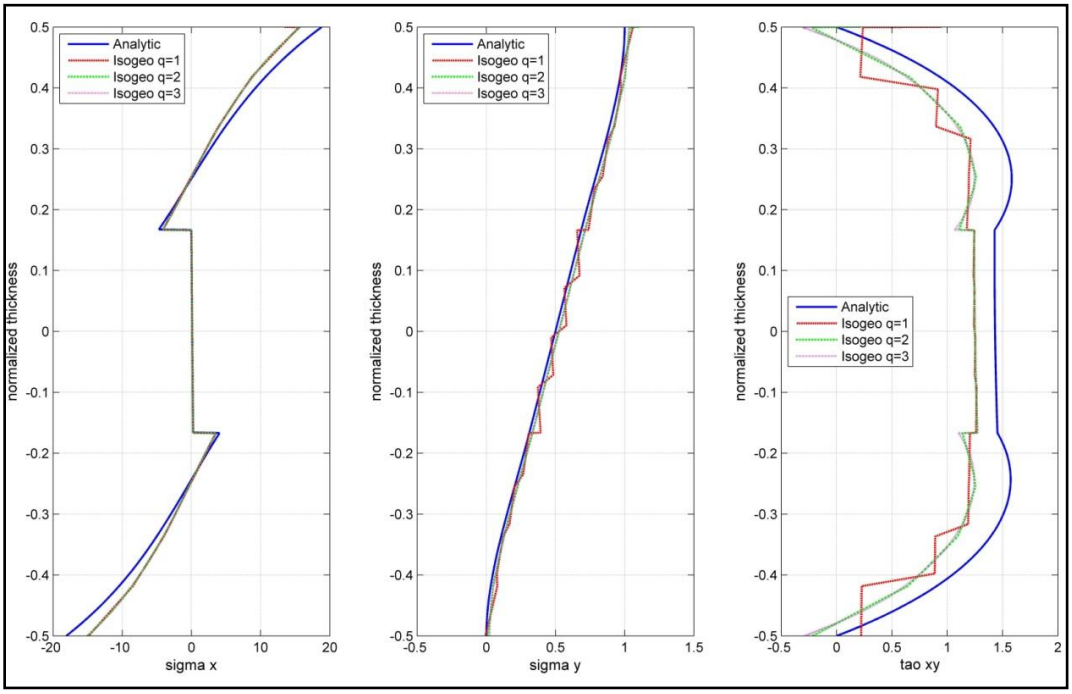

Figure B.3 : Stress results for 4 elements along the length and 4 elements per layer by using linear basis functions.

APPENDIX B.4

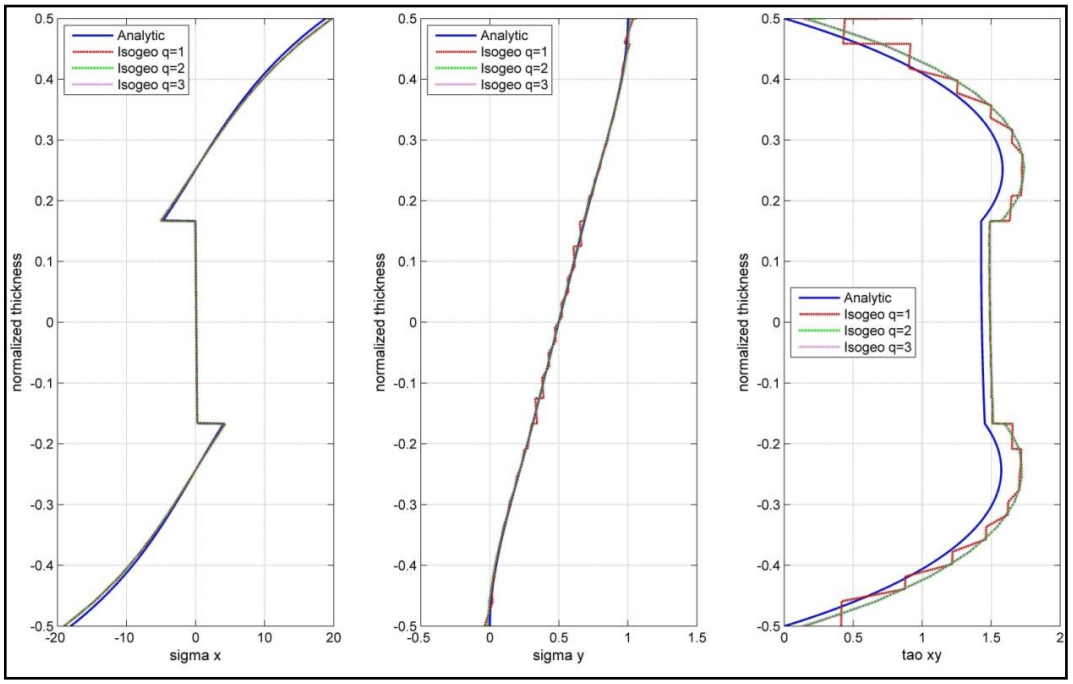

Figure B.4 : Stress results for 4 elements along the length and 8 elements per layer by using quadratic basis functions.

APPENDIX B.5

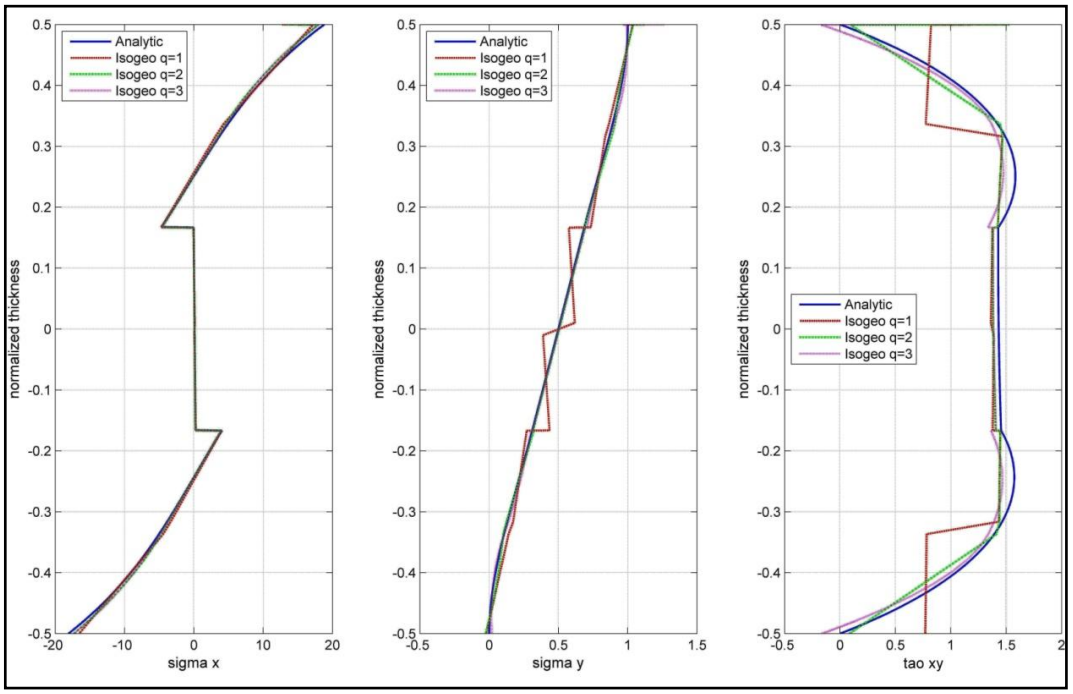

Figure B.5 : Stress results for 8 elements along the length and 2 elements per layer by using linear basis functions.

APPENDIX B.6

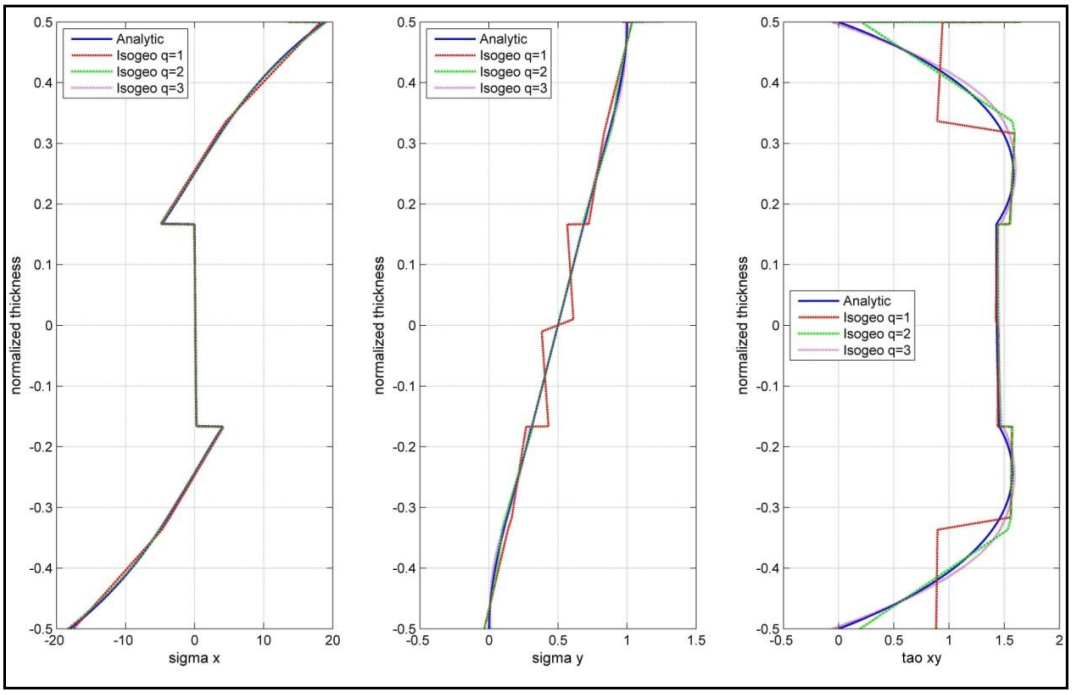

Figure B.6 : Stress results for 8 elements along the length and 2 elements per layer by using quadratic basis functions.

APPENDIX B.7

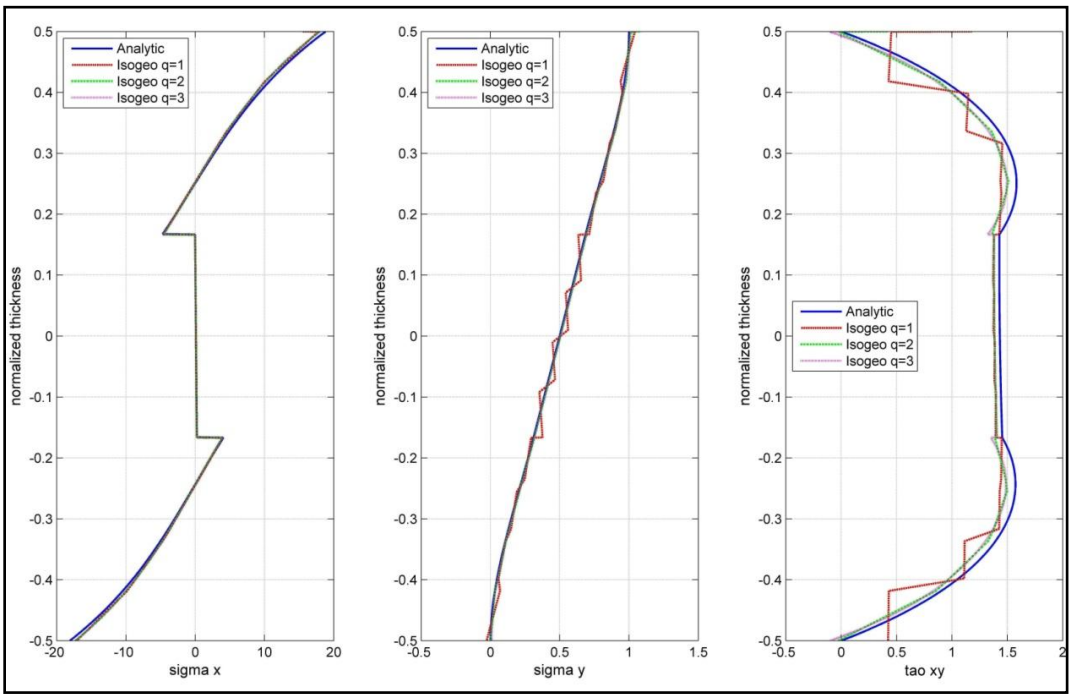

Figure B.7 : Stress results for 8 elements along the length and 4 elements per layer by using linear basis functions.

APPENDIX B.8

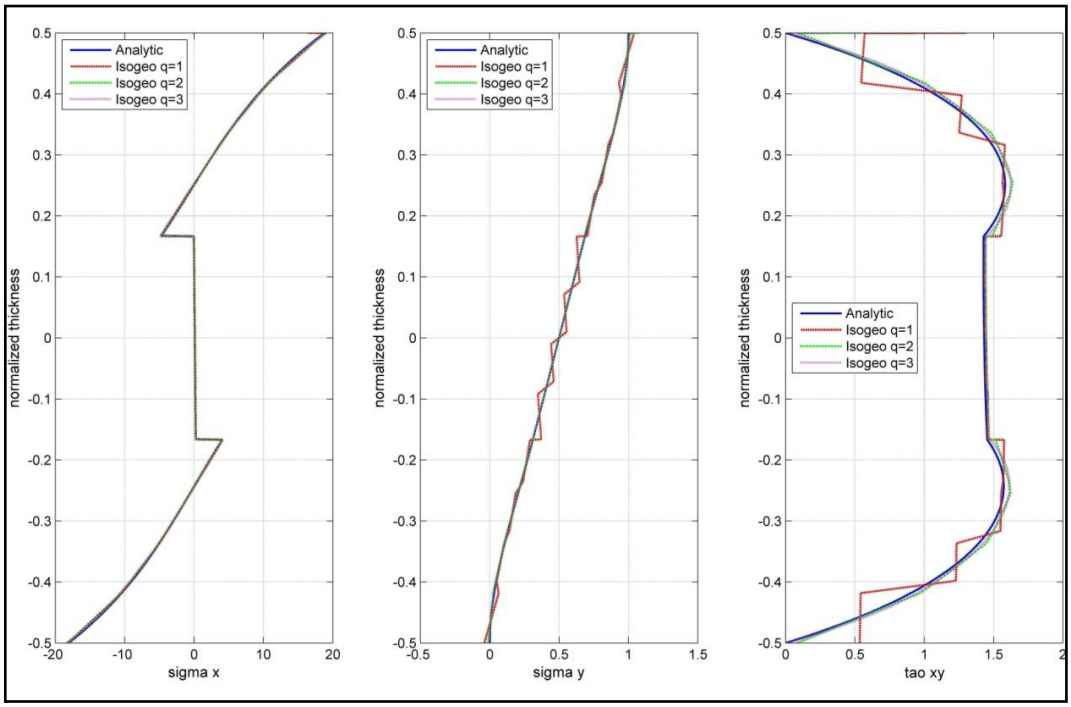

Figure B.8 : Stress results for 8 elements along the length and 4 elements per layer by using quadratic basis functions.

APPENDIX B.9

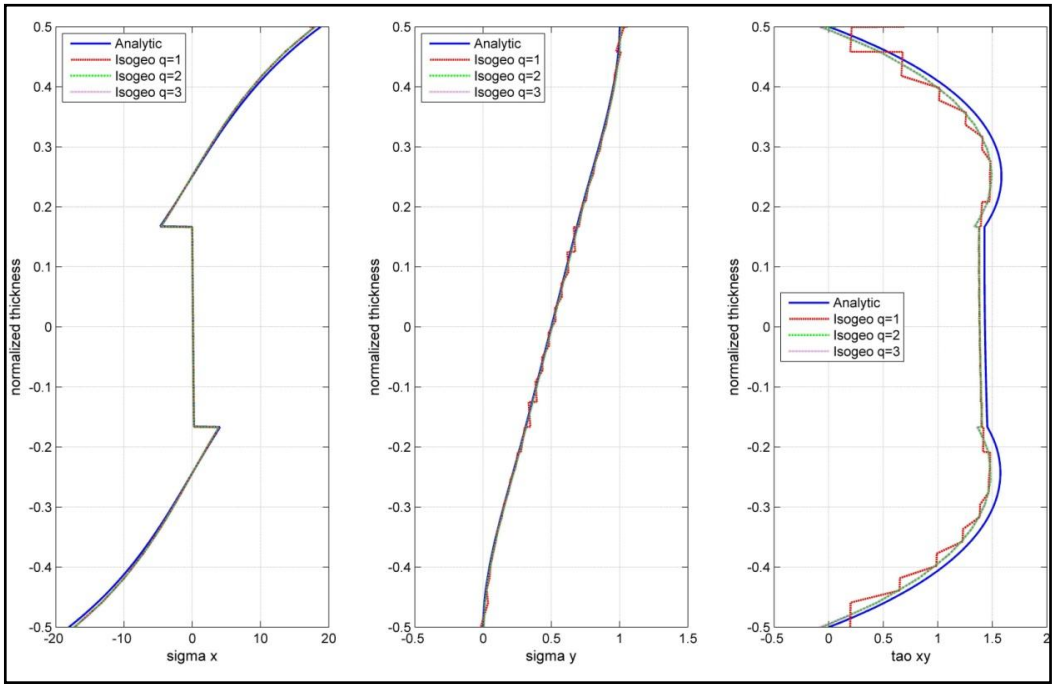

Figure B.9 : Stress results for 8 elements along the length and 8 elements per layer by using linear basis functions.

APPENDIX B.10

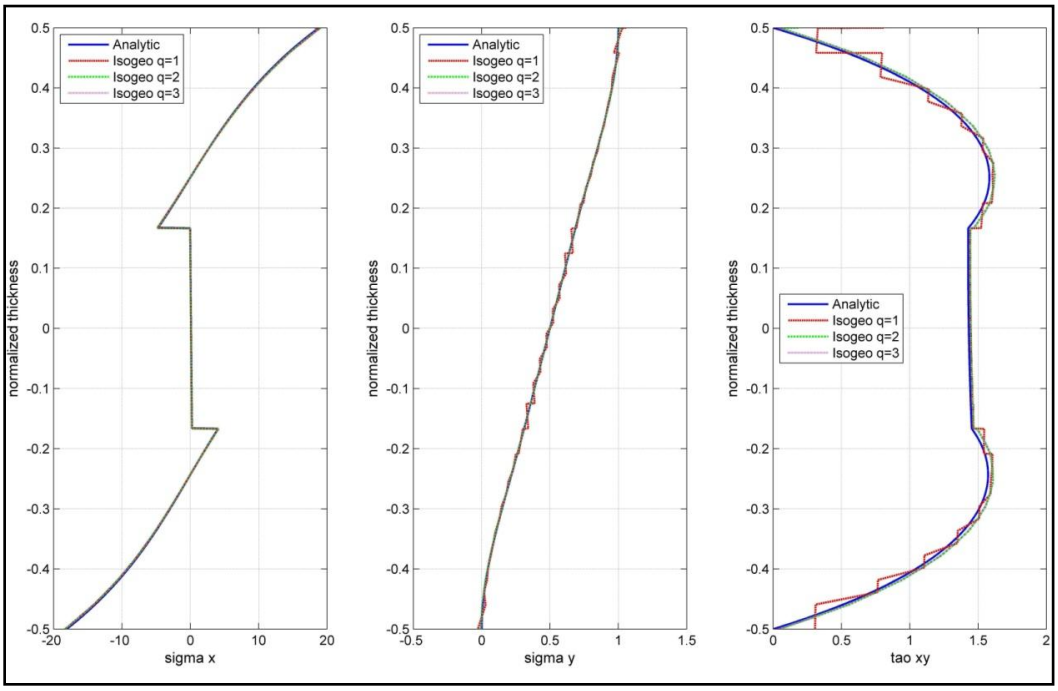

Figure B.10 : Stress results for 8 elements along the length and 8 elements per layer by using quadratic basis functions.

APPENDIX B.11

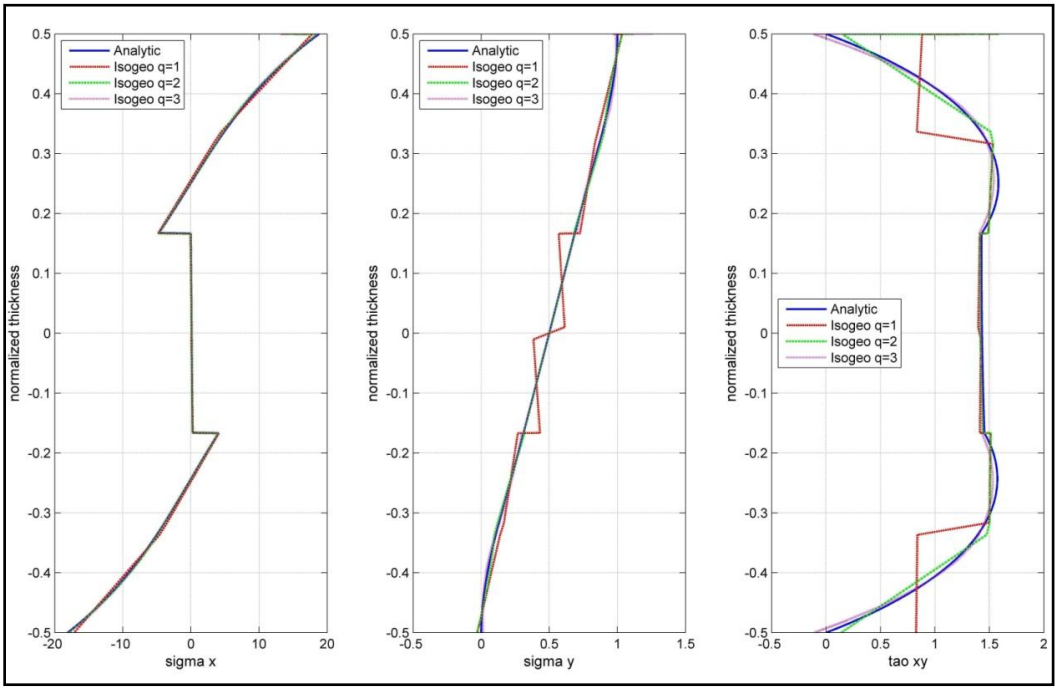

Figure B.11 : Stress results for 16 elements along the length and 2 elements per layer by using linear basis functions.

APPENDIX B.12

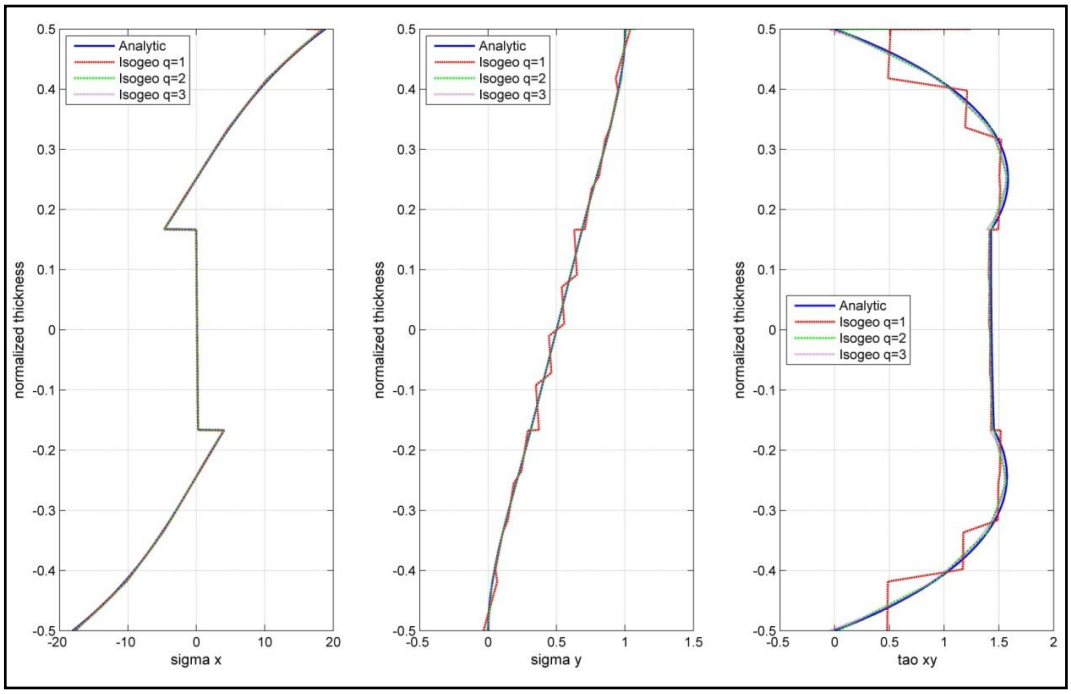

Figure B.12 : Stress results for 16 elements along the length and 4 elements per layer by using linear basis functions.

APPENDIX B.13

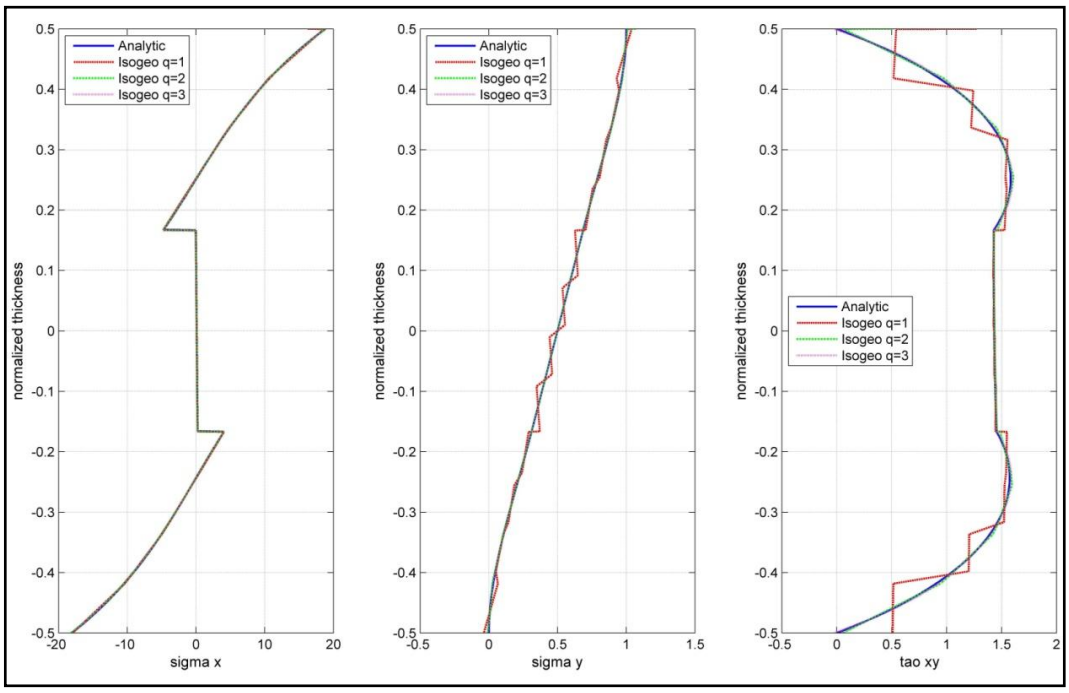

Figure B.13 : Stress results for 16 elements along the length and 4 elements per layer by using quadratic basis functions.

APPENDIX B.14

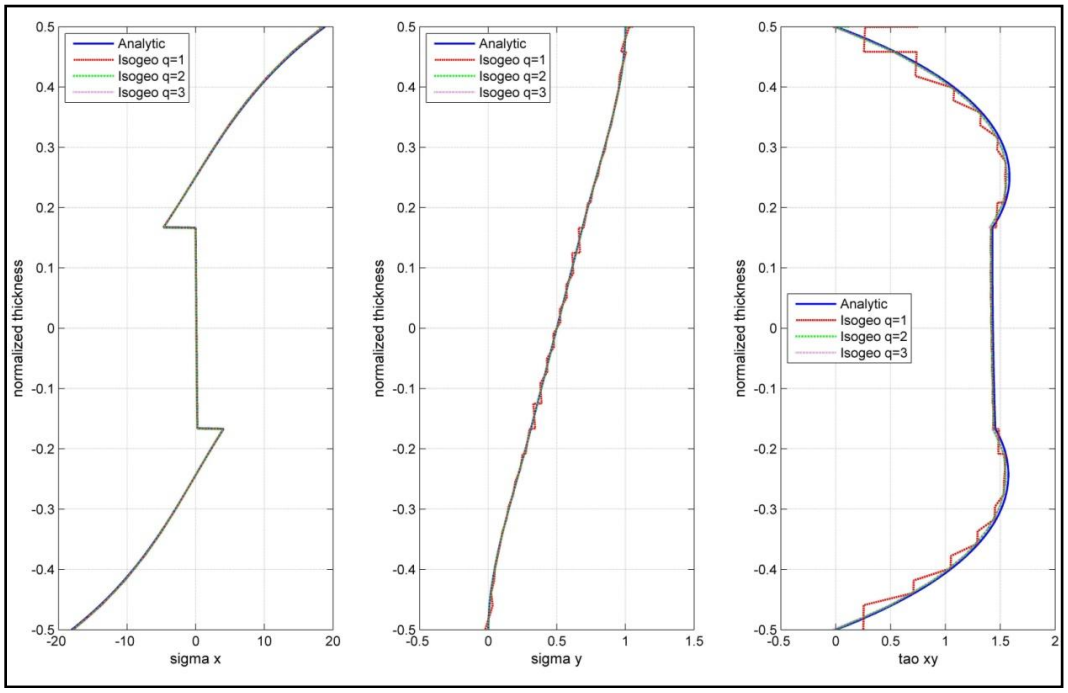

Figure B.14 : Stress results for 16 elements along the length and 8 elements per layer by using linear basis functions.

CURRICULUM VITAE

Name Surname: Murat DEMIRTAŞ

Place and Date of Birth: İZMİT/10.11.1985

Address: Büyükdere Mah. Mühendis Şevket Sok. 16/3 Sarıyer/İstanbul

E-Mail: demirtasmurat85@gmail.com

B.Sc.: Astronautical Engineering